Université de Strasbourg

ÉCOLE DOCTORALE DES SCIENCE DE LA VIE ET DE LA SANTE (ED414)

Laboratoire de Génétique médicale, INSERM UMRS_1112, Strasbourg

Thèse Présentée par :

Daniel AJOY MORENO

Soutenue le : **15 décembre 2020**

pour obtenir le grade de : **Docteur de l'université de Strasbourg**

Discipline/ Spécialité : Aspects moléculaires et cellulaires de la Biologie

Non-invasive pharmacological treatment of retinal degeneration in the Bardet-Biedl Syndrome and related ciliopathies

THÈSE dirigée par :
Mme. Hélène DOLLFUS   **Professeur, Université de Strasbourg**

ENCADREMENT SCIENTIFIQUE :
M. Vincent MARION   **CR1 INSERM**

RAPPORTEURS :
Mme. Rocío Herrero Vanrell   **Professeur, Universidad Complutense de Madrid**
M. Mathias SEELIGER   **Professeur, Eberhard-Karls Universität Tübingen**

EXAMINATEUR INTERNE :
M. David HICKS   **DR INSERM, Université de Strasbourg**

To my family and friends

Acknowledgments

Before starting the exposition of the work done the last three years, I would like to take some time to thank all the people who was walked with me these last three years.

First of all, I would like to extend my gratitude to professor Hélène Dollfus and my scientific supervisor Dr. Vincent Marion for giving me the opportunity of doing my thesis in this laboratory.

I would also like to thanks my thesis committee Rocío Herrera Vanrell and Mathias Seeliger for taking the time of reading and evaluating my work and participating in my thesis defence. I would also like to thanks David Hicks, for taking the time to evaluate the evolution of my project and following it as part of the mid-thesis committee and now part of my thesis jury.

A big thanks to the people that have been with me during these 3 years of work. Without them this period would have been significantly more complicated. Thanks to Agnès for being the first person showing me how the lab worked and the techniques I have used during these years. Thanks to Katia for the talk during the long PCR times and all the help she has given me with the mice. Thanks to Clarisse for all the support, corrections and cheese, it was really great starting the thesis along with you. Thanks to Cathy also for all the support and for putting up with me and my questions all these years and of course for the little plant I have at home. Thanks to Catherine (also Cathy) for all the advice, encouragement, support and good mood, even after working with us. While not part of our lab, a big thanks to Celes for all the support, shared coffees and for making the last period of my thesis easier. I thank all of them for helping me learn and grow, without you this work would not have been possible. I would also like to thank the rest of the team, the ones thar are working and the ones that left: Ariane, Vero, Alejandro, Tiphaine, Aline, Jean, Nico, Corinne…Thanks to Amandine and Laurie for the short time we have shared, I hope you are able to keep being positive and bring new energy to the group. I also want to wish luck to the new people which I have not known much, Adella and Gaëlle. Thanks to our ex-neighbour team. Thanks, Jérémie for all the chocolate and bad movie references (Oh, hi Mark). Thanks to Chiara and good luck with your thesis.

Next, of course, I would like to thanks the people from the Ocuther project. It has been an amazing experience and opportunity being able to work with some of them but also share and discuss with all the people from this project. Especially, Stephen, Ada, Anam, Chiara and Amir. It was a great experience starting the thesis with you and getting to know you over all the Ocuther meetings and travels. Also, thanks to Marco, for his work in this collaboration that made my thesis possible.

I cannot forget in these acknowledgments, the people that have supported me while not being a direct part of my thesis. Thanks to Ali, Alex, Alberto, Cris, Cecilia, Adri thanks for being with me after all these

Non-invasive pharmacological treatment of retinal degeneration in the Bardet-Biedl Syndrome and related ciliopathies.

Preface

This thesis was done in the context The Ocuther Network, coordinated by Professor Arto Urtti, University of Eastern Finland. It was funded by the European Union's Horizon 2020 Research and Innovation Programme under the Marie Skłodowska-Curie Grant Agreement № 722717. The main aim of this project is the formation of several PhD students in the field of ocular drug delivery. The Ocuther network studies different methods for drug delivery to the ocular tissues as well as searches to increase the knowledge on the eye pharmacokinetics. Some of the projects included in the Ocuther Network are related to formulation of liposomes, hydrogels or the use of sonophoresis for enhancing ocular drug delivery. In the case of my thesis, the Ocuther Project was performed in the UMRS_1112 laboratory consisting of two groups at the Strasbourg University (France): 1) group 1 works in close relation with a reference centre for patients with Rare Eye syndromes of the Strasbourg University Hospital (CARGO) and is performing molecular characterization of the patients with rare genetic eye diseases, this centre is coordinated by Pr. Hélène Dollfus, director of this thesis; 2) group 2 by which this thesis was supervised focuses on the development of treatments for the ciliopathies, that in turn, could potentially be used in these patients. The coordinator of this group 2 and scientific supervisor of the thesis is Dr. Vincent Marion.

List of contents

List of Tables

List of Figures

List of Abbreviations

BAB	**Blood-aqueous barrier**
BBS	**Bardet-Biedl syndrome**
BRB	**Blood-retinal barrier**
	Centre de référence pour les Affections Rares en Génetique
CARGO	**Ophtalmologique**
DDS	**Drug delivery system**
DLS	**Dynamic light scattering**
ERG	**Electroretinogram recording**
ER	**Endoplasmic Reticulum**
GBZ	**Guanabenz**
IRD	**Inherited Retinal Degeneration**
IS	**Inner segment**
IVT	**Intravitreal Injection**
MN	**Micro needles**
MNPs	**Magnetic Nanoparticles**
MSC	**Mesenchymal stem cells**
MW	**Molecular Weight**
OS	**Outer segment**
PCR	**Polymerase chain reaction**
PR	**Photoreceptor**
TEM	**Transmission Electron Microscopy**
UPR	**Unfolded protein response**
US	**Ultrasounds**

I. Introduction

1.Introduction

Therapies for inherited retinal degenerations took a step forward with the development and FDA approval of the gene therapy for RPE65 related Leber Congenital Amaurosis. However, the great number of genes associated with inherited retinal degeneration (IRD) and the phenotyping overlapping between them make diagnostics a difficult task. In this context, the search for therapies targeting common pathways that lead to photoreceptor death can be important to delay vision loss on patients with this type of retinal degeneration. Our laboratory, has studied thoroughly different IRD with a focus in one group of IRD called ciliopathies. The work of this thesis continues previous work in our group that have studied the possibility of modulating stress pathways in one emblematic ciliopathy, the Bardet-Biedl syndrome. The aim of this thesis is to test Magnetic Nanoparticles loaded with these compounds. We will test the potential of these nanoparticles as drug delivery systems guided with magnetic fields for drug delivery to the retina after topical application. The need to test this kind of delivery system stems from the challenge that represents the effective drug delivery to the retina due to numerous anatomical and physiological barriers that exists in the eye. We collaborated with OZ Bioscience in this project a French company partner of the Ocuther project that have been working in formulation and optimization of these nanoparticles.

1.1. Ciliopathies, a brief introduction:

The primary cilium (Figure 1) is a microtubule-based structure found in almost all vertebrate cells. It acts as an antenna for the cell receiving signals from the extracellular environment such as proteins, mechanical stimuli or light (Malicki & Johnson, 2017). The importance of these structures in the cell is highlighted by the existence of a broad group of diseases related to genetic mutations of the genes encoding for ciliary proteins. These diseases, called ciliopathies, affect a variety of tissues and organ systems due to the widespread distribution of the cilia in the body. Nonetheless, ciliopathies preferentially affect organs such as the kidney, the retina or the central nervous system. Alteration of the cilia can appear as non-syndromic (one organ only affected), such as isolated kidney diseases (nephronophtisis, polycystic kidney diseases) or isolated retinal dystrophies. On another hand, it can be syndromic, as for example Bardet-Biedl syndrome (BBS) or Joubert syndrome. It has been described that there are at least 187 genes related to 35 ciliopathies and around 241 candidate genes that could be related to ciliopathies (Reiter & Leroux, 2017).
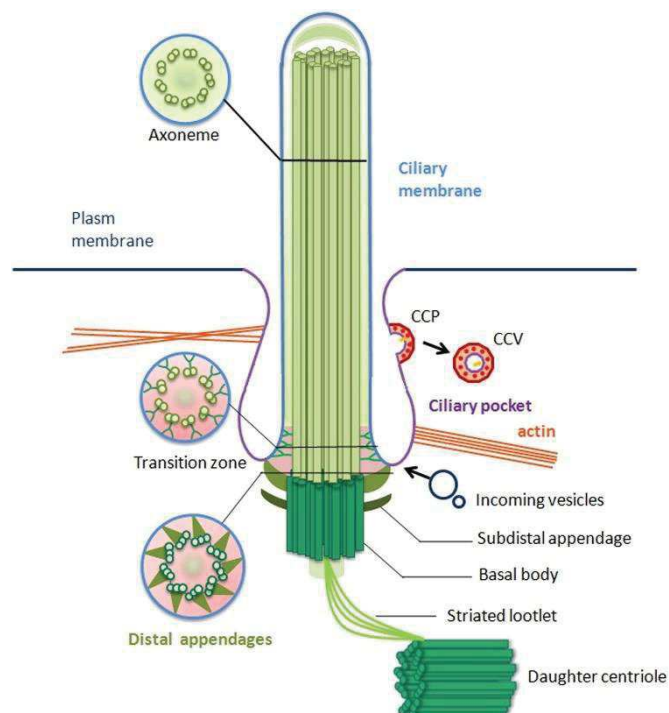
Figure 1. Structure of the primary cilium. It presents a "9+0" axoneme different from the one found in motile cilium. It presents Y-shaped bridges spawning from the transition between duplets and triplets, forming the transition zone. Mother and daughter centrioles are connected by striated lootlets. The actin network anchored in the ciliary pocket facilitates the cilia orientation. Figure from (Ke & Yang, 2014).

The photoreceptor cell (PR) is well known to be a modified cilium. Retinal degeneration linked to ciliopathy is caused by defects on the ciliary structure. The inner segment (IS), where all the biosynthesis and metabolism of the photoreceptors is carried on, is connected to the outer segment

(OS) of the PR , where the phototransduction takes place, by the connecting cilium (Figure 2) (May-Simera et al., 2017). The connecting cilium acts as a highway between both segments allowing the passage of proteins between them. One common mechanism of photoreceptor death in retinal degeneration in ciliopathies is related to the interruption of the protein circulation between both segments (Wright et al., 2010) When this circulation is interrupted the proteins that are not able to cross to the OS begin to accumulate in the endoplasmic reticulum (ER) of the IS, the protein accumulation will finally activate a stress pathway called the Unfolded Protein Response (UPR) (Ron & Walter, 2007). Once this mechanism is activated it can lead to apoptosis and induce retinal degeneration (Starr et al., 2018).
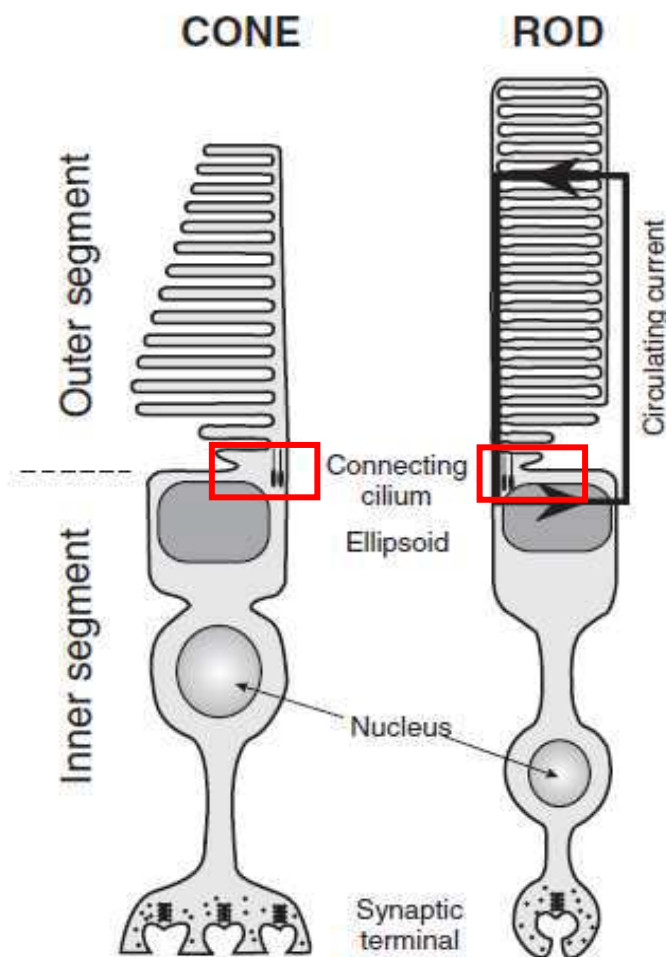
Figure 2. Photoreceptor cell structure. The connecting cilium localization is highlighted by the red rectangle. Adapted from Visual transduction from rod and cone photoreceptors (Lamb & Burns, 2004).

1.2. The Bardet-Biedl syndrome:

The prevalence of the disease depends highly on the studied population varying from an estimated prevalence of 1:13500 in isolated regions (Gouronc et al., 2020) to 1:160000 in Northern Europe (Waters & Beales, 2011). BBS is caused by up to 24 genes involved in the proper function of the primary cilia. The location of BBS proteins is variable: at the level of the basal body in the case of BBS 13, 15 and 15 or as part of the intraflagellar transport system in the case of BBS 19, 20 and 22. But in many cases more classically they are involved in the BBSome a (composed by BBS 1, 2, 4, 7, 8, 9) the formation of which is ensured by a chaperonin complex (BBS6, 10 and 12).

The mayor clinical findings in this syndrome are: an early-onset rod-cone degeneration (RP), renal dysfunction , obesity, polydactyly, learning difficulties and genital malformation (Forsythe et al., 2018). Diagnosis for this disease is based in the presence of four of these clinical symptoms or the presence of three of these symptoms along with two other minor signs such as speech or developmental delay, dental abnormalities, diabetes mellitus, congenital heart disease, ataxia, anosmia or brachydactyly/syndactyly (Beales et al., 1999). As mentioned, before the impairment of circulation of proteins between the IS and OS have been proved in ciliopathies as a mechanisms for cell death (Wright et al., 2010). This has also been studied in different BBS animal models and two mechanisms related to the impairment of circulation of proteins have been shown as possible causes for apoptosis. In one case the mechanisms found was the accumulation in the OS of proteins that are not native to this portion of the cell (Datta et al., 2015). The other mechanism has been more thoroughly studied in our laboratory and is the activation of the UPR due to the accumulation of proteins in the IS (Mockel et al., 2012; Brun et al., 2019).

1.2.1. Unfolded Protein Response:

The accumulation of proteins in the ER, independently of the cause, is referred as ER stress. In order to maintain the ER functions the UPR is activated (Hetz et al., 2020). The initiation of this response involves the interaction of the Bip chaperone with three ER transmembrane enzymes (Figure 3), the inositol-requiring enzyme 1 (IRE-1), activating transcription factor 6 (ATF6) and the protein kinase R-like endoplasmic reticulum kinase (PERK) (M. Wang & Kaufman, 2016). Under stress conditions the Bip chaperon dissociates from these three enzymes in order to help in the folding of unfolded proteins accumulated in the ER. Once dissociated the three UPR enzymes are able to activate the UPR (Bertolotti et al., 2000). The UPR modifies the rate of protein synthesis in order to reduce the amount of protein accumulation. It also affects protein folding, maturation and quality control as well as

increases the elimination of misfolded proteins through autophagy and ER-associated protein degradation. (Hetz et al., 2020).
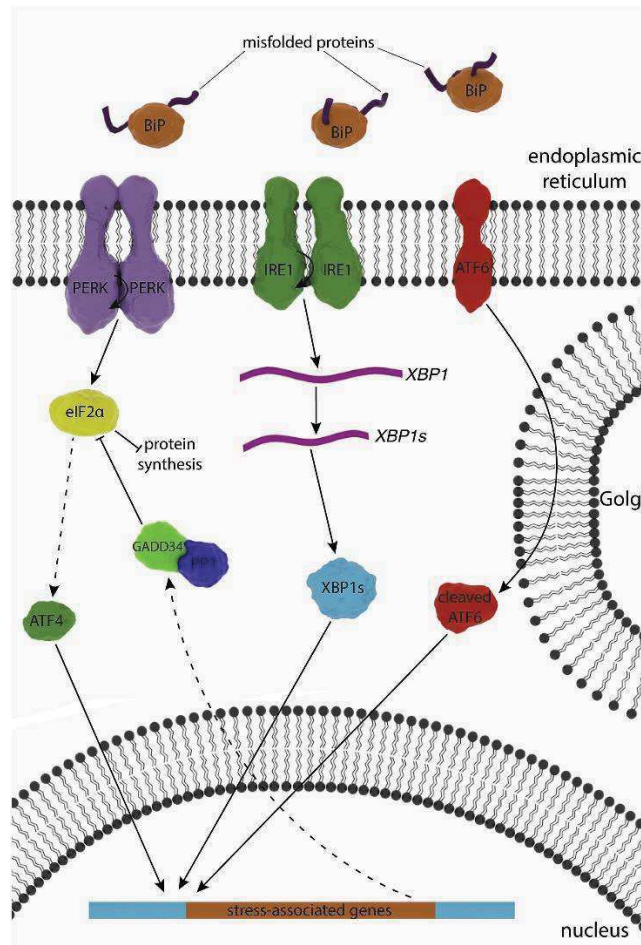
Figure 3. UPR pathway. Representation of the three branches and cascades of the UPR pathway. (Gorbatyuk et al., 2020)

1.2.2. Pharmacological Modulation of the Retinal Unfolded Protein Response in Bardet-Biedl Syndrome:

Previous work in our laboratory has shown that the modulation of the UPR that causes PR cell death in the BBS is possible (Mockel et al., 2012). This modulation was achieved using three different drugs: valproic acid (VPA), guanabenz (GBZ) and a caspase 12 inhibitor and it resulted in an increase in PR survival coupled with the preservation of light perception in the treated mice. While not treating the cause of the disease, the reduction of the apoptosis could increase the therapeutic window in these patients for the use of gene therapies by maintaining the PR cells alive. This study showed that VPA is capable to increase the concentration of the Bip chaperone while GBZ is able of increasing the levels of p-EIF2α via inhibition of the GADD34 phosphatase. Finally, the inhibition of caspase 12, specifically activated with the UPR, was achieved with a selective inhibitor. The three compounds used were able

to restore the retinal function of the *Bbs12^{-/-}* treated mice as shown using electroretinogram recordings (ERG). This was achieved by decreasing the apoptosis in the PR cells. The treatment was also able to increase the ONL layer thickness as well as decreasing the dilatation of the ER.

The work presented in this thesis continues the investigation of these compounds using novel technologies for retinal drug delivery.

1.3. Common routes for drug delivery:

In this section we will refer to the most commonly used drug delivery routes (Figure 4) for the treatment of different ocular diseases.

1.3.1. Topical application:

This is the most commonly used route for the application of drugs for the treatment of ophthalmologic diseases (Urtti, 2006). While this method is simple to use and can be auto administered it presents several disadvantages. Some patients might have problems with the instillation of the eyedrops and incorrect instillation can lead to the non-productive loss of drug and use of unnecessary additional medication (Tatham et al., 2013). On the other hand, one problem with the use of self-applied eyedrops is the lack of adherence of the patients, that also leads to a decrease in therapeutic efficiency. Peak concentration of drugs is found in the anterior chamber around 20-30 minutes after eyedrop application (Urtti et al., 1990) but most of the administered dose is cleared by aqueous humour turnover and systemic absorption of the drugs within 2 minutes after application (Davies, 2000).

1.3.2. Intravitreal injection:

Intravitreal injection (IVT) is the most commonly used method for drug delivery to the retina and the posterior chamber of the eye. IVTs are used for instance for the delivery of anti-VEGF proteins (bevacizumab, ranibizumab, aflibercept) to patients suffering from the wet form of age-related macular degeneration. These injections should be given every one or two months, but in practice the compliance is poor and the injections are given at longer intervals (Cohen et al., 2013; Holz et al., 2015). This decreases the efficacy of the AMD treatments and there is a need for longer acting IVT. Anti-VEGF proteins are highly potent compounds with large intravitreal half-lives that are relatively well tolerated at high doses, these characteristics are what make IVT delivery possible for these compounds. Smaller or more lipophilic compounds with shorter half-lives would need short intervals between injections, which would significantly increase the number of injections in the case of chronic disease. The

repeated injections could present problems related to the negative side effects of the IVT such as retinal detachment or vitreous haemorrhage (Jager et al., 2004).

1.3.3. Systemic administration:

Drug delivery to the retina from the systemic blood circulation is possible. The main disadvantage of this delivery route is the existence of the blood retinal barrier that limits greatly the access of the drugs to the retina and the anterior chamber. While it is possible for drugs to reach the ocular tissues, high concentrations are needed and systemic side effects are a common occurrence (Eljarrat-Binstock et al., 2010). Drugs that can target the central nervous system could potentially overcome the blood-retinal barrier as they are similar to the blood brain barrier (Himawan et al., 2019).

1.3.4. Subretinal injection:

This method is the preferred method for the delivery of retinal gene therapies. While the method is highly effective in delivering the compounds to the retina it also results in a transient retinal detachment due to the injection of the compounds directly in the subretinal space, which is the space between the PR and the retinal pigmented epithelium (RPE) layer (Peng et al., 2017). This retinal detachment caused by the injection might be a problem when frequent re-injections of the treatment are needed as the damage resulting from the detachment can offset the potential benefits of the treatment applied.
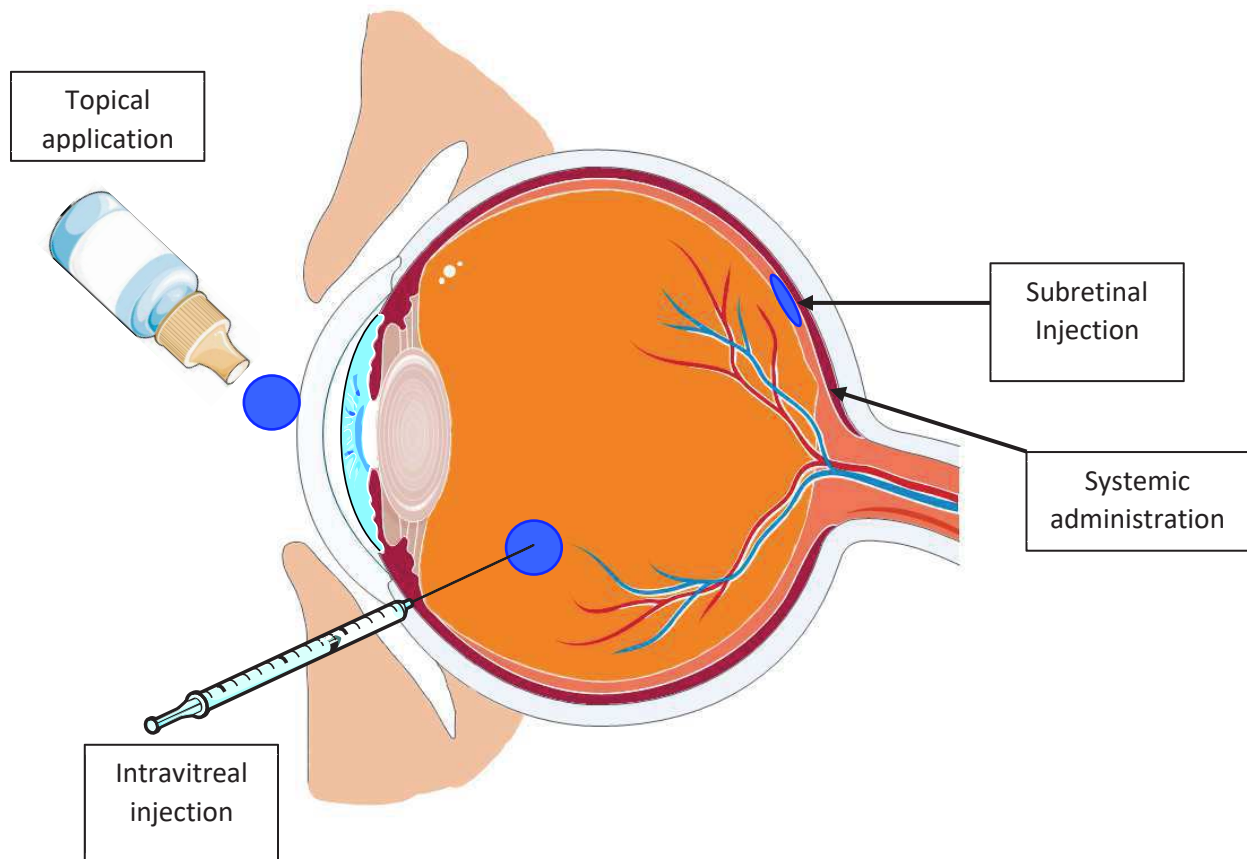
Figure 4. Representation of the eye and the most commonly used methods for drug delivery to the ocular tissues. The four most common pathways are represented on the image. This figure was drawn using the image bank of Servier Medical Art. Servier Medical Art by Servier is licensed under a Creative Commons Attribution 3.0 Unported License.

1.4. Anatomical and physiological barriers of the eye:

1.4.1. Precorneal factors

Precorneal factors are the first factors that influence the amount of drug absorbed after eyedrop application. They limit the amount of drug that is in contact with the ocular surface thus limiting the total amount of drug that can potentially penetrate the eye. Drug losses start directly after eyedrop application, a part of the drop can spill to the cheek or the lower eyelid due to poor instillation technique, high drop volume or blinking caused by the eyedrop (Singh & Ahmad, 2011; Moosa et al., 2014). Next, a major portion of the instilled eyedrop will be drained from the surface of the eye through the nasolacrimal duct, which maintains pre-corneal fluid volume at 7-10 µl while most commercial eyedrop dispensers produce eyedrops of about 25-50 µl. Drainage rate is influenced by several factors (Agrahari et al., 2016). The drainage of the drug to the nasal cavity leads to systemic absorption of the drug. In a similar manner, the drug that flows to the conjunctival sac can also be systemically absorbed

through local vasculature reducing even more the amount of drug available (Urtti, 2006). Finally, the drug that remains in contact with the ocular surface will be immediately diluted in the tear film. The tear film influences the amount of drug that can penetrate the cornea in two ways. First, the remaining drug diluted in the tear film is subjected to the tear turnover, meaning that over time, the drug will be washed away (Eljarrat-Binstock et al., 2010). Finally, it is possible for the drugs to interact with proteins present in the tear film reducing even more the amount of drug that can cross the cornea (Agrahari et al., 2016). Due to these pre-corneal factors it has been determined that up to 90% of the instilled eyedrop is cleared within 2 minutes after instillation (Davies, 2000).

1.4.2. Corneal factors

After being affected by the pre-corneal factors, instilled drugs can be absorbed through two routes. The first one is called the corneal route and the second one is the non-corneal route and is comprised of the sclera and conjunctiva. The cornea is a highly selective barrier composed of five different layers with an overall average thickness of 0.5 mm (Doughty & Zaman, 2000). Three of the layers are cellular layers (epithelium, stroma and endothelium) and the other two are interface layers (Bowman's and Descemet's membrane) (Robinson, 1993) (Figure 5). The two more important barriers of the cornea are the corneal epithelium and the corneal stroma. The corneal epithelium is the first barrier to penetration inside the eye, it contains 5-7 layers of cells connected by tight junctions with a paracellular diameter of 2 nm. In general, the corneal epithelium limits the paracellular passage of hydrophilic drugs while allowing transcellular diffusion of lipophilic drugs. On the other hand, the stroma is composed of hydrated collagen and glycosaminoglycans which act as a diffusional barrier to highly lipophilic drugs (Bucolo et al., 2012; Huang et al., 2018). This organization means the cornea acts as a barrier to most hydrophilic and lipophilic drugs. Only small molecules with an adequate lipophilicity can cross through these barriers. Finally, the corneal endothelium is a monolayer of polarized cells with specialized transport function. It allows the passage of macromolecules between the stroma and the aqueous humour (Barar et al., 2008). In the case of the endothelium, passage is limited mostly depending on the size of the molecules and not on the characteristics of the compounds. Finally, the charge of the compounds also influence permeation through the tissue. Corneal surface has a negative charge, thus positively charge molecules are able to bind to the surface and increase its permeability across the tissue (Liaw et al., 1992).

1.4.3. Conjunctiva and sclera (Non-corneal route):

Compounds that are not able to permeate the cornea and are not absorbed into the systemic circulation can in turn access the interior of the eye through the conjunctiva and sclera. This route is thus the preferred route for large molecules, proteins or hydrophilic compounds. When compared to the corneal route, uptake of drugs can be up to one order of magnitude higher (Eljarrat-Binstock et al., 2010). This differences in uptake are partially explained by the relative leakiness of the tissue when compared to the cornea. The surface area of the conjunctiva could also influence the higher uptake as its surface is up to 17 times larger than the corneal surface in humans. The conjunctiva is the tissue that covers the inside of the eyelids and the anterior surface of the eyeball. It is formed by two different layers, first, the epithelium, consisting in a 5 to 15 layers of epithelial cells connected by tight junctions acts as a permeability barrier for hydrophilic drugs (Hosoya et al., 2005). However, these tight junctions have a larger pore radius than that of the cornea with a radius of 3 nm in the bulbar portion and 4.9 nm in the palpebral portion. (characterization of paracellular and aqueous penetration routes in cornea, conjunctiva and sclera) and particles of up to 300 nm have been reported to cross the conjunctiva (Salamanca et al., 2006). The second layer that forms the conjunctiva is the stroma, composed of nerves, lymphatic and blood vessels. This layer attaches loosely to the sclera. The rich vasculature nature of this tissue means that a large amount of the administered drugs will be washed away by the systemic circulation (Ahmed & Patton, 1985). Drugs that are not washed to the systemic circulation will cross from the conjunctiva to the sclera. The composition of the sclera is mainly an extracellular matrix formed by collagen and mucopolysaccharides (S. H. Kim et al., 2007), the porous space in the collagen network varies between a diameter of 25 to 300 nm (Hämäläinen et al., 1997). It is also a poorly vascularized tissue in comparison to the conjunctiva, therefore, systemic loss is less than that of the conjunctiva. This lack of vascularization along the high surface of close to 16.3 cm^2 means that the scleral tissue is generally more permeable to solutes than the conjunctiva and cornea. The charge of the drugs also affects the passage through the sclera, in this portion positively charged compounds have a lower permeability as the matrix is negatively charged and compounds with positive charge will bind to the matrix slowing their progress. Once the drug has permeated through the sclera there are several pathways that they can follow. It can cross to the anterior chamber and be mixed with the aqueous humour or it can also permeate to the choroid and from there to the systemic circulation or to the RPE and retina (Ranta & Urtti, 2006). The choroid is a vascular tissue that supplies blood to the retina. It is composed of fenestrated capillaries with pores of up to 60-80 nm (Bill et al., 1980). It is supported by the Bruch's membrane that is an elastic membrane composed also by the basal membrane of the RPE. From the choroid, the compounds can reach the retinal tissue but first they have to cross the retinal blood barrier formed by the RPE. Passage through the choroid is also

influenced by the charge of the compounds as positively charged compounds interact with this tissue (Cheruvu & Kompella, 2006).

1.4.4. Anterior Chamber

Drugs that permeate from the corneal or the non-corneal route and reach the anterior chamber of the eye will be mixed with the aqueous humour. Usually peak drug concentration is reached around 20-30 minutes after the eyedrop administration, but due to the aforementioned barriers the concentration can be up to two orders of magnitude lower than the applied concentration (Urtti et al., 1990). Once in the anterior chamber there are two mechanisms with which drugs are eliminated, the aqueous humour turnover and blood flow from the anterior uvea. Aqueous humour is produced in the posterior chamber by the ciliary processes and then flows to the anterior chamber. The aqueous humour turnover will wash the drug from the anterior chamber independently from the characteristics of the drugs at a rate of 3 µl/min. Second, drugs can be absorbed into the venous blood flow from the uvea. This mechanism depends on the drug characteristics as it will depend on their capability to penetrate across the endothelial walls of the vessels. For this reason, clearance will be higher for lipophilic drugs than for hydrophilic drugs with a clearance rate that can be up to 20-30 µl/min. Another factor that can interfere with the movement of the compounds inside the anterior chamber is the melanin binding. In the case of the anterior chamber melanin is found in both the iris and the ciliary body, meaning that the compounds reaching the aqueous humour can bind to the melanin in these tissues and form a reservoir that is released gradually to the surrounding cells, increasing the activity time of these compounds (Urtti, 2006).

While the aforementioned factors affect drugs that reach the anterior chamber through the corneal or non-corneal route, compounds that arrive from the blood circulation have to reach a different barrier, in this case the blood-ocular barrier. It can be divided in the blood-aqueous barrier (BAB), present in the anterior chamber and the blood-retinal barrier (BRB), present in the posterior chamber. The BAB presents an endothelial and an epithelial component in the anterior chamber. The endothelial portion is formed by the vasculature of the iris and the ciliary muscle while the epithelial portion is formed by the posterior pigmented and non-pigmented epithelium of the iris. Horseradish peroxidase, with a diameter of 4 nm have been reported as not being able to escape the iris or the ciliary vessels and thus do not reach the anterior chamber from the circulation (del Amo et al., 2017). Identical results have been reported for the epithelial portion of the BAB (Raviola, 1974, 1977). The BAB not only regulates the crossing of compounds from the circulation to the anterior chamber but also regulates aqueous humour turnover, thus it influences the clearance of drugs through this pathway. The permeability of the BAB is difficult to determined separately from the permeability of the BRB. This is because drugs administered systemically crosses both the BRB and BAB and also elimination of drugs

from the vitreous can occur through both of them. We will discuss the mechanisms of elimination of drugs from the vitreous in the next section.
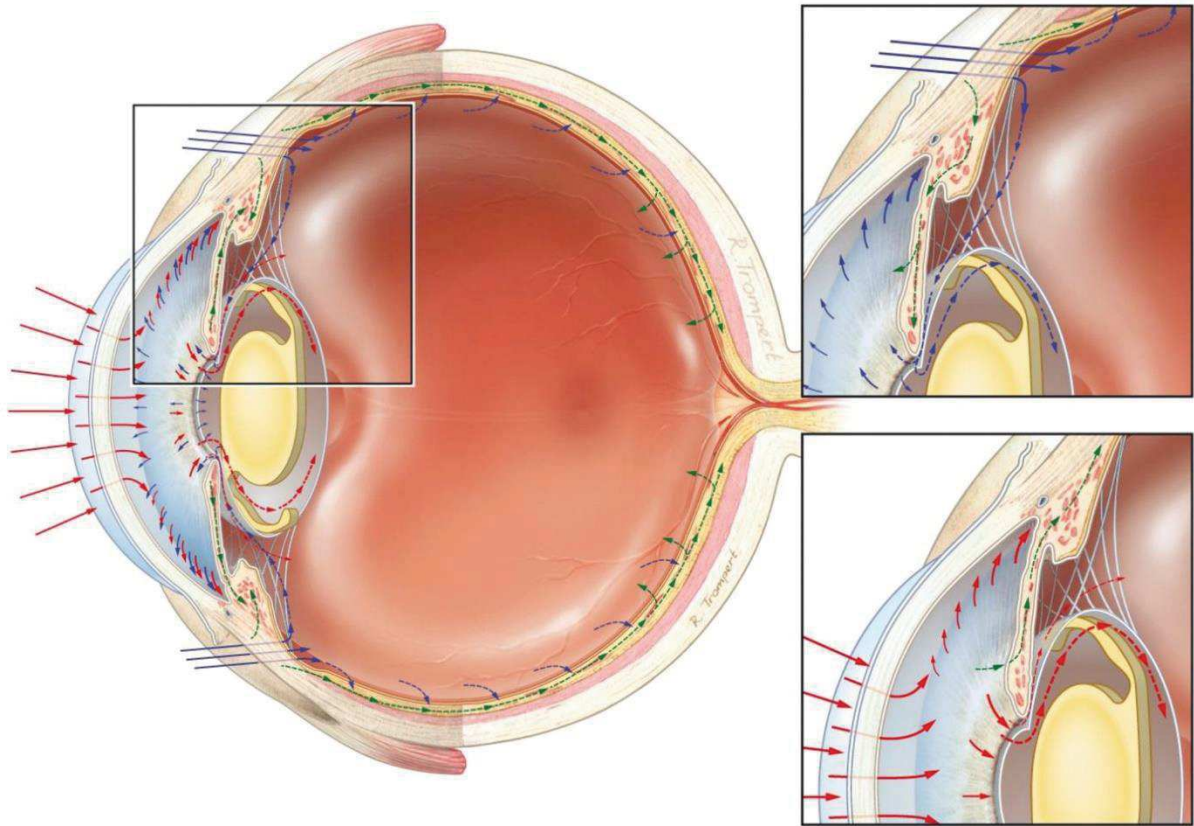
Figure 5. Ocular drug delivery routes. Red arrows show the corneal drug delivery route, through the cornea to the anterior chamber and elimination through the trabecular meshwork or iris. Blue arrows show the non-corneal drug delivery route, through the sclera and conjunctiva to the choroid, retina or the posterior chamber with further elimination through the anterior chamber. Green arrows show the possibility of compounds migrating from the anterior to the posterior chamber (as shown in the lower magnification of the corneal route.) In the upper magnification (non-corneal route) green arrows show the passage of compounds from sclera and conjunctiva to the retina and choroid. Figure from (Bertens et al., 2018).

1.4.5. Vitreous

The vitreous humour is mostly composed of collagen and hyaluronan, which gives the vitreous and overall negative charge (Le Goff & Bishop, 2008). Compounds that reach the vitreous can exit the posterior chamber via two pathways depending on the characteristic of the drug. The first pathway is available for all type of drugs that reach the vitreous and is called the anterior pathway. This route is based in the diffusion of the drugs from the vitreous to the aqueous humour. Once the drugs diffuse from the vitreous to the aqueous humour, they will be eliminated with the aqueous humour turnover through the BAB. The second pathway

depends on the capacity of the compounds to cross the blood ocular barriers. This means that this route is mostly available for small molecules with lipophilic properties and they will be eliminated through the BRB. These two mechanisms explain why the half-life of big molecules and proteins can be up to several days while small molecules stay in the vitreous for hours only.

1.4.6. Retina

Drugs can reach the retina from two sides, either from the vitreous or from the systemic circulation. Each one of these sides have to deal with different barriers that limits the amount of drug reaching the retinal tissue.

Diffusion from the vitreous to the retinal tissue is mainly limited by the inner limiting membrane. The main component is a network of collagen and glycosaminoglycans, in humans the pore size for this structure is suggested to be around 10 nm and it presents a negative net charge. This pore size allows the crossing of small molecules and of biologics below a molecular weight (MW) of 100 kDa through the vitreous (Jackson et al., 2003).

Finally, the blood retinal barrier limits the access of compounds from the circulation to the retina. This barrier present two different components, the inner blood ocular barrier formed by the retinal capillaries and the outer blood retinal barrier formed by the RPE. The permeability of the retinal capillaries is hard to assess (del Amo et al., 2017), small molecules such as glycerol have been reported to be able to permeate these capillaries (Thornit et al., 2010). These compounds present a size smaller than the typical size of tight junctions (2 nm). The second component of the blood retinal barrier is the RPE, a cellular monolayer found between the choroid and the photoreceptors with important functions in the homeostasis of the neural retina. Contrary to what was shown in the retinal capillaries, glycerol was not shown to cross the RPE in vivo in monkeys (Smith & Rudt, 1975). Overall, the RPE acts as a barrier mostly for hydrophilic and larger molecules while allowing the passage of small lipophilic molecules (Pitkänen et al., 2005).

1.5. Overcoming the ocular barriers

1.5.1. Physical forces to overcome the ocular drug delivery barriers:

1.5.1.1. Electrical fields:

Electrical forces have been studied in order to increase the permeation of certain barriers to different compounds, in this case we can differentiate between two methods, one is called iontophoresis and the other one is called electroporation. The approaches using iontophoresis use low intensity electrical currents while the approaches using electroporation use relatively high intensity electrical fields with a short pulse duration (Banga et al., 1999).

1.5.1.2. Iontophoresis:

The application of an electrical current increases the permeability of the compounds due to electrorepulsion (affecting only charged compounds) and electroosmosis (affects both charged compounds and compounds with neutral charge) (Guy et al., 2000).The amount of drug delivered is dependent on the applied current, the duration of the application and the surface area contacted (Kalia et al., 2004). The application of the electrical current produces a convective solvent flow due to the voltage difference imposed across charged membranes (Marro et al., 2001). How the compounds move under the influence of the electrical current depends both on their size and charge as well as on the electrical features of the membrane. Small molecules move mainly due to electrorepulsion (Huang et al., 2018), while on the other hand the movement of macromolecules depend on the charge to MW ratio. For example, negatively charged compounds with a low charge to MW ratio seem to move primarily due to electroosmosis. On the other hand, negative molecules with high charge to MW ratio seem to move mainly due to electrorepulsion (Chopra et al., 2010). This approach has been extensively studied for both transcorneal and transscleral drug delivery (Huang et al., 2018). One device developed for ocular iontophoresis is the EyeGate® II. This system has already been tested in humans, for example, for the control of post cataract operation inflammation (Wirostko et al., 2017), it has also been tested in anterior uveitis patients (M. A. Patane et al., 2010), patients with dry eye disease (Michael A. Patane et al., 2011) and in scleritis patients (O'Neil et al., 2018).

1.5.1.3. Electroporation:

In the case of electroporation, the increase in the permeation of the drugs is due to a direct effect of the electrical current on the plasma membrane of the cells (Neumann & Rosenheck, 1972). The electrical current induces the formation of pores in the membranes resulting in the diffusion of the compounds. I*n silico* simulations have been used in order to understand the mechanisms of pore formation in the cell membranes (Tieleman, 2004). Studies using this method have been mainly done in order to increase gene therapy delivery. Enhanced gene therapy has been observed in neonatal mouse retina (T. Matsuda & Cepko, 2004; Takahiko Matsuda & Cepko, 2007; de Melo & Blackshaw, 2018), the cornea (Hao et al., 2009) and the suprachoroidal space (Touchard et al., 2012).

1.5.1.4. Sonophoresis:

Sonophoresis is done with the use of ultrasounds (US), which involves the use of frequencies higher than 20 kHz. There are several mechanisms through which US enhance the permeability of the biological barriers. These mechanisms can be divided into thermal and non-thermal. Nonetheless, the exact contribution of each mechanism to this increase in permeability remains undetermined (Lentacker et al., 2014). However, cavitation is usually considered the predominant mechanism that enhances the permeability of the biological membranes (Mitragotri et al., 1995).Sonophoresis has been studied for the enhancement of drugs both through the sclera and to the posterior chamber. For transscleral drug delivery sonophoresis have been used in combination with injected microbubbles as a more efficient approach for drug delivery, mostly for gene delivery. One example was the increase of transfection efficacy of pEGFP-N2, a fluorescent plasmid injected in the rabbit cornea (Sonoda et al., 2006). Focused ultrasounds have been shown to be able to increase delivery of systemically applied drugs to the retina. Injection of microbubbles and delivery of ultrasounds through the cornea was able to briefly disrupt the blood retinal barrier increasing the amount of MRI contrast observed in the vitreous humour (J. Park et al., 2012).

1.5.1.5. Microneedles:

Conventionally, hypodermic needles have been used for delivery of intraocular therapies. As an alternative to f hypodermic needles, microneedles (MN) which have dimensions in the range of a few micrometres up to 200 μm can be used. Classification of the MN depends on the characteristic of the MN and how they deliver the compounds, mainly 3 types of MN have been studied for ocular drug delivery. The first one is solid MN coated with the compounds, in this case, the MN pierces the tissue allowing the coating to dissolve immediately after. The needle will create a small channel where the

coating will be dissolved increasing local delivery (Jiang et al., 2007). The second type of MN studied for ocular drug delivery are hollow MN, the MN pricks the tissue and then the compounds stored in the hollow space of the needle is released (Gardeniers et al., 2003). Finally, dissolving MN have been developed, they are made with biodegradable polymers with drugs encapsulated within their matrix. Since degradation of the MN is needed this type of MN is used for sustained delivery of compounds over time (J.-H. Park et al., 2005). MN have already been studied for the delivery of drugs to the cornea (Y. C. Kim et al., 2014), sclera (Thakur et al., 2014) and suprachoroidal space (S. R. Patel et al., 2011).

1.5.2. Advances in drug delivery systems

1.5.2.1. Punctum plugs:

The principle behind punctum plugs is simple, a biocompatible device is inserted in the tear duct, blocking tear drainage. In addition to blocking tear drainage, these plugs can also be formulated in order to act as a controlled drug delivery system. This is the case, for example of travoprost (OTX-TP) and dexamethasome (OTX-DP) containing punctum plugs. Both have completed phase III clinical trials for glaucoma (NCT02914509) in the case of OTX-TP and for chronic allergic conjunctivitis and inflammation post cataract surgery in the case of OTX-DP (NCT02988882, NCT02736175).

1.5.2.2. Implants:

Another option of controlled drug delivery to the eye for prolonged periods is the use of implants. These implants can be inserted in different portion of the eyes such as the sclera or the conjunctival sac. One example of implants developed for ocular drug delivery is the LX201, a silicone based episcleral implant for delivery of Cyclosporine-A that has been studied to prevent corneal graft rejection (NCT00447642). Other implants used for drug delivery to the anterior chamber are Lacrisert® and DSP-Visulex. Lacrisert® is a conjunctival sac implant that has been used in patients with dry eye disease with some side effects such as foreign body sensation or blurry vision. DSP-Visulex have completed phase II clinical trials for the treatment of anterior uveitis (NCT02914509), it is a conjunctival implant containing dexamethasone.

1.5.2.3. Emulsions:

Emulsions are composed of two immiscible phases. Emulsions can be divided roughly in two types, water in oil emulsions or oil in water emulsions. Usually oil in water emulsions are preferred as they are better tolerated and produce less ocular irritation (Gote et al., 2019).This type of delivery system present high drug loading capacities, high bioavailability and biocompatibility (Y. Wang et al., 2018). One example of commercially available emulsion is Restasis® an oil in water emulsion of cyclosporine A, this was the first FDA approved treatment for dry eye disease (Ames & Galor, 2015). Durezol® is an emulsion of an anti-inflammatory corticosteroid, difluprednate, that has been studied for the management of postoperative ocular inflammation and pain (Korenfeld et al., 2009).

1.5.2.4. In situ gelling systems:

In situ gelling systems have been developed in order to try and improve the retention time of the drugs on the ocular tissues. Depending on the monomers and crosslinkers used in the formulation of the gels it is possible to formulate stimuli-responsive gels such as gels that either degrade or form depending on pH, light or temperature stimuli (L. Lim et al., 2014). Gel systems have been studied for different ophthalmic applications such as vitreous substitutes or intraocular lenses formulation (Cooper & Yang, 2019). There is one clinical trial using hydrogels for improvement of delivery of Cyclosporine A in the form of eyedrops for dry eye disease (NCT03676335). Moreover, several hydrogels are commercially available and several patents have been filled for the use of this type of delivery system (Y. Wu et al., 2019).

1.5.2.5. Liposomes:

Liposome are vesicles formed by an aqueous core and a lipophilic bilayer. This structure allows for the encapsulation of both hydrophilic and hydrophobic drugs. In the formulation of these vesicles the bilayer is usually composed of phospholipids similar to the ones present on the cell membrane (Agarwal et al., 2016). Some of the approaches using liposomes include eyedrops for the treatment of dry eye disease. One example is the liposome formulation of vitamin A palmitate and vitamin E, Lacrisek®. This eyedrop have already been tested in dry eye patients (Meng et al., 2019) with better results than the non-liposomal formulation of PEG and hyaluronic acid based aqueous formulation of vitamin B12, Rebalance®. The major advantage of the liposomal formulation being the capacity of decreasing tear film osmolarity and increasing tear film stability (Garrigue et al., 2017). Liposome have also been studied for the treatment of retinal diseases, being one example, the use of topical applied

liposomes containing bevacizumab. The study from Davis et al, have shown the presence of bevacizumab on the retinal tissue of rats and rabbit after topical application of their annexin A5-conjugated liposomes (B. M. Davis et al., 2014). GSH-conjugated, PEGylated liposomes carrying a cyclic nucleotide analogue CN03 have been shown to be able to produce photoreceptor protection after systemic delivery (Vighi et al., 2018).

1.6. Magnetic Nanoparticles:

Nanoparticles are characterized by a size of approximately 100 nm, high surface-area-to-volume ratio offering interesting possibilities for example, for drug delivery. In this regard, magnetic nanoparticles (MNPs) are of special interest due to the fact that they can be manipulated using magnetic fields (Cardoso et al., 2018), they present no immunogenicity and its surface can be modified in several ways leading to high biocompatibility (Guo et al., 2018). All these characteristics have led to the development of MNPs for several uses such as imaging or drug delivery systems with different cores and coatings studied for a large amount of applications.

One of the fields where MNPs have been more widely studied is their use as contrast agents for imaging where they are replacing traditional contrast agents such as gadolinium that had poor body clearance (Cardoso et al., 2018). MNPs present several characteristics that make them great tools as contrast agents, their surface can be tuned to control their circulation or retention times within the body. The concentration of imaging agent can also be controlled during the synthesis of the MNPs. Finally, iron-based MNPs presents exclusive magnetization properties that result in enhanced contrast under MRI at very low concentrations (Fatima & Kim, 2018). However, in some cases such as haemorrhages where the iron from the blood creates artifacts on the image the use of MNPs is less optimal (K. Wu et al., 2019). Nonetheless, further functionalization of the MNPs allows for a high target specificity, allowing specific imaging of tumours such as gliomas. MNPs conjugated with chlorotoxin have been shown to present a high specificity for these tumours (Sun et al., 2008), making them great tools for targeted imaging. While mostly being studied as contrast agents for MRI there have been studies that have also studied the potential of MNPs for multimodal imaging (Reguera et al., 2017), this is the combination of two imaging techniques, for example MRI and computed tomography. MNPs have been studied for use in combinations of MRI+computed tomography (Naha et al., 2014) or MRI+positron emission (Evertsson et al., 2017).

The characteristics of the MNPs have also drawn the attention as potential tools in oncology. MNPs have been used either for hyperthermia treatments, drug delivery or as diagnostic tools (Zhang et al.,

2018). As we have mentioned before the use of MRI and functionalized MNPs as contrast agents are a potent tool for targeted imaging of tissues. Moreover, many treatments have been shown the efficacy of the use of MNPs as drug delivery system in cancer, these includes chemotherapy agents (Arya et al., 2011; Barraud et al., 2005) or even gene therapy (Han et al., 2010). The possibility of improving the delivery efficacy of chemotherapy agents is very appealing as it would lead to a decrease in the doses needed and thus a decrease in the negative side effects. The possibility of moving the MNPs with the use of external magnetic fields have led to the development of MNPs for hyperthermia in cancer. In this case the MNPs are injected locally to the tumour and subjected to an alternate current magnetic field that will be converted in heat through several mechanisms depending on the characteristics of the MNPs (Hedayatnasab et al., 2017). This approach has the advantage of being localized, however, the efficiency of this method is still not optimal and several approaches are being studied in order to further understand and improve the use of MNPs for hypothermia (Cardoso et al., 2018; Zhang et al., 2018).

While different types of MNPs have been designed and tested for several purposes not so many of them have made it to the clinical use. Most of the MNPs approved for clinical use are MRI agents and some are used for the intravenous iron replacement treatment of anaemia in patients with chronic kidney disease (Lu et al., 2010). In our work we are interested in the potential of MNPs for targeted drug delivery. The main factors affecting MNPs for drug delivery are the size and physiochemical impact of the MNPs, their biocompatibility, strength of the magnetic field needed, target distance or vascular blood supply (Mirza et al., 2020).

1.6.1. Magnetic nanoparticles for ocular use:

The advances in nanotechnology and magnetic nanoparticles have also been carried over to the field of ophthalmology where the potential uses of magnetic nanoparticles have been also studied for different applications. We will first discuss studies that try to observe basic parameters of the MNPs such as toxicity or distribution and afterwards we will also discuss studies that aim at specific uses of the MNPs such as cell transplant or the use of MNPs as delivery system for molecules.

1.6.1.1. Toxicity of magnetic nanoparticles:

The possible toxicity of the MNPs is a concern that has been studied by many groups that try to develop them as a drug delivery system. Since the term nanoparticle only classifies by size, there are several different types of cores and coatings that have been studied in order to assess their toxicity. Most

studies assess the toxicity of their nanoparticles while also testing their distribution or other characteristics, but some studies are also dedicated to the toxicity of MNPs. Raju et al studied dextran coated 50 nm MNPs and 4μm polystyrene coated MNPs (Raju et al., 2011). In this study both injections in the anterior chamber and IVT were studied. Neither of these types of injection was shown to increase the intraocular pressure for a period of up 5 weeks, nonetheless, no measure was taken after injection of the MNPs. They did not observe signs of glial activation after the injections but the 4μm particles produced a decrease in the number of corneal endothelial cells after injection in the anterior chamber. On the other hand, 50 nm particles did not alter at any point the ocular histology. Finally, no significant decrease was observed in the electroretinogram of the injected mice when compared with the untreated animals. As commented before, most of the studies carried on with nanoparticles also assess the possible toxicity of particles used. In most of the case no toxic effect is observed while in one study signs such as a slight infiltration of ED-1 immunopositive activated microglia/macrophages was observed but no further retinal inflammation or phagocytosis of MNPs was reported.

1.6.1.2. Distribution of magnetic nanoparticles:

Being able to assess the movement of the particles is essential to know if they are able to reach the target, this could be even more important when the attempts of directing the treatment is done with an external force such as a magnet placed outside the targeted tissue. Thus, the distribution of the MNPs have been studied using several methods (Table 1) from magnetic resonance imaging (MRI) to microscopy or radioactive compounds.

Dengler et al. used cobalt nanoparticles with technetium (Dengler et al., 2010). They administered the nanoparticles systemically and applied a magnet positioned in front of the eyes of the mice for 30 minutes, at this time no successful delivery of MNPs through the vasculature of the eye had been reported. Using the radioactive marker, they observed high signal in liver, lung and spleen. Nonetheless, they also observed a high concentration of nanoparticles in the ocular tissues but there is no analysis of the location of the nanoparticles within the tissues.

One tool that can potentially be used to examinate the nanoparticles inside the ocular tissue is MRI. One of these studies by Raju et al. studied Iron oxide particles of two different types, one with a size of 50 nm and dextran coating and another of 4 μm and a polystyrene coating (Raju et al., 2012). Both types of nanoparticles were observed 1 hour after IVT but the 50 nm particles were not observed when full MRI scanning was performed. To be able to observe the 50 nm particles the eyes had to be enucleated and imaged alone. Finally, the 4 μm were observed by MRI at 5 weeks post-injection. Harrison et al. used a partial optic nerve injury model to analyse the biodistribution of their multimodal

nanoparticles (Harrison et al., 2012). The nanoparticles were formulated with poly (glycidyl methacrylate) (PGMA) and contained iron oxide and rhodamine B both for the distribution analysis. These particles were injected in a partial transection of the optic nerve and a decrease over time of the signal in MRI was observed. With fluorescence the particles were also observed in the injection site but 3 days after they could be observed also close to the injury site. Some particles were also observed in the retinal ganglion cells possibly due to retrograde transport of the nanoparticles along the axons. They could also observe a slight increase in infiltration of ED-1 immuno positive activated microglia/macrophages but there was not a significant phagocytosis of the particles. Finally, Tzameret et al also studied the distribution of magnetic nanoparticles, in this case after suprachoroidal injection (Tzameret et al., 2019). With MRI the nanoparticles were observed in the back of the eye up to 30 weeks following injection. However, MRI cannot differentiate between the different ocular tissues, thus it is not always possible to differentiate if the MNPs are in the retina or only on the posterior chamber with this method. The localization in the retinal tissue was assessed with Prussian blue and the nanoparticles were found in the choroid, sclera and in the debris zone, a characteristic zone of the animal model they used, 2 hours after injection. It is interesting to note that particles were also found in the photoreceptor outer nuclear layer at 1-week post injection whereas they did not observe any nanoparticle in this layer before. However, 12 weeks after injection no nanoparticle could be observed in any retinal layer. Finally, no changes on retinal structure or retinal function were observed in this study as there were no retinal thinning nor ERG differences between the injected and non-injected mice. MRI have also been used to follow injected cells photoreceptor precursor cells (Ma et al., 2019) in this study the uptake of 100 nm magnetite particles with dextran coating had no effect in the proliferation or the differentiation capacity of the photoreceptor cell precursors used. These particles were then injected in the subretinal space of College of Surgeons rats. Using MRI, they were able to track the injected cells for up to 12 weeks. The cells labelled with the magnetic nanoparticles were able to delay the loss in retinal function as shown in ERG, the ERG response was maintained at the same levels than the animals injected with non-labelled photoreceptors.

The distribution of nanoparticles has also been studied in non-rodent animal models. The nanoparticles were observed after injection in *xenopus laevis* embryos (Giannaccini et al., 2014). The injection of the nanoparticles did not affect the development of the ocular tissues suggesting that these nanoparticles are not toxic. Nanoparticles were observed to localize mainly to the posterior segment independently of the injection site. The nanoparticles seem to migrate to the RPE in this model, with most of the nanoparticles observed in this portion of the eye as soon as 6 hours after the injection. Moreover, this study proved that the superficial charge of the nanoparticles used had no effect on their migration. Finally, they also studied if the migration of the nanoparticles towards the

RPE could be observed in other species, thus nanoparticles were injected in zebrafish embryos and the same localization of the nanoparticles was observed one day after the injection. The same group studied the possibility of functionalizing the nanoparticles in order to target the choroid after injection (Giannaccini et al., 2017). In this case Carboxylic acid-stabilised iron oxide nanoparticles were covalently linked (peptide bond) to recombinant VEGF and injected in zebrafish embryos. One day after injection these functionalized particles were able to cross the previously shown RPE location towards the developing choroid. Moreover, the functionalization with the recombinant VEGF did not seem to cause any angiogenic effect in the eye of the injected fishes.

Model used	MNPs used	Magnet application	Year	References
C57Bl/6 mice	Cobalt nanoparticles (Turbobeads®) with Technetium 99	Yes	2010	(Dengler et al., 2010)
Sprague Dawley rat	Iron oxide particles: 50 nm dextran coated 4μm polystyrene coated	No	2012	(Raju et al., 2012)
Female PVG Hooded rats	PGMA-Iron oxide nanoparticles with PEI modification on the surface	No	2012	(Harrison et al., 2012)
Xenopus laevis and zebrafish	Magnetite nanoparticles of 252 nm	No	2014	(Giannaccini et al., 2014)
Zebrafish	Carboxylic acid-stabilised iron oxide nanoparticles covalently linked to VEGF or PLL	No	2017	(Giannaccini et al., 2017)
Royal College of Surgeons rat model	Iron oxide core coated with Human serum albumin with hydrodynamic diameter 43 ± 5 nm	No	2019	(Tzameret et al., 2019)
Royal College of Surgeons	Magnetite nanoparticles 100 nm Ø with dextran coating	No	2019	(Ma et al., 2019)

Table 1. Studies dedicated to the analysis of the distribution of MNPs.

1.6.1.3. Magnetic nanoparticles in cell transplants:

The use of MNPs has been proposed to aid in cell transplant on the ocular tissues. In this case two different uses for MNPs have been studied, one is the marking of MNPs to aid in cell tracking and the other one is the use of MNPs for targeted delivery of the cells. The results in the different studies indicates that the use of magnetic field is indeed effective in the targeting of the transplanted cells to the desired tissue with no serious adverse effects observed in the different type of cells functionalized with the different nanoparticles. Studies have been carried mainly for four different groups of cells: corneal endothelium cells, mesenchymal stem cells, PR and RPE cells (Table 2).

Two studies have attempted to use MNPs to improve the delivery of mesenchymal stem cells (MSC) for different uses, one for targeting the retina and another one for targeting the trabecular meshwork. Yanai et al studied the possibility of guiding magnetized MSC to the retina either after intravitreal injection and after systemic administration (Yanai et al., 2012). They studied the magnetizing capacity of two different MNPs, one coated with dextran sulphate and one coated with starch, their results suggested that the MNPs coated with starch were better both in term of magnetizing the MSC and in terms of cell survival after incubation with this type of MNPs. This study also showed that the use of a magnet external to the eye could affect the localization of the magnetized MSC as they localized them in a circle corresponding to the perimeter of the magnet. After systemic administration of the MSC they could also observe marked cells in both the outer and inner retina, while cells treated with intravitreal injection without the magnet showed only marking in the inner retina. Moreover, systemic administration of the magnetized MSC lead to an increase of hepatocyte growing factor (HGF) and IL-10 in the retinas of the mice treated with the magnet when compared with the mice where systemic administration of the MSC was done without the use of magnetic fields, showing that the use of magnetic fields could enhance the anti-inflammatory effects of treatment with MSC. The study by Snider et al. showed the use of magnetized of MSC targeting for the treatment of glaucoma as the trabecular meshwork presents reduced cellularity in glaucoma patients (Snider et al., 2018). In this case using Prussian blue cells were magnetized nanocubes of ither 20 or 200 nm. Higher concentrations of iron were needed with the 20 nm particles in order to obtain similar cell concentration at the site of the magnet. The steering of the nanoparticles can be seen as fast as 15 minutes after injection with similar results in cell concentration at times up to 60 minutes. Moreover, the conjugation of MSC and magnetic nanoparticles did not affect cell survival and the multipotency of these cells was also maintained after magnetization.

Corneal endothelial cells losses the capacity to proliferate in a mature state (Joyce, 2003) therefore therapies using cell transplantation coupled with the possibility of directing them with MNPs have attracted the attention of several research groups. Internalization of MNPs does not affect the

functions of the rabbit cultured endothelial cells (Bi et al., 2013) in this case they used iron core MNPs coated with dextran, showing no effect of the MNPs in cell adhesion, cell morphology or proliferation. This study also proved that the internalization of the MNPs did not affected the pump function of these cells or the expression of markers such as ZO-1, Ki-67 and nestin. Mimura et al. studied the possibility of using magnetized corneal endothelial cells for targeted delivery to the cornea (Mimura et al., 2005). They used cultured endothelial cells obtained from rabbit corneas and magnetized them for injection in the anterior chamber. In this case they placed a magnet in the eyelid of the injected eyes in order to steer the cells. The study lasted for 12 months; at the end of this period they could observe that the animals treated with the magnetized cells presented transplanted cells in the central cornea. Several positive factors were observed in the animals treated with the magnetized cells when compared to their control groups such as the lack of corneal opacities, lesser corneal oedema and the presence of transplanted cells in the central cornea. Other studies have studied the possibility of functionalizing human corneal epithelium cells in order to use magnetic nanoparticles for aiding in transplanting these cells. Patel et al. tested three types of MNPs none of the types used reduced cell viability or decreased light transmission through the cells in a statistically significant manner (S. V. Patel et al., 2009). They were able to show that the donor cells were only found in the corneal stroma of the human anterior segment perfusion organ culture model when a magnet was used for the experiment. Other study done with human corneal epithelium tested nanoparticles of 50 nm of diameter (Moysidis et al., 2015), the internalization of these nanoparticles did not affect the viability of the cells nor the expression of several markers such as ZO1 or ATP1A1. They tested *in vitro* the mobility of the nanoparticles and could assess that the use of the magnet increased the density of the cells present in the surface of a hydrogel lens model. Finally, human corneal endothelial cells have been also tested for delivery to the rabbit cornea (Xia et al., 2019) no effect of the internalization of the MNPs on the viability and function of the cells was observed. In this study they were able to observe that the animals treated with magnetic cells presented a clearer and less inflamed cornea. It is also possible that the magnetic cells prevent excess fibrous deposition in the model used for this study where Descemet membrane was stripped. The use of the magnet in this study prevented the accumulation of cells in other areas than the cornea such as the iris.

The possibility of combining MNPs with cells has also been studied for the delivery of retinal cells such as the photoreceptors and RPE. RPE cells showed significant toxicity when exposed to particles of a diameter of 15 nm (*Feraheme* particles) when conjugated with either Heparin or protamine (Grottone et al., 2014). In this study the non-conjugated form of these particles was not internalized by the cells and thus presented no effect on cell movement as opposed to the other types of nanoparticle tested. Another study using ARPE-19 cells (Ito et al., 2005) used liposomes using magnetite at their core. In

I. Introduction

this case the magnetic liposomes were then internalized by the ARP-19 cells. They showed that uptake of the iron particles did not have an effect on the cell proliferation. In this study the use of the magnet was studied in order to cultivate multi-layered sheets of RPE, their results show that with the use of the magnet the ARPE-19 cells were able to form a sheet that was able later to be transferred.

Model used	MNPs used	Cell type used	Magnet application	Year	References
New Zealand White rabbit	Spherical iron powder (Cosmo Bio, Tokyo, Japan)	Corneal endothelium cells	Yes	2005	(Mimura et al., 2005)
ARPE-19 cell culture	Magnetite core 10 nm	RPE cells	Yes	2005	(Ito et al., 2005)
Human anterior segment perfusion organ culture model	Magnetite core nanoparticles of 300 and 900 nm Ø Iron oxide nanoparticles of 100 nm Ø	Corneal endothelial cells	Yes	2009	(S. V. Patel et al., 2009)
S334ter-4 rats	FluidMAG-DXS (coated with dextran sulfate) and fluidMAG-D (coated with starch)	Mesenchymal stem cells	Yes	2012	(Yanai et al., 2012)
Rabbit corneal endothelial cells	Iron oxide core 50 nm of size with dextran coating	Corneal endothelial cells	No	2013	(Bi et al., 2013)
ARPE-19 cells	Iron oxide core 300 nm Ø with silicone coating Iron oxide core 100 nm Ø with lipid coating	RPE cells	Yes	2014	(Grottone et al., 2014)

	100 nm Ø nanoparticle with dextran coating 15 nm Ø nanoparticle with carboxymethylether coating					
Human corneal endothelial cells	MACS MicroBeads functionalized with Rat anti-mouse IgG1	Corneal endothelial cells	Yes	2015	(Moysidis et al., 2015)
Porcine perfused *ex vivo* anterior chambers	20 and 200 nm iron oxide nanoparticles	Mesenchymal stem cells	Yes	2018	(Snider et al., 2018)
New Zealand White rabbits	50 nm nanoparticles	Corneal endothelial cells	Yes	2019	(Xia et al., 2019)

Table 2. Studies dedicated to the assessment of the potential of MNPs for improvement of ocular cell transplant.

1.6.1.4. Magnetic nanoparticles as drug delivery systems:

Another important study used for MNPs are delivery systems (Table 3). The possibility of steering the particles using magnetic fields are an interesting characteristic for the delivery of compounds to the ocular tissue. It is interesting to note that up to this date no MNPs for non-invasive, injection-free delivery to the ocular tissues have been developed (Zahn et al., 2020).

Gene therapy is one of the fields where the potential of MNPs as delivery system have been studied. The study of Prow et al. tested MNPs and non-magnetic particles for gene delivery using either intravitreal or subretinal injection (Prow et al., 2008). The MNPs used in this study are coated with streptavidin and had also biotin-labelled transcriptionally active PCR products. New Zealand white rabbits were used for intravitreal injection and Dutch Belted rabbits were used for subretinal injections; in both cases the animals were examined 7 days after the injections. The results for the intravitreal injection showed no inflammatory response elicited by the injection of the MNPs and no gross anatomical changes after 7 days. The MNPs were the least toxic particles used in this study but some vacuoles were observed in the RPE of the animals treated with MNPs. Intravitreal injection

showed the MNPs near the vessels in the surface of the retina while the subretinal injection group presented the MNPs mostly in the RPE layer. As for the transfection capacities of the MNPs it was observed that most of the transfected cells were RPE or possibly phagocytic cells existing in the vitreous (for the intravitreal injection group), it is noteworthy that this study was carried on without the application of an external magnetic field.

Other studies have attempted to use the MNPs as drug delivery systems using different methods. The study from Mousavikhamene et al. tested the use of MNPs as drug delivery system for compounds present in a simulated periocular space for transscleral drug delivery (Mousavikhamene et al., 2017). Human scleral tissue was used in a two-chamber model with the scleral tissue placed as a membrane between the two chambers This model simulated the blood flow by replacing the fluid present in the donor chamber. In this study they used iron oxide MNPs were loaded with diclofenac sodium. For this study the same iron core was coated using different proportions of surfactant and polymers, resulting in particles with ranges varying from 60 nm to 640 nm. Two of the particles were used in order to analyse the transscleral drug permeability, in this case the size of the particle was roughly 60 and 417 nm. The presence of the magnet increased the passage of nanoparticles between the two chambers and across the scleral tissue but the effect was more prominent for the smaller particle of 60 nm. Without the magnet the smaller particles were cleared more easily from the donor chamber than the larger particles. Other studies have attempted to use the MNPs as drug delivery systems for the treatment of retinal diseases. This was done as MNPs are able to localize to the retina, mainly the RPE, in an independent manner after IVT. In one of these studies neurotrophins were loaded in 50 nm MNPs (Giannaccini et al., 2018) . The loading of the neurotrophins on the nanoparticles showed that, not only they maintained their functions but they were also more stable than the free factors. The conjugated MNPs were able to protect the retina from oxidative stress induced damage as shown by the reduction of the apoptosis observed in the inner nuclear layer and the ganglion cell layer of the animals that were injected with the conjugated MNPs. It is important to note that treatment with the free neurotrophins was not able to protect the retina from ROS damage. Finally, the use of MNPs have also been studied for the treatment of diabetic retinopathy. Amato et al. published preliminary data (Amato et al., 2018) that was continued in another study (Amato et al., 2020) for the study of magnetite nanoparticles with a size of 50 nm functionalized with somatostatin analogue octreotide were used. The used of the MNPs showed no alteration of the retinal morphology in retinal explants treated with MNPs only. The use of MNPs shows to improve the effect of the compounds use as the protective effect could be observed when the concentrations used on the retinal explants were of 0.001 μM when the compound alone had the lower significant effect at 0.01 μM. This study also analysed the *in vivo* localization of the particles (in two *Balb/c* mice). In this case they observed the

same distributions as other studies where the MNPs were localized mostly in the outer retina/RPE layer 24 hours after the injection. However, it is interesting to note that 5 days after the injection they could also observe the MNPs in both the ganglion cell layer and the inner nuclear layer, which was not observed in previous studies. These observations highlight the need of more studies to better understand the movement of the particles in the ocular tissues.

Model used	MNPs used	Application	Magnet application	Year	Reference
New Zealand white and Dutch Belted rabbits	Streptavidin coated magnetic nanoparticles with Biotin-labeled transcriptionally active PCR products	Gene therapy	No	2008	(Prow et al., 2008)
Human scleral tissue	Iron oxide nanoparticles	Transcleral drug delivery	Yes	2017	(Mousavikha mene et al., 2017)
Zebrafish	Magnetite nanoparticle with a size of 50 nm Functionalized with NGF, BVNF or BSA	Neurotrophin delivery to the retina	No	2018	(Giannaccini et al., 2018)
C57BL/6J mice *Balb/c* mice for IVT	Magnetite nanoparticles 50 nm core functionalized with somatostatin analog octreotide	Somatostatin analog octreotide delivery to the retina	No	2020	(Amato et al., 2020)

Table 3. Studies dedicated for the use of MNPs as drug delivery system for the ocular tissues

1.7. Purpose of the thesis:

As we have seen, eyedrops are one of the most used routes of application for drugs in ophthalmology. However, the existence of several anatomical and physiological barriers means that this method is not useful for drug delivery to the retina. The work on the thesis addresses the need of drug delivery tools for targeted treatment of retinal diseases in collaboration with OZ Bioscience, an industry partner of the Ocuther project. They have been in charge of the design, formulation, optimization and loading of the MNPs with our compounds. In this collaboration we have theorized that by using an external magnetic field we could greatly improve the drug delivery from the ocular surface to the retina. As we have seen there are several studies using MNPs for different purposes on the eye, but very few of them study the use of MNPs for drug delivery and none of them have attempted the use of magnet to guide MNPs after topical application. Thus, we have tried to address basic questions related to the use of MNPs guided by a magnetic static field that have not been addressed *in vivo*. In another collaboration, with the Ocular Pharmacology group from the University of Eastern Finland we were able to assess the distribution of MNPs on the ocular tissues after topical application of these MNPS in mice. Further studies will be carried on in rats in the future. Using the same MNPs we have assessed the safety of this drug delivery system *in vitro* and *in vivo.* Moreover, we have tested if a single application of our treatment in Bbs$^{-/-}$ mice was able of modulating the UPR pathway described before and preserve the retinal function of the treated animals.

.

II. Material and Methods

2. Materials and methods

2.1. Materials

2.1.1. Solutions and Buffers:

Name	Composition	Use
Lysis buffer	Tris/HCl 0,1M pH 8,5, EDTA 5mM pH 8,0, SDS 0,2%, NaCl 0,2M	Genotyping
Proteinase K solution	Proteinase K at a concentration of 0,3μg/ml	
TE buffer	Tris/HCl 10mM pH 8,0, EDTA 1mM pH 8,0	
Glucose 10%	D-(+)-Glucose-Monohydrate diluted in PBS	Eyedrop instillation
NP01 solution	Negatively charged MNPs+ MiliQ Water	
NP02solution	Positively charged MNPs+ MiliQ Water	
VPA solution	VPA solution in MiliQ water at a concentration of 12mM	
GBZ solution	GBZ solution in MiliQ water at a concentration of 15μM	
Fixation solution	in 2.5% Glutaraldehyde and 2.5% Para-formaldehyde in Cacodylate buffer (0.1M, pH 7.4)	Transmission Electron Microscopy
RIPA Buffer	150 mM NaCl0, % Triton, 0.5% sodium deoxycholate. 0.1% SDS (sodium dodecyl sulphate), 50mMTris-HCl pH 8.0, protease inhibitors	Western Blot
TBS (10x)	Trizma HCl, NaCl, ultra-pure water (adjust to final pH of 7.6)	
TBST	TBS 10x, ml ultra-pure water, Tween 20 (10%)	
Blocking solution	Milk 5%, TBST 0,1%	

Table 4. solutions and buffers used.

2.1.2. Antibodies for Western Blot (WB):

Name	Conditions	Source
Mouse monoclonal anti-eIF2α	1/1000; 5 % milk	Cell Signalling #2103S
Rabbit polyclonal anti-p-eIF2α	1/1000; 5 % milk	Cell Signalling #9721S
Rabbit monoclonal anti-Bip	1/1000; 5 % milk	Cell Signalling #3177S
Chicken anti-rabbit IgG-HRP	1/2500; 5% milk	Santa Cruz Biotechnology #2955
Goat anti-mouse IgG-HRP	1/2500; 5% milk	Santa Cruz Biotechnology #2060

Table 5. Antibodies used for WB

2.1.3. Primers:

Genes	Primer	sequences 5' - 3'
Bbs1	A	TCT CCT TGC TCC CTC TCA AA
	B	CCT GGA AAT GGA GAG ATG GA
	LTR	AAA TGG CGT TAC TTA AGC TAG CTT GC
Bbs10	4054	ACA AAT ACA ATT GAT CAT CGA TGT G
	4057	ACC TCC CCA CTT GAA CGA GGT CT
	4058	GTT GCC TGG CTT GGG TGG CA
Bbs12	4511	AGT TGA TGT CTA TCA ATA ACT GCC A
	4514	ACA CCT CCA CTG CTG TTC CTG CC
	4515	CTT CTC GAG CTT AAG GTC GAC CTG

Table 6. Primers used for genotyping.

2.1.4. Software:

Software Name	Used for	Source
ERGVIEW	ERG recording analysis	OcuScience
ImageJ	Analysis of ER dilatation	Free software
MRIcroGL	MRI analysis	Free software

Table 7. Softwares used for data analysis.

2.2. Methods used for the formulation and characterization of the MNPs:

The formulation and characterization of the MNPs was carried on by Marco Bassetto from the Ocuther Project as a collaboration with OZ Bioscience. In the next section the methods used for the formulation and characterization of our MNPs will be briefly described.

2.2.1. Synthesis of Iron oxide MNPs

Classical co-precipitation of iron salts following the Massart method with few modifications was used for the synthesis of the MNPs. Ferrous and ferric ions in solution (1:2 stoichiometry) were precipitated in an oxygen free atmosphere by adding ammonium hydroxide. This mixture was heated to 80°C and kept at this temperature for 30 minutes under stirring.

Negative MNPs were synthetized adding TEOS (Tetraethyl orthosilicate) and THPMP (3-(tryhydroxysilylpropyl) methyl-phosphonate monosodium salt) in one shot and stirring the mix for 2 hours. This resulted in the in-situ co-condensation of two silanes yielding a silicon oxide layer presenting negative surface phosphonate groups.

The synthesis of the positive MNPs capping of the crystals was achieved by the addition of Zonyl FSA followed by the addition of a solution of cationic polymer such as polybrene, poly-L-lysine, polyethylenimine or proprietary ionizable amphiphilic block co-polymers. The iron content of the MNPs was quantified by colorimetric assay.

2.2.2. Particle morphology assessment

Transmission electron microscopy (TEM) was used to assess the particles morphology, size and distribution using a JEOL (JEOL, Montpellier, FR). All the samples were sonicated and then 1-2 µl of single MNPs were placed on holey carbon film covered copper grids and left drying before analysis. The average MNPs size and cumulative size distribution was obtained with 100 single objects measures.

2.2.3. Powder x-ray diffraction

X-ray diffraction was used in order to assess the magnetic core's crystallinity, chemical composition and size. A Bruker D8 Focus diffractometer was used. Measurements were recorded in the 15-115 Ɵ-2Ɵ range with step size of 0.02 and 1.2 s/step acquisition. Freeze dried samples were loaded on a plastic slit and rotated at 15 rpm at 25°C. The crystal size was derived from peak's enlargement using the Williamson-Hall equation.

2.2.4. Loading procedure and quantification

Two different solutions were used for the loading procedure, one at a concentration of 15 µM for the GBZ solution and another at a concentration of 12mM for the VPA solution, both loading solutions were prepared with MiliQ water. Then, the MNPs were diluted separately, the negatively charged particles were diluted using the GBZ solution while the positively charged particles were diluted using the VPA solution until a concentration of 1 mg Fe/ml were obtained. The quantification of the drug adsorbed on the MNPs surface was quantified using high-performance liquid chromatography.

2.3. Methods used for the *in vivo* testing of the MNPs:

2.3.1. Mice husbandry:

All experimental procedures were approved by the local ethical committee of Strasbourg University. Animals were kept in the central animal facility of the Faculty of Medicine of the University of Strasbourg.

2.3.1.1. Husbandry:

Homozygous *Bbs1^{-/-}* (R. E. Davis et al., 2007)*, Bbs10^{-/-}* (Cognard et al., 2015)*, Bbs12^{-/-}* (Mockel et al., 2012) were generated by crossing heterozygous *Bbs1^{+/-}, Bbs10^{+/-}, Bbs12^{+/-}* mice. The mice were bred and kept in individually ventilated cages in humidity- and temperature- controlled rooms on a 12 hours light/dark cycle with *ad libitum* access to food and water. Heterozygous mice were used for breeding as the homozygous mice are not able to produce offspring. These three different mice models were chosen as previous work in our laboratory has shown that they all share the activation of the UPR pathway.

Relevant mouse models are bred on a C57BL/6N background and crossbreeding with the C57BL/6J strain to remove the strain associated interfering Rd8 mutation which interferes with the retinal phenotype.

2.3.1.2. Genotyping:

In order to identify mice with the adequate genotypes for our studies the litters obtained from our breeding were genotyped.

2.3.1.3. Genomic DNA extraction:

The genotyping of the mice obtained by reproduction of the different *Bbs^{+/-}* was done using genomic DNA extracted from finger tissues cut in the first days of life (between 5 and 10 days after birth). For the extraction the tissue was digested using a lysis buffer and proteinase K solution. The tissue was incubated at 55° degrees in the mix overnight. The DNA was then precipitated using isopropanol. After precipitation the DNA was resuspended in the TE buffer.

2.3.1.4. Polymerase chain reaction:

The previously extracted DNA was used for polymerase chain reaction (PCR). This technique is based on the possibility of amplifying a specific DNA region using polymerase enzymes guided by specific primers. The primers used are shown in the table (M3) we used a Taq polymerase enzyme catalogue # D4545, Sigma-Aldrich). The cycles for the PCR consisted in: 3 minutes at 94°C for the initial denaturation of the DNA, a 3-step cycle: 30 seconds at 94°C for denaturation, 30 seconds at 62° for the hybridization of the primers and the DNA and 30 seconds at 72°C for the elongation. This cycle is repeated 30 times before a final elongation phase of 5 minutes at 72°C degrees. The product was then deposed in an 2% agarose gel. For the visualization of the bands an DNA intercalant agent (Ethidium bromide) was used and the bands were revealed using UV light.

2.4.2. Treatment with MNPs as eyedrops

2.4.1. General experimental flowchart:

We started our experiments in 14-days old mice with the application of the treatment. This age was chosen as it correlates to the day the mice open the eyes for the first time. We then waited 2 weeks after the treatment to assess the effects of the treatment in 1-month old mice. We decided to study the effects of the treatment at this age as our laboratory has previously studied the phenotype of the different $Bbs^{-/-}$ mice at this age. General treatment flowchart is shown in Figure 6.
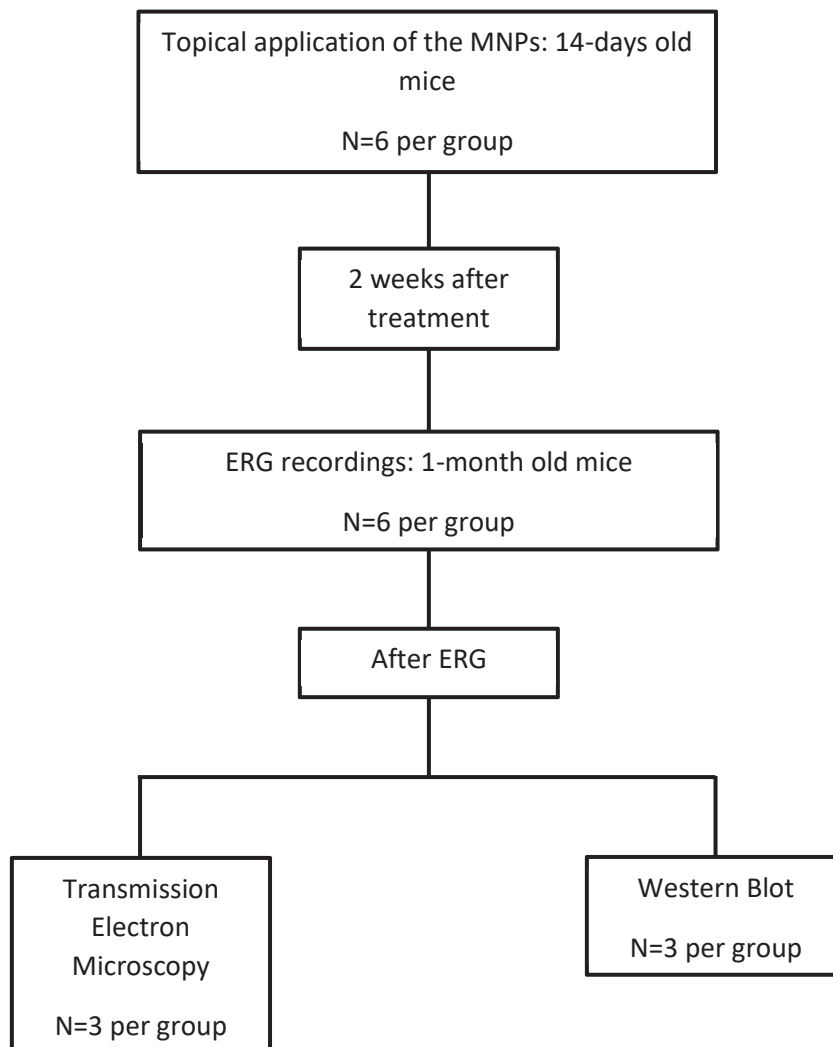
Figure 6. Experimental flowchart. This flowchart was repeated for each one of our treatment groups.

For our experiments only one eye was treated per mice but we analyzed both the treated eye and the contralateral untreated eye. This was done in order to see if the treatment of one eye had any effect on the untreated eye.

2.4.2. MNPs *in vivo* testing:

2.4.2.1. Toxicity tests:

To assess the possible toxicity of the MNPs iron core mice were treated with unloaded MNPs $Bbs^{+/+}$ the groups are shown in table 8. In this case only ERG was recorded and no TEM images were acquired.

Mice model	Treatment
$Bbs^{+/+}$	Mix of unloaded MNPs (NP01+NP02)
$Bbs^{-/-}$	NP01 unloaded+NP02 loaded

Table 8. Mice treated to test the toxicity of the unloaded MNPs.

2.4.2.2. Biological effect of the loaded MNPs:

To assess if the loaded MNPs were able to produce an effect *in vivo* we treated different mice separated in groups as shown in Table 9.

Mice model	Treatment
$Bbs^{+/+}$	Mix of loaded MNPs (NP01+NP02) undiluted
$Bbs^{+/+}$	Mix of loaded MNPs (NP01+NP02) 1/25 dilution
$Bbs^{+/+}$	Mix of loaded MNPs (NP01+NP02)1/50 dilution
$Bbs^{-/-}$	Mix of loaded MNPs (NP01+NP02) undiluted
$Bbs^{-/-}$	Mix of loaded MNPs (NP01+NP02) 1/25 dilution
$Bbs^{-/-}$	Mix of loaded MNPs (NP01+NP02)1/50 dilution
$Bbs^{-/-}$	VPA and GBZ solutions
$Bbs^{-/-}$	NP01 loaded+NP02 unloaded
$Bbs^{-/-}$	NP01 unloaded+NP02 loaded
$Bbs^{-/-}$	Unloaded MNPs

Table 9. Mice treated to test the biological effect of the loaded MNPs.

2.4.2.3. Nanoparticle application:

For the preparation of the eyedrop for treating one mouse 5 µl of NP01 is mixed with 5µl of NP02 and 10 µl of glucose at 10% for a total eyedrop volume of 20 µl. Different dilutions of NP01 and NP02 were used in our experiments as shown in the tables 9 and 10, undiluted MNPs present a concentration of 1mg/ml of iron for both MNPs. For the topical application of the diluted MNPs NP01 and NP02 were previously diluted and then mixed following the same proportions as the non-diluted MNPs. Unloaded MNPs were diluted using ddH2O while the Loaded MNPs were diluted using the GBZ solution for NP01 and the VPA solution for NP02.

Mice were treated under anesthesia using Domitor® (Medetomidine, 6.5µg/g body weight) and Ketamine (665 µg/g body weight). The instillation of the eyedrop was done in two times. First 10 µl were applied with a pipette and the magnet was positioned behind the ear of the mice (Figure 7). After 5 minutes from the first instillation had elapsed another 10 µl of the solutions were applied. The treatment was done in two times to avoid the eyedrop from falling directly after application as 20 µl is too large for the size of the mice eye. The eyedrop was left on the surface of the eye for a total of 30 minutes counting after the first 10 µl instillation. Once the 30 minutes passed the magnet was removed from behind the head of the mice and the eyedrop was carefully wiped. Then, ocrygel was used to cover the eye to avoid excessive drying of the cornea. Mice were kept under controlled temperature conditions until fully awake.
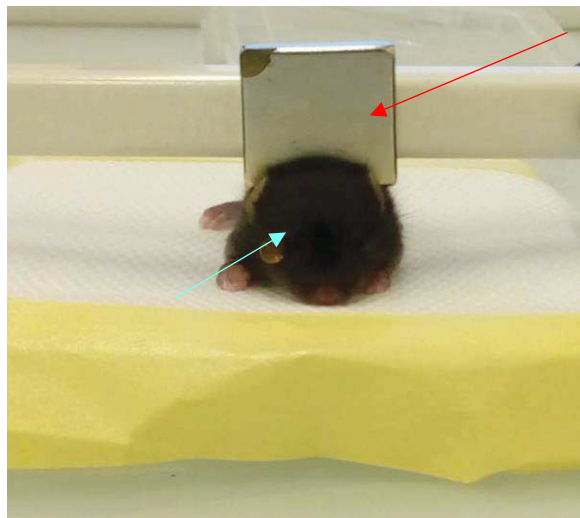

*Figure 7. Experimental setup for topical application of the treatment. **Red arrow points to the magnet. Blue arrow points to the eyedrop.***

2.4.3. Electroretinogram:

The ERG is a non-invasive technique that allows to measure the retinal response after a controlled light stimulus. For our project we performed Flash ERG, in this modality we used different flashes separated in time and with growing intensities. After the flash the retina produces a small electrical signal with the start of the light perception by the PR. The electric current started by the PR that will continue through the other neurons in the retina will be received by electrodes positioned in the surface of the eye, amplified by the recorder and later analyzed. For our experiments we have measured only the a-wave of the ERG (Figure 8) corresponding to the PR response. A-wave measures are important as the goal of the treatment is to preserve the retinal function via the modulation of the apoptosis of PR cells. Thus, ERG recording is a direct measure of the treatment efficacy.

ERG was recorded two weeks after the application of the treatment in 1-monht old mice using a HMsERG system (Ocuscience). Mice were dark-adapted overnight (for at least 12 hours) and anesthetized by intraperitoneal injection of Domitor® (Medetomidine, 7.6µg/g body weight) and Ketamine (760 µg/g body weight) before the experiment. The pupils are dilated with atropine 0,3% eyedrops. The recordings were carried out in dim red light (Philips) in order to maintain the dark adaptation of the mice. For the ERG one ground electrode is placed next to the tail and two reference electrodes are placed subcutaneously under the skin of the cheeks. Recording electrodes were placed on the corneal surface and a methylcellulose gel and a contact lens are used to improve the contact with the surface. ERGs standard procedure was used according to manufacturer's protocol (Ocuscience). Briefly, the protocol consisted in recording a dark-adapted ERG (Scotopic ERG) after photonic stimuli with intensities ranging from 0.1 to 25cd.s/m2. For the Photopic ERG recording, obtained after a period of light saturation, ERG the intensities ranged from 0.01 to 25cd.s/m2. ERG results were amplified and captured digitally by ERG View system 4.3 (Ocuscience).
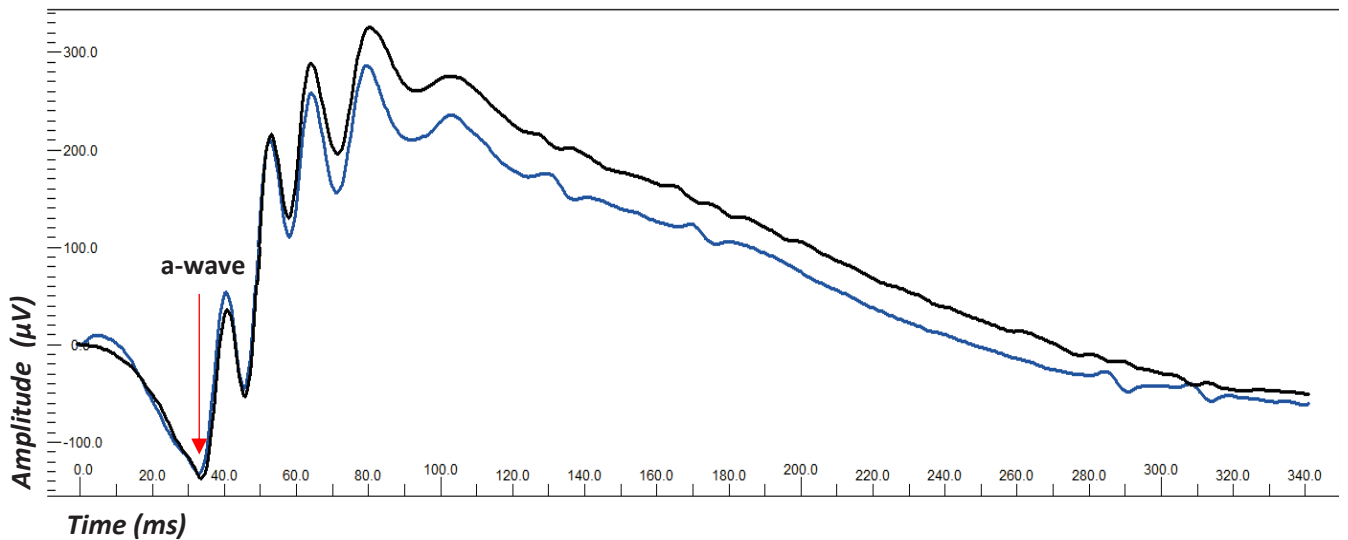
Figure 8. Representative ERG trace. The arrow points to the negative deflection of the ERG corresponding to the a-wave or PR response to light.

The analysis of the ERG recording was carried on using the ERGVIEW program (OcuScience). The a-wave was measured by measuring the first negative deflection observed in the recording.

2.4.4. Eye dissection:

After ERG, eyeballs were harvested and prepared either for TEM or for WB. Dissections of the eye were performed with the eye submerged in Ames medium supplemented with glucose (concentration of 6,5 mg/ml). For the samples used in TEM imaging the anterior part of the eye along with the lens were removed. To achieve this the cornea was pierced with a needle, then a micro-scissor was used in order to separate the cornea from the posterior chamber of the eye by cutting over the corneal limbus. Then the lens is removed using pincers. Finally, the tissue was fixed (as explained in the next section). For WB the retina was separated from the ocular tissues and frozen using liquid nitrogen. Then the tissues were conserved at -80° until used.

2.4.5. Transmission electron microscopy (TEM)

Samples were fixed by immersion in 2.5% Glutaraldehyde and 2.5% Para-formaldehyde in Cacodylate buffer (0.1M, pH 7.4), post fixed in 1% osmium tetroxide in 0.1M Cacodylate buffer and then dehydrated through graded alcohol (50, 70, 90, 100%) and propylene oxide for 30 minutes each. Samples were embedded in Epon™ 812 (Sigma-Aldrich)). Semi-thin sections were cut at 2μm with an ultra-microtome (Leica Ultracut UCT, Leica Biosystems) and stained with Toluidine blue, and

histologically analyzed by light microscopy. Ultrathin sections were cut at 70nm and contrasted with uranyl acetate and lead citrate and examined at 70kV with a Morgagni 268D electron microscope. Images were captured digitally by Mega View III camera (Soft Imaging System).

ImageJ was used for measuring the thickness of the outer nuclear layer on Toluidine blue staining sections. The optic nerve was used for orientation with measures starting at 500 µm distance from the optic nerve with a total of 5 measures taken with 100 µm intervals between each measure, 3 eyes were used for group.

ImageJ was also used for the measure of the area of the pictures occupied by the ER. Three pictures were examined by animal. The area occupied by ER was measured in three different pictures for each animal and the averages was compared. In order to be able to assure equivalency between the animals measured, we measured a similar number of objects between each picture.

2.4.6. Western blot

The Western blot assay allows the immunologic marking of specific proteins present in a protein extract. Then the signal obtained from the antibody marking of the proteins can be used to semi-quantitative analyze the protein concentration of the extract by measuring the differences on the signals obtained for each sample.

Protein extraction:

Total protein was extracted from retinal tissues in RIPA buffer supplemented with an antiprotease cocktail ("Complete EDTA-free", Roche), 1 mM NaVO4 and 25mM NaF. The tissue was dissociated and then it was sonicated for 30 seconds. Protein concentration was determined by Bradford assay (Bio-rad protein assay, cat. #500-0006, Bio-rad laboratories GmbH, Mûnchen).

Western Blot:

For our experiments, a total of 20 µg of proteins per sample were supplemented with 1x Laemmli Sample Buffer (Ref#1610747, BioRad) and β-mercaptoetanol and denatured for 15 min at 95°C. The denatured proteins where then separated by electrophoresis using a 10% polyacrylamide gel (Ref: 5678034 Biorad Stainfree) and TGX 10X running buffer. This was done in order to separate all the proteins based on their molecular weight. The separated proteins were transferred from the gel to

PVDF membranes membranes (Ref: 170-4157, Biorad). The transfer was verified using Biorad's stain free technology. The membranes were then blocked using 5% milk for 1 hour at 4°C. The membrane was incubated at 4°C overnight with primary antibodies diluted in 5% milk shown on table 5. The membrane is washed and then incubated with the second antibodies conjugated with horseradish peroxidase for 1 hour at room temperature. The blots were visualized using Super signal® West Femto (Ref: 34095, thermo scientific) and the ChemiDoc™MP Imaging System.

The quantification of the proteins was later done using the Image Lab software from BioRad. Normalization of the quantification was done using with the total amount of protein loaded as observed in the membrane using the BioRad Stainfree techonology.

2.4.7. Statistical analysis

For the statistical analysis we used the software Graphpad Prism 8. Since the size of our groups is too small to assess with certainty the Normal distribution of our samples, we compared our groups using non-parametric tests, namely the Mann-Whitney test. We represent our results as averages ± SEM. The differences between groups was considered significant when $p < 0,5$ and was represented by an asterisk.

2.5. Experiments in Collaboration with the Ocular Pharmacology group from the University of Eastern Finland:

One of the most important aspects of the Ocuther project is the interaction between the different partners of the project. As part of the thesis project we have collaborated with the Ocular Pharmacology group from the University of Eastern Finland, under the direction of Pr. Arto Urtti. The Ocular Pharmacology group has a wide and long experience in the study of the ocular pharmacokinetics. During the time of the exchange in the University of Eastern Finland we tried to answer the basic questions about the mobility if the MNPs after topical application and how they would behave if they reached the inside of the eye. With this in mind we decided to use magnetic resonance imaging (MRI) in order to observe the MNPs after treatment. For the analysis of how the MNPs behave we had two different approaches, one topical and one using IVT. The objective was to understand how would the MNPs reach the retina and how would the magnet or absence of magnet influence the mobility of the MNPs. This set of experiment was hindered partially by the COVID outbreak as the University of Eastern Finland was partially closed. For the project this meant that the experiments were delayed for the period of the exchange and they will not be finished by the end of the thesis.

2.5.1. Imaging of animals treated by topical application

For the topical application of the MNPs we used mice. The focus of these experiments was to observe how the MNPs behave after topical application and if the magnet had any impact on the treatment. The experimental groups are shown in table 10. A total of 3 mice were used for each group. These mice were 2-month-old mice as using smaller animals as the ones normally used for the treatment would difficult the acquisition of images due to size constraints.

Group	Treatment	Magnet application
Group 1	NP01	Yes
	NP02	
Group 2	NP01	No
	NP02	
Group 3	Mix	Yes
Group 4	Mix	No

Table 10. Mice treated topically for MRI.

For this study we wanted to observe if there were any differences between NP01, NP02 and the mix of both MNPs in terms of mobility, penetration on the ocular tissues and time of permanence on the tissues. Due to the characteristics of the imaging technique some changes were done to the MNPs instillation protocol.

The images were acquired right after the application of the MNPs and 24 hours after the application of the treatment.

2.5.1.1. Nanoparticle application:

The first change in the protocols of the MNPs application is the concentration used for the treatment, higher concentrations of MNPs were used: 16mg/ml for NP01 and 8 mg/ml for NP02. Secondly, we reduced the volume of the applied eyedrop. Finally, the application time of the treatment was 45 minutes instead of 30. These changes were done in order to optimize the images obtained after the topical application of the MNPs.

2.5.1.2. MRI imaging:

For the imaging mice were imaged just after the application of the MNPs thus no additional anesthesia was used. For the imaging 24 hours after application inhaled isoflurane was used. Each eye was imaged separately, and the mice was placed laying on the side. The images were acquired with a repetition time of 1200ms, and echo time of 3.7 ms between pulses, effective echo time of 29.6 ms and a spatial resolution with a Field of View 6.4 x 6.4 x 4.8 mm, matrix 64x64x48 (spatial resolution 100 µm) for the experiments using mice. For the experiments using rats we used a repetition time of 1000ms, echo time of 5.4 ms between pulses, effective echo time of 43.2 ms and a spatial resolution with a Field of View 26x10x10 mm, matrix 208x80x80 (spatial resolution 125 µm).

2.5.2. Imaging of animals treated by IVT

To better understand how the MNPs would behave once inside the eye we used IVT in order to ensure that we would be able to observe MNPs inside the eyeball. In this case we tried different concentrations in order to see what the optimal concentration for imaging would be. The groups for this experiment are shown in table 11. These are ongoing experiments that will be continued by the Ocular Pharmacology group of the University of Eastern Finland. For the study 3 month old rats were used.

Group	Treatment	Concentration	Number of animals
Group 1	NP01 + control eye	0.5 mg/ml	1 rat
Group 2	NP01	0.5 mg/ml	1 rat
	NP02		
Group 3	NP01	0.25 mg/ml	1 rat
	NP02		
Group 4	NP01	0.125 mg/ml	1 rat
	NP02		
Group 5	NP01	0.0625 mg/ml	2 rats
	NP02		

Table 11. Mice treated with IVT for MRI.

We acquired MRI images in the following time points:

1. After injection
2. One day after injection
3. One week after injection
4. Two weeks after injection
5. One month after injection

One month after injection, we also decided to apply the magnet in the group 2 of our treatment in order to see if it could elicit any movement in the MNPs. This was done in order to assess if the magnet could affect the MNPs that were already in the vitreous. For this experiment the magnet was placed in front of the eye of the animal (Figure 9) instead that in the back of the eye. The change in position was decided as the preliminary imaging showed that the MNPs were closer to the back of the eye, thus, placing the magnet in front of the eyes would allow for a wider movement of the MNPs inside the posterior chamber.

Figure 9. Experimental set-up for the assessment of magnetic field effect on IVT injected MNPs. Since the MNPs were already in the back of the eye we changed the position of the magnet in order to assess the effect of the magnetic field on the movement of the particles

III. Results

3.Results

3.1. Results 1: In vivo phenotypic and molecular characterization of retinal degeneration in mouse models of three ciliopathies:

During the duration of the thesis I have been able to participate in one paper not directly related with the Ocuther project but describing and comparing various ciliopathy mouse models. This section will highlight the main results of this paper and also how these results correlate with the main project.

3.1.1. Synopsis:

Preliminary data have shown that UPR was activated in a mice model for BBS and that it was possible to pharmacologically modulate the UPR activation. These findings raised the question if this stress pathway was also activated in other ciliopathy models, as finding common pathological mechanisms for these diseases would be a breakthrough for developing treatment for these rare diseases. In the study different models, namely, $Bbs1^{M390R/M390R}$ (henceforth $Bbs1^{-/-}$), $Bbs10^{-/-}$, $Cep290^{-/-}$ and $Alms^{foz/foz}$ were analysed in term of retinal function (assessed by using ERG recordings), retinal structure (studied using TEM images and immunofluorescence) and UPR activation (assessed using qPCR for UPR related proteins). Comparison between the different models showed that the $Alms^{foz-foz}$ mice did not show activation of the UPR and the degeneration of this model occurred later than in the other models. However, the $Bbs1^{-/-}$, $Bbs10^{-/-}$, $Cep290^{-/-}$ models presented a faster retinal degeneration than the $Alms^{foz-foz}$. Upregulated levels of known UPR genes as well as mislocalization of Rhodopsin, signs that were also found in all the models except the $Alms^{foz-foz}$, apparently showing that this model does not present UPR activation.

Participation on this project and correlation with the main project:

For this project I participated in the immunofluorescence staining for the $Bbs1^{-/-}$, $Bbs10^{-/-}$ $Bbs12^{-/-}$ models as well as with the microscopy image acquisition. I also took part in the manuscript writing and correction.

Correlation with the main project:

As mentioned in this study, the ciliopathies present a high heterogeneity with overlapping phenotypes. We have proved that different BBS models presented the activation of the same stress pathway, the UPR. Since this pathway causes apoptosis in these models, modulation of the UPR with our treatment can benefit the different $Bbs^{-/-}$ models.

In vivo phenotypic and molecular characterization of retinal degeneration in mouse models of three ciliopathies

Agnès Brun[a,1], Xiangxiang Yu[a,1], Cathy Obringer[a], Daniel Ajoy[a], Elodie Haser[a], Corinne Stoetzel[a], Michel J. Roux[b], Nadia Messaddeq[b], Hélène Dollfus[a], Vincent Marion[a,*]

[a] INSERM, Laboratoire de Génétique Médicale, UMR_U1112, Ciliopathies Modeling and Associated Therapies Team (CMAT), Fédération de Médecine Translationnelle de Strasbourg (FMTS), Institut de Génétique Médicale D'Alsace (IGMA), Université de Strasbourg, 11 Rues Humann, Bâtiment 3, 67085, Strasbourg, France [b] Institut de Génétique et Biologie Moléculaire et Cellulaire (IGBMC), 1 Rue Laurent Fries, 67400, Illkirch-Graffenstaden, France

A B S T R A C T

Cilia are highly conserved and ubiquitously expressed organelles. Ciliary defects of genetic origins lead to ciliopathies, in which retinal degeneration (RD) is one cardinal clinical feature. In order to efficiently find and design new therapeutic strategies the underlying mechanism of retinal degeneration of three murine model was compared. The rodent models correspond to three emblematic ciliopathies, namely: Bardet-Biedl Syndrome (BBS), Alström Syndrome (ALMS) and CEP290-mediated Leber Congenital Amaurosis (LCA). Scotopic rodent electroretinography (ERG) was used to test the retinal function of mice, Transmitted Electron microscopy (T.E.M) was performed to assess retinal structural defects and real-time PCR for targeted genes was used to monitor the expression levels of the major apoptotic Caspase-related pathways in retinal extracts to identify pathological pathways driving the RD in order to identify potential therapeutic targets. We found that BBS and CEP290-mediated LCA mouse models exhibit perinatal retinal degeneration associated with rhodopsin mislocalization in the photoreceptor and the induction of an Endoplasmic Reticulum (ER) stress. On the other hand, the tested ALMS mouse model, displayed a slower degeneration phenotype, with no Rhodopsin mislocalization nor ER-stress activity. Our data points out that behind the general phenotype of vision loss associated with these ciliopathies, the mechanisms and kinetics of disease progression are different.

Introduction

Ciliopathies, a group of rare genetic diseases, can be either of nonsyndromic or syndromic nature in which retinal degeneration (RD) is a cardinal clinical feature (Bujakowska et al., 2017; Estrada-Cuzcano et al., 2012). Ciliopathies contain a spectrum of disorders ranging from isolated RD such as in a sub group of Leber Congenital Amaurosis (LCA) (i.e: Cep290), to complex syndromes with multiple organs dysfunction such as, for example, Bardet-Biedl Syndrome (BBS), Alström Syndrome (ALMS) and the lethal manifestations in the Meckel-Gruber syndrome (Adams et al., 2007; Mockel et al., 2011; Waters and Beales, 2011). These syndromes are caused by mutations in different genes coding for proteins with distinct roles and cellular localizations within the ciliated cells (Cui et al., 2013; Estrada-Cuzcano et al., 2012; Knorz et al., 2010; Reiter and Leroux, 2017). Interestingly, the retinal degeneration presents in many ciliopathies is often of early onset leading to severe visual impairment but can exhibit variable progression phenotypes. For example, RD is characterized by an initial photophobia with nystagmus in Alström syndrome in the first months of life, whereas the first symptoms will be evident only after a few years with nyctalopia and visual field deficiency in BBS (Hamel, 2006; May-Simera et al., 2017). The fact that such differences exist in the RD progression combined with the myriads of mutated genes, lead us to hypothesize that there might be different mechanisms at play at the level of the photoreceptor cell in these different ciliopathies. In view of the heterogeneity, the large number of genes and mutations involved in RD, identifying such mechanistic differences behind these retinal phenotypes is of prime importance in order to properly stratify the patients with future appropriate therapy.

Currently, there is no treatment available for RD; one clinical trial showed the efficacy of gene therapy in LCA (Russell et al., 2017) but it is specific of RPE65 gene mutations. The identification of common

III. Results

Gene	Oligo name	Sequence(5'-3')
Bbs10	4054	ACA AAT ACA ATT GAT CAT CGA TGT G
Bbs10	4057	ACC TCC CCA CTT GAA CGA GGT CT
Bbs10	4058	GTT GCC TGG CTT GGG TGG CA
Cep290	M11336	TGG AAG ACC AGG CTT CAG AG
Cep290	M11340	GGC TCA CTG TGA TCT TGT GC
Cep290	W11338	GTA AGT GCC CGA CAG CTA CC
Cep290	W11339	AGC GCA GTG CAG AGT ATG TG
Rd8	F1	GTGAAGACAGCTACAGTTCTGATC
Rd8	R	GCCCCATTTGCACACTGATGAC
Rd8	F2	GCCCCTGTTTGCATGGAGGAAACTTGGAAGACAGCTACAGTTCTTCTG
Alms	Forward	ACA ACT TTT CAT GGC TCC AGT
Alms	Reverse	TTG GCT CAG AGA CAG TTG AAA

mechanisms could allow the development of therapeutics applicable to RD regardless of the affected gene and the type of mutation. RD in the ciliopathies is linked to the structure of the photoreceptor itself. The photoreceptors outer segment is connected to the inner segment via the connecting cilium (May-Simera et al., 2017; Sjostrand, 1953). This connecting cilium is a protein highway that allows the efficient connection between the biosynthetic active inner segment and the light detecting outer segment for the visual process to start upon photonic impulse. In ciliopathies, ciliary proteins are defective and therefore are no longer able to play their respective roles in the photoreceptor. One of the commonly associated mechanism to photoreceptor apoptosis in the ciliopathies is a defective intraflagellar transport (IFT) of proteins between the two segments (Wright et al., 2010). This defect ultimately causes protein accumulation in the IS, which in turn triggers a proapoptotic unfolded protein response (UPR) associated with an ER-stress (Mockel et al., 2012; Starr et al., 2018). Previously, we have proved that UPR activation occurs in a Bbs12 model, leading us to develop a pharmacological approach (GIVin). The treatment slowed RD in our mouse model (Mockel et al., 2012). Other studies targeting non-ciliopathy models have also shown that UPR is an interesting pathway to target in slow RD presenting ER stress. However, RD mechanisms for other emblematic ciliopathies still need to be characterized. We therefore used mice models for three iconic ciliopathies namely BBS, LCA (CEP290) and ALMS to analyze and compare their respective retinal phenotypes while measuring the key components of the UPR pathway.

To date 21 genes (BBS1-BBS21) have been identified in BBS (Heon et al., 2016). Half of these proteins are involved in two major BBS protein complexes, the Bbsome complex containing 7 of the BBS proteins (BBS1, 2, 4, 5, 7, 8 and 9) (Nachury et al., 2007) and the BBSchaperone complex containing three BBS proteins (BBS 6, 10 and 12) (Seo et al., 2010). The pro-apoptotic mechanism of RD associated with Bbs12 has already been characterized in a mouse model (Mockel et al., 2012) and apoptosis was shown to be induced by a deleterious protein accumulation in the IS, leading to the activation of the UPR pathways. We, therefore, determined whether the other BBS proteins could induce the same type of events leading to RD. In the LCA model we studied the centrosomal protein 290 (CEP290), also known as the LCA10 protein, mutations in this gene may lead to various ciliopathies and remarkably a recurrent mutation in intron 26 of CEP290 is a frequent cause of LCA (Garanto et al., 2015). CEP290 protein is known to be involved in photoreceptor development and when mutated leads to early-onset retinal degeneration (Garanto et al., 2015). Finally, in ALMS, only one gene (ALMS1) has been identified to date. In human patients, ALMS is characterized by early onset cone-rod dystrophy leading to blindness but the mechanism behind this phenotype remains elusive (Marshall et al., 2007).

Material and methods

2.1. Generation of knockout mice and animal husbandry

All experimental procedures were approved by the local ethical committee of Strasbourg University. Bbs1$^{M390R/M390R}$ (henceforth Bbs1$^{-/-}$), Bbs10$^{-/-}$, Cep290$^{-/-}$ and Alms$^{foz/foz}$ mice with their control wild type littermates were generated as described previously (Arsov et al., 2006; Cognard et al., 2015; Davis et al., 2007; Mockel et al., 2012). Stock Cep290$^{tm1.1Jgg}$/J mice were developed by replacing exons 36, 37 (schematic representation of the mutated allele in Supplementary Fig. 1). Relevant mouse models were bred on a C57BL/ 6N background and crossbreeding with the C57BL/6J strain to remove the strain-associated interfering Rd8 mutation which interferes with the retinal phenotype (Mattapallil et al., 2012). Mice were kept and bred in humidity- and temperature-controlled rooms on a 12 h light/dark cycle on normal chow and water ad libitum. PCR-genotyping were carried out using KAPA Mouse Genotyping Kit (Catalog#KK7302, Kapa Biosystems, Woburn, Massachusetts, USA), primers used for genotyping are listed in Table 1 in supplementary data.

2.2. Electroretinogram

Electroretinograms (ERGs) were performed at the indicated time points with the HMsERG system (Ocuscience®, Kansas City, Missouri, USA). Mice were dark-adapted overnight and then anesthetized by intraperitoneal injection of Domitor® (Medetomidine, 7.6 μg/g body weight) and Ketamine (760 μg/g body weight). The experiments were carried out in dim red light (Catalog #R125IRR, Philips, Suresnes, France). ERGs standard procedure was used according to manufacturer's protocol (Ocuscience®, Kansas City, Missouri, USA). Briefly, the protocol consisted in recording a dark-adapted ERG (Scotopic ERG) after photonic stimuli with intensities ranging from 0.1 to 25 cd s/m^2. ERG results were amplified and captured digitally by ERG View system 4.3 (Ocuscience®, Kansas City, Missouri, USA). The a-wave (corresponding to the first negative deflection) for the scotopic responses was recorded and analyzed.

2.3. Histology and immunofluorescence

Eyeballs were harvested after ERG examination and were fixed 1 h in 4% formalin (Catalog#F5554-4L, Sigma-Aldrich, Saint-Louis, Missouri, USA) at 4 °C, and then incubated sequentially in 10%, 20% and 30% sucrose solutions for 1 h. Eyeballs were then transferred into Optimal Cutting Temperature Compound™ (OCT™, Catalog# 4583, Tissue-Tek® OCT™, Sakura® Finetek, Torrance, California, USA) and frozen in liquid nitrogen. 7 μm cryosections were cut with Cryostat Leica CM1950 (Catalog# 14 0477 8001, Leica Biosystems, Wetzlar, Germany). Eye sections were treated for Haematoxylin-Eosin staining. The thickness of photoreceptor (ONL), inner nuclear layer (INL), outer

Table 2.
Antibodies used

ntibodies	talog	mpany
odopsin mouse monoclonal	AB5316	emicon
oat-anti mouse Alexa Fluor® 594	11032	ïtrogen

segment (OS) and inner segment (IS) were measured five times at 100 μm regular intervals, the first one was measured at 500 μm distance from the optic nerve. For immunofluorescence, cryosections were postfixed in 4% formalin for 3 min and then permeabilized with 0.01% TritonX-100 in PBS (Catalog #ET330, Euromedex, France) for 5 min. Sections were incubated 30 min in 1%BSA (Catalog #A7030-100G, Sigma-Aldrich, USA) in PBS at room temperature, then incubated overnight with primary antibodies diluted in blocking buffer at 4 °C. Sections were then incubated for 1 h at room temperature with the secondary antibody. Nuclei were counterstained with Hoechst (#D1306, Invitrogen, Carlsbad, California, USA). Slices were then mounted with Vectashield® Mounting Medium (Catalog #H-1000, Vector Laboratories, Burlingame, California, USA). Images were acquired on a Leica SP8 confocal microscope with either a HC PL APO CS2 63x/1.40 or 40x/1.30 oil immersion lens, driven by the LAS X software (Leica, Weitzlar, Germany). Antibodies used are listed in Table 2 in supplementary data.

2.4. Transmission electron microscopy (T.E.M.)

The samples were fixed by immersion in 2.5% Glutaraldehyde and 2.5% Para-formaldehyde in Cacodylate buffer (0.1M, pH 7.4), post fixed in 1% osmium tetroxide in 0.1M Cacodylate buffer for 1 h at 4 °C and then dehydrated through graded alcohol (50, 70, 90, 100%) and propylene oxide for 30 min each. Samples were embedded in Epon™ 812 (Sigma-Aldrich, Saint-Louis, Missouri, USA). Semi-thin sections were cut at 2 μm with an ultra-microtome (Leica Ultracut UCT, Leica Biosystems, Wetzlar, Germany) and stained with Toluidin blue, and histologically analyzed by light microscopy. Ultrathin sections were cut at 70 nm and contrasted with uranyl acetate and lead citrate and examined at 70 kV with a Morgagni 268D electron microscope. Images were captured digitally by Mega View III camera (Soft Imaging System). The thickness of the photoreceptor ONL, INL and OS + IS were measured five times at 100 μm regular intervals on Toluidin blue stained sections, 3 mice were used for per genotype. Nuclei of ONL were counted, on Toluidin blue stained sections. At least 20 rows were counted in each section and 3 eyes were used for each genotype.

2.5. RNA extraction and real-time PCR

Retinal tissues were harvested as previously described (Mockel et al., 2012). RNA extraction was performed using Trizol® reagent (Catalog #15596-018, Invitrogen®, Life Technologies™, Carlsbad, California, USA) and Tissue Ruptor® (Catalog #9001272, Qiagen, Venlo, Nederland). RNA samples were treated with DNase (TURBO™ DNA-free Kit, Catalog #AM1907, Ambion®,
Life Technologies™, Carlsbad, California, USA) prior to reverse transcription using the iScript® cDNA synthesis kit (Catalog#170–889, BioRad, USA). Self-design primers were purchased from Sigma-Aldrich. Quanti-tech Primers were purchased from Qiagen, Courtaboeuf, France (Table 3). Real-Time PCR was performed using the iQ SYBR® Green Supermix (Catalog#170–8886, BioRad, USA) on C1000TM thermo-cycler (CFX96, Real-Time System, Bio-Rad, USA). Real-time PCR was carried out according to the following cycle: initial hold at 95 °C for 30 s and then 39 cycles at 95 °C for 5s and 60 °C for 30s. Quantitative gene expression was calculated by the $2^{\Delta\Delta Ct}$ method relative to the reference gene, Gapdh. Primers used for real-time PCR are listed in Table 3 in supplementary data.

Table 3
Primers used for real-time PCR.

ne	ference	mpany
u-Bbs10-Rt-F1	GCTTAGCAGGGATGGAG	gma-Aldrich
u-Bbs10-Rt-R1	GCAGAGCCTGGGAAATAG	gma-Aldrich
ms1 F	GATTTGCCTTTGCTGACA	gma-Aldrich
ms1 R	CCTCTGTAAGTGGATGC	gma-Aldrich
spase3	n_Casp3_2_SG QT01164779	agen
spase6	n_Casp6_2_SG QT00494921	agen
spase7	n_Casp7_1_SG QT01058085	agen
spase9	n_Casp9_1_SG QT00133280	agen
spase12	n_Casp12_2_SG QT00495376	agen
p	n_Hspa5_1_SG QT00172361	agen
iop10	n_Ddit3_2_SG QT01749748	agen
rk	n_Eif2ak3_1_SG QT00147329	agen
pdh	n_Gapdh_3_SG QT01658692	agen

2.6. Organotypic culture

The retinas were transferred, with retinal pigmented epithelium side down, to a nitrocellulose culture membrane (catalogue number PICMORG50; Millipore, Molsheim, France) and cultivated as previously described (Mockel et al., 2012). Specific gene silencing with lentiviruses that carried a shRNA sequence for Alms1 (catalogue numbers sc108080 (Ctl), sc-72345-V (Alms1)); Santa Cruz Biotechnology, Tebu Bio, Yvelines, France) was performed by adding 20 μl of a viral suspension containing 10^5 infectious units to the culture medium overnight. The infected explants were then washed and cultured for 3 days, with half the medium refreshed daily. Explants were not maintained longer in culture to avoid unspecific apoptosis in the different retinal layers.

2.7. Statistical analysis

Student's t-test (two-tailed) was applied to all data (two samples). Statistical tests were performed using GraphPad/Prism version 5. All data in bar charts show mean ± SEM. $p < 0.05$ is considered to have significant differences.

Results

3.1. Bbs classical retinal apoptotic phenotype

To assess if mutations in other BBS proteins were inducing RD through the same pro-apoptotic pathophysiological mechanism as the one associated with Bbs12 (Mockel et al., 2012), two BBS models, Bbs10$^{-/-}$ mice model and Bbs1$^{M390R/M390R}$ mice model have been characterized and compared. The retinal phenotype for Bbs1 M390R/M390R has been previously characterized (Davis et al., 2007). In both mice models, histology and RNA analysis were performed on 14-daysold retinas and ERG were performed on 3-month-old mice. 3-month-old Bbs10$^{-/-}$ mice showed a significant decrease in light detection capacity measured by ERG compared to control mice (Fig. 1A). Toluidinblue staining showed that 14-days-old Bbs10$^{-/-}$ retina present a significant reduction of the retinal thickness in IS, OS, ONL and INL compared to wild type mice (Fig. 1B, Supplementary Fig. 2A) associated to a decreased of the number of ONL nuclei (Supplementary Fig. 2A). The outer and inner segments of the photoreceptors are completely disorganized but with a correctly formed axonemal microtubules in the connecting cilium as observed by T.E.M (Fig. 1B, Supplementary Fig. 2B) and previously described in Bbs10$^{-/-}$ mice (Cognard et al., 2015) and in other BBS mouse models (Davis et al., 2007; Dilan et al., 2018; Hsu et al., 2017; Mockel et al., 2012). In 14-days-old Bbs10$^{+/+}$ control retinas, rhodopsin was localized in the OS, while rhodopsin is mislocalized in the IS and the ONL in Bbs10$^{-/-}$ retinas (Fig. 1C, Supplementary Fig. 2C). The mRNA levels of key UPR proteins were
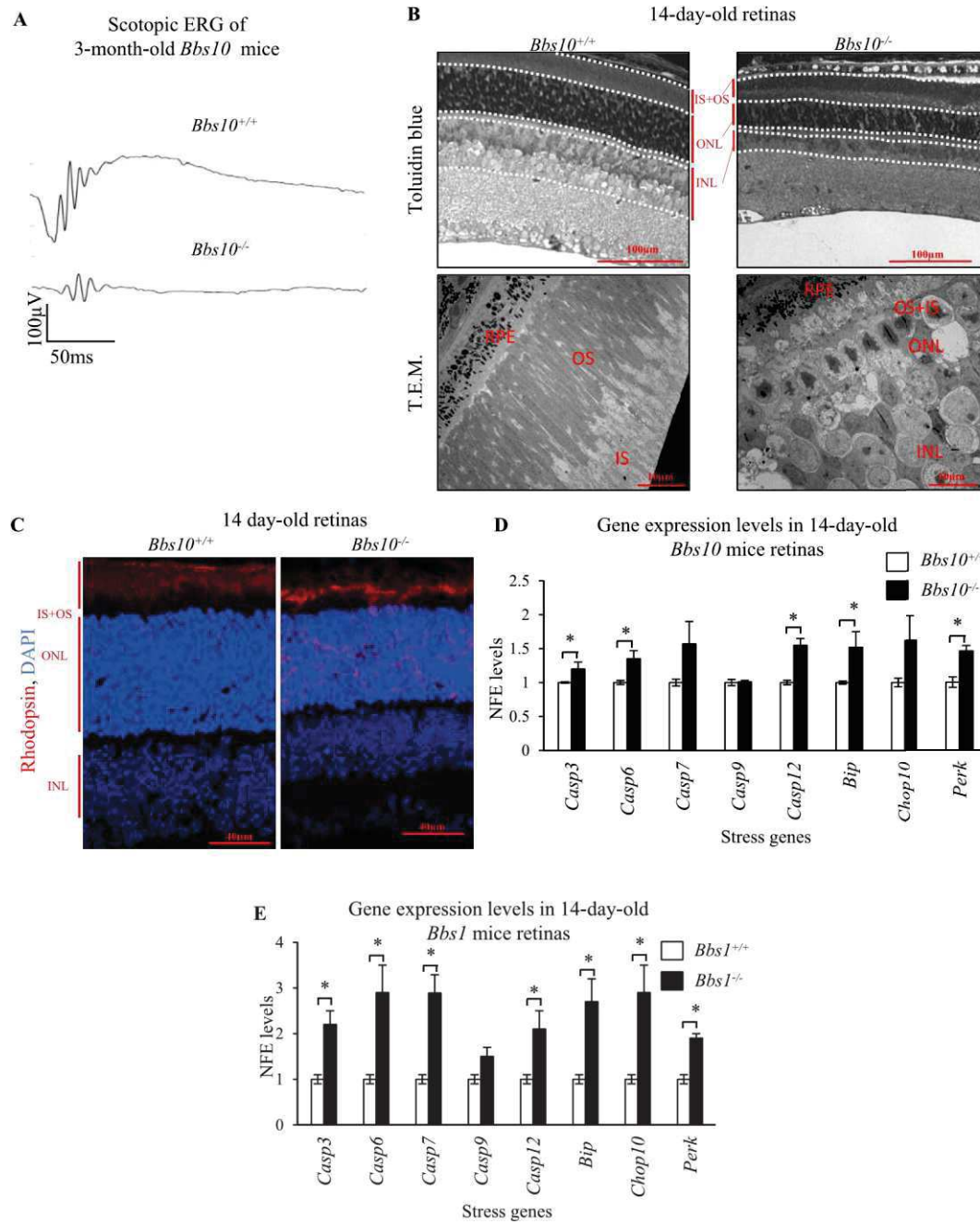
Fig. 1. Retinal phenotype and molecular characterization of Bbs10 and Bbs1 mice.

A) Scotopic ERG of 3-month-old Bbs10 mice (n = 5), *: P ≤ 0.05; B) Toluidin blue staining (Scale bar: 100 μm) and transmission electron microscope (T.E.M) (Scale bar: 10 μm) of 14-day-old Bbs10 mice retinas (n =3). RPE: Retinal Pigment Epithelium, OS: Outer Segment: IS: Inner segment, ONL: Outer Nuclear Layer, INL: Inner Nuclear Layer; C) Immunofluorescence of rhodopsin (red) and counterstained nuclei in DAPI on 14-day-old Bbs10 mice.(n =3) (Scale bar: 40 μm); D) Stress genes normalized fold expression (NFE) in 14-day-old Bbs10 mice (n = 3), *: P ≤ 0.05; E) Stress genes NFE in 14-day-old Bbs1 mice (n = 3), *: P ≤ 0.05. (For interpretation of the references to colour in this figure legend, the reader is referred to the Web version of this article.)

measured in 14-day-old Bbs10$^{-/-}$ mice retinas. Endoplasmic reticulum (ER) stress genes such as Bip and Perk, are significantly increased in Bbs10$^{-/-}$ mice retinas. Caspase 12 along with other caspase effectors like Caspase 3 and Caspase 6 are also significantly increased (Fig. 1D). Similarly, we characterized the Bbs1 $^{-/-}$ mice to confirm the UPR activation as a common mechanism in BBS models. The Bbs1$^{-/-}$ mouse model (Davis et al., 2007) exhibits similar retinal degeneration as the other tested BBS model (Bbs10 and 12) (Mockel et al., 2012). The UPR related set of genes was also upregulated in the 14-day-old Bbs1$^{M390R/M390R}$ retina (Fig. 1E) as in Bbs10 $^{-/-}$ retina. These data indicate that

the inactivation of the BBS1 protein of the Bbsome triggers the same pro-apoptotic pathway as BBS10.

3.2. LCA-Cep290-mouse model shares the same pro-apoptotic, UPR-mediated mechanism with the Bbs

To verify if this LCA mouse model could share the same pro-apoptotic mechanism as BBS as part of the ciliopathy family, the same experimental approach than BBS was used. At 1-month-old, no ERG signal was detected in Cep290$^{-/-}$ mice. (Fig. 2A). Histological studies at 14 postnatal days on Toluidin-blue stained sections showed a disruption and thinning of retinal layers (IS/OS and ONL) in the Cep290$^{-/-}$ retina
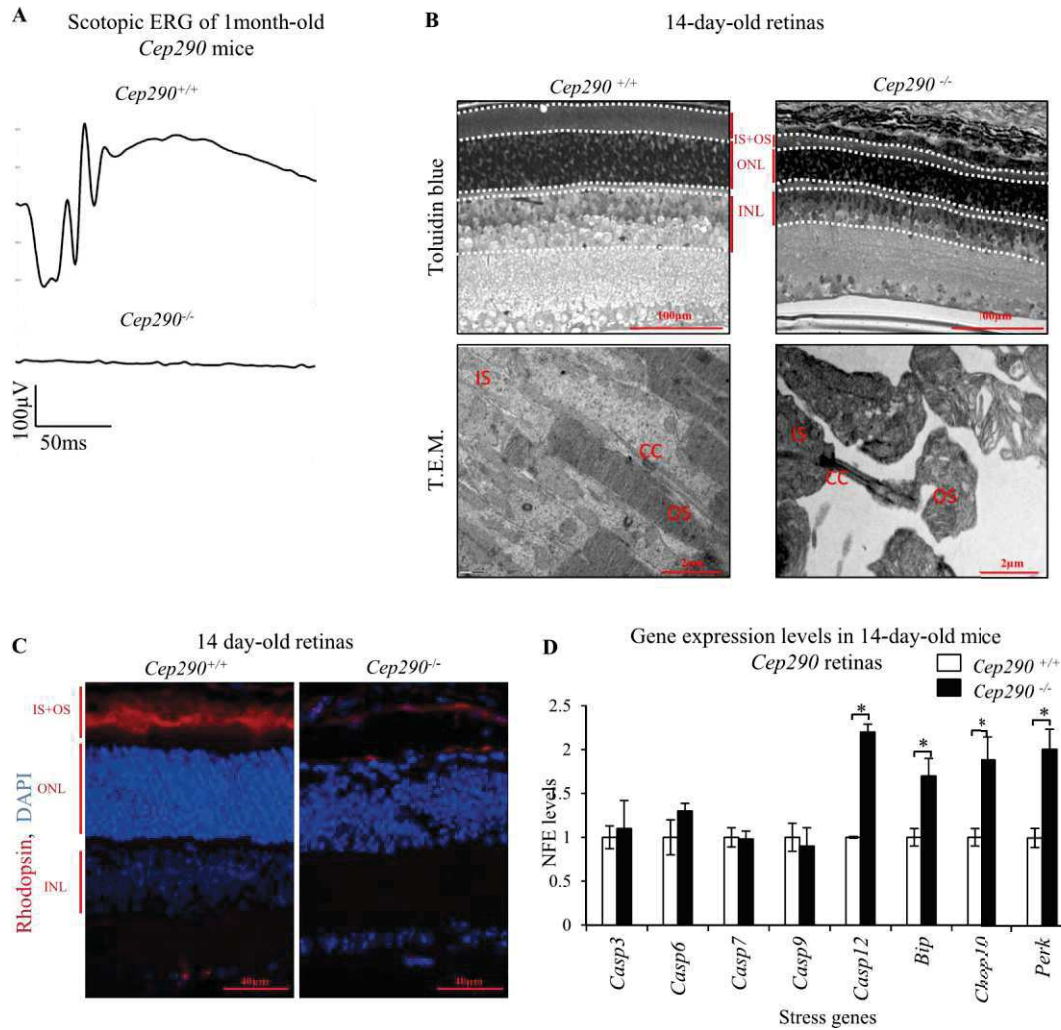
Fig. 2. Retinal phenotype and molecular characterization of Cep290^{-/-} mice.

A) Scotopic ERG of 1-month-old Cep290 mice (n =3); B) Toluidin blue staining (Scale bar: 100 μm) and T.E.M (Scale bar: 2 μm) of 14-day-old Cep290 mice retinas. (n =3) OS: Outer Segment: IS: Inner segment, ONL: Outer Nuclear Layer, INL: Inner Nuclear Layer, CC: Conecting Cilium; C) Immunofluorescence of rhodopsin (red) and counterstained nuclei in DAPI on 14-day-old Cep290 mice.(n =3) (Scale bar: 40 μm).). The space between the RPE and the OS is due a detachment of the RPE during preparation.; D) Stress genes NFE in 14-day-old Cep290 mice retinas *: P ≤ 0.05. (For interpretation of the references to colour in this figure legend, the reader is referred to the Web version of this article.)

(Fig. 2B, Supplementary Fig. 3A). A decrease of nuclei number in the ONL of Cep290^{-/-} retina has been observed but it was not statistically significant. T.E.M. analysis revealed the presence of a normal axomal microtubules of the connecting cilium without intact photoreceptors outer segment (Fig. 2B, Supplementary Fig. 3B), which correlates with no ERG signal in Cep290^{-/-} mice. On 14-day-old Cep290^{+/+} control retinas, immunostaining for rhodopsin showed that rhodopsin localizes in the OS. In contrast, on 14-day-old Cep290^{-/-} retinas, rhodopsin was observed in the limits between IS and ONL and in the ONL (Fig. 2C, Supplementary Fig. 3C). The exact location is complicated pinpoint as the IS and OS are severely decreased. At this same age, an upregulation of key genes of the UPR pathway namely Bip, Chop10, Perk and Caspase12 (Fig. 2D) is also observed in the retinas of Cep290^{-/-} mice.

3.3. Alms1 foz/foz retinal degeneration phenotype

Next, we focused on the retinal phenotype associated with the ALMS syndrome. We investigated the retinal phenotype in the spontaneous mutant mouse line, the Fattie Aussie mouse (Alms1foz/foz) (Arsov et al., 2006). Interestingly, the ERG measurements in 1-month-old Alms1foz/foz mice did not present any significant attenuation of scotopic ERG responses compared to wild

type mice at the same age (Fig. 3A). The ERGs were consistent with the retinal morphology; no difference in retinal thickness was observed in 1-month-old Alms1foz/foz versus control Alms1+/+ on retinas H&E staining (Fig. 3B and C). On the other hand, flat electroretinograms were obtained in 1-year-old Alms1foz/foz (Fig. 3D), suggesting a slow degenerative process of the retina. Concomitantly, significant thinning of the IS/OS and ONL was measured in 1-year-old Alms1foz/foz (Fig. 3E and F). In order to identify any temporal tipping point in the ALMS-related retinal phenotype, we monitored the a-wave amplitude of scotopic ERGs, through time over a 9-month period (Fig. 3G). Interestingly, the a-wave amplitude of the Alms1foz/foz rapidly decreased through time. By plotting the a-wave amplitude evolution for the two genotypes, we identified an intersecting point at 7 weeks. We thus started focusing on the Alms1foz/foz retinas at 7 weeks postnatal. T.E.M analysis of the Alms1foz/foz photoreceptors revealed swelling of the IS together with the presence of vacuoles in the cytoplasm as indicated by asterisks (Fig. 4A) and an intact axonemal structure of the connecting cilium in photoreceptors (Supplementary Fig. 4A). Rhodopsin transport was maintained in Alms1foz/foz retina, as rhodopsin was primarily detected in the OS of the photoreceptor (Fig. 4B, Supplementary Fig. 4B). Real-time PCR on the 7-week-old
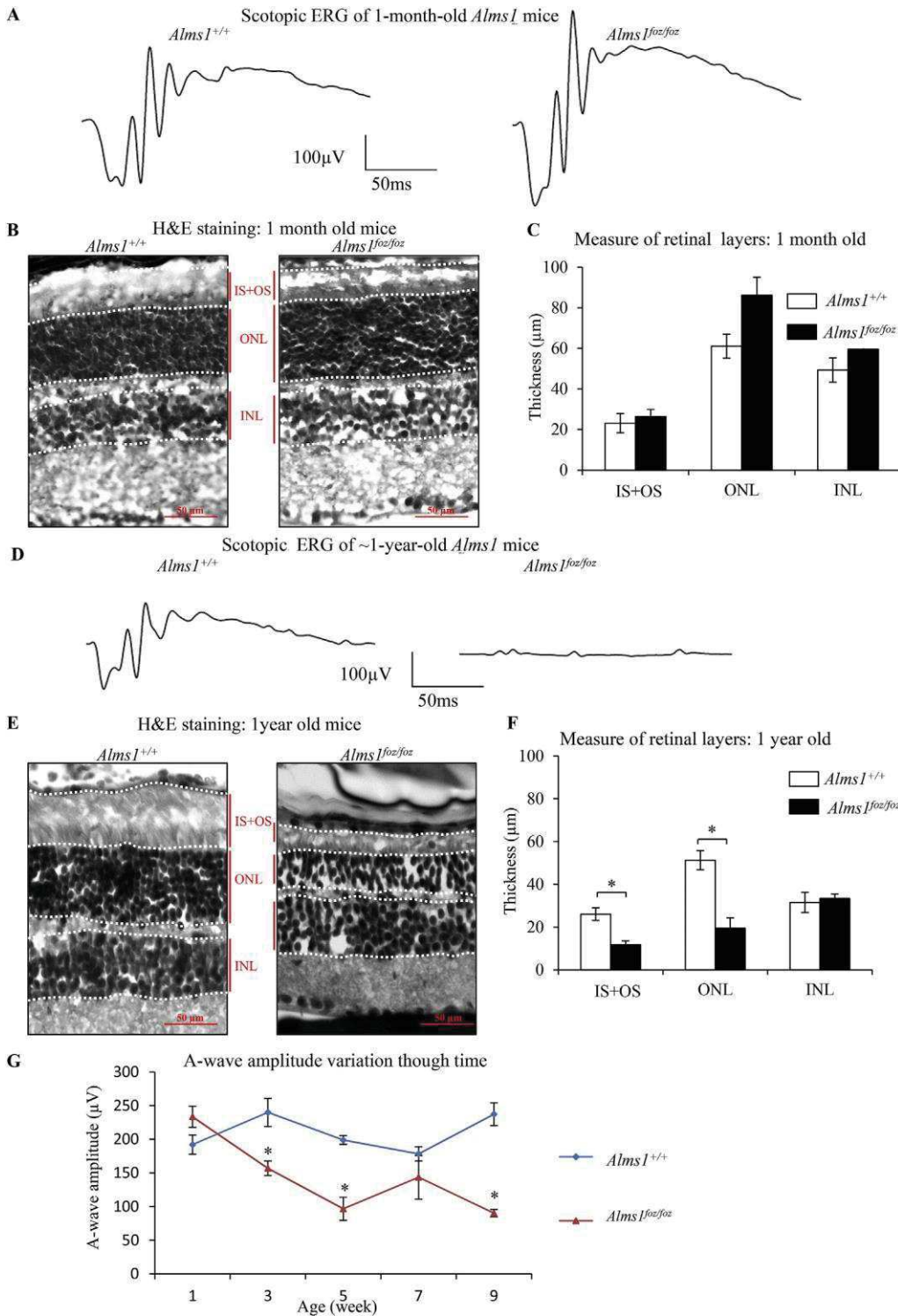
III. Results

A Scotopic ERG of 1-month-old *Alms1* mice

Alms1^{+/+}   *Alms1*[foz/foz]

100μV
50ms

B H&E staining: 1 month old mice

Alms1^{+/+}   *Alms1*[foz/foz]

IS+OS
ONL
INL
50 μm   50 μm

C Measure of retinal layers: 1 month old

Alms1^{+/+}
Alms1[foz/foz]

D Scotopic ERG of ~1-year-old *Alms1* mice

Alms1^{+/+}   *Alms1*[foz/foz]

100μV
50ms

E H&E staining: 1year old mice

Alms1^{+/+}   *Alms1*[foz/foz]

IS+OS
ONL
INL
50 μm   50 μm

F Measure of retinal layers: 1 year old

Alms1^{+/+}
Alms1[foz/foz]

G A-wave amplitude variation though time

Alms1^{+/+}
Alms1[foz/foz]

Fig. 3. Retinal phenotype and molecular characterization of Alms1[foz/foz] mice.
A) Scotopic ERGs recording showed retinal function of Alms1^{+/+} and Alms1[foz/foz] mice at 1 month-old. B&C). H&E staining (Scale bar: 50 μm) and retinal thickness measurement of 1 month-old Alms1^{+/+} and Alms1[foz/foz] mice retinas (n =3) OS: Outer Segment: IS: Inner segment, ONL: Outer Nuclear Layer, INL: Inner Nuclear Layer; D) Scotopic ERGs recording showed retinal function of Alms1^{+/+} and Alms1[foz/foz] mice at 1-year-old. E& F) H&E staining (Scale bar: 50 μm) and retinal thickness measurement of 1year-old Alms1^{+/+} and Alms1[foz/foz] mice retinas (n = 3), *: P ≤ 0.05. G) Evolution of the ERG a-wave amplitude as a function of age for Alms1^{+/+} and Alms1[foz/foz] mice.

retinas for the key UPR genes did not show any significant difference in expression level in Alms1[foz/foz] (Fig. 4C) suggesting that the associated phenotype was not linked to the UPR pathways.

Next, we used the organotypic culture approach and culture 14-dayold WT retinas to knock-down Alms1 using a lentiviral approach as previously performed (Mockel et al., 2012). 3 days post-infection, realtime PCR analysis showed a 40% decrease in Alms1 expression level (Fig. 4D) with no difference in expression level of the key UPR-related genes (Fig. 4E) as expected without total absence of Alms1. The ALMSmediated retinal degeneration in the Alms1[foz/foz] mice is not primarily UPR-related.

Discussion

RD associated with ciliopathies leads to major visual impairment and understanding the underlying pathogenesis is a prerequisite to define therapeutic options. Describing the pro-apoptotic mechanism underlying ciliopathy-related RD will help to design the therapeutic agents that could hamper the degeneration. With this aim, we studied different murine models for three emblematic ciliopathies, and
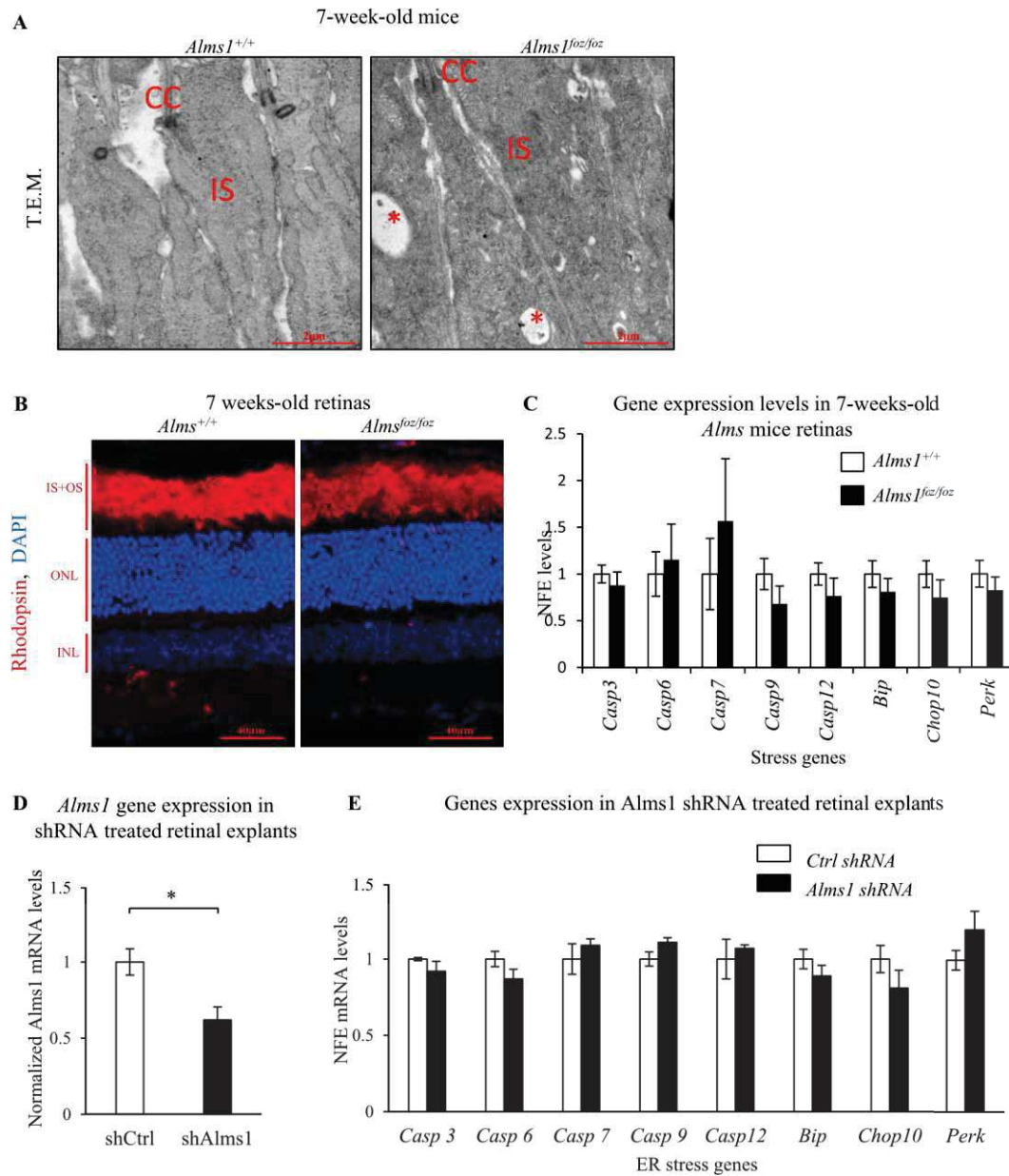
Fig. 4. Ultrastructure of retinas and pathogenic genes expression in 7-week-old Alms1$^{foz/foz}$ mice retinas.

A) T.E.M. of 7-week-old Alms1 mice retina (n = 3) (Scale bar: 2 µm), asterisks indicate the presence of vacuoles in the IS cytoplasm CC: Connecting Cilium; B) Immunofluorescence of localization of rhodopsin (red) and counterstained nuclei in DAPI at 7-week-old on Alms1 mice retina. (n = 3) (Scale bar: 40 µm). OS: Outer Segment: IS: Inner segment, ONL: Outer Nuclear Layer, INL: Inner Nuclear Layer; C) ER stress genes expressions in 7 week-old Alms1 mice retina (n =3). D) Alms1 gene expression in shRNA treated retinal explants (n = 3), *: P ≤ 0.05. E) Stress genes NFE in Alms1 shRNA treated retinal explants (n = 3), *: P ≤ 0.05. (For interpretation of the references to colour in this figure legend, the reader is referred to the Web version of this article.)

interestingly we could differentiate between UPR-related RD, including the Cep290-LCA and three tested BBS mouse models, and non-UPRrelated RDs, namely the ALMS mouse model. Interestingly, the progression rate and the severity of the retinal phenotype in these different mouse models of ciliopathies might be related the UPR pathway as indeed the two UPR-related ciliopathies (BBS and LCA) showed a faster retinal degeneration compared to the ALMS UPR-independent ciliopathies.

Our results showed that, associated to Rhodopsin trafficking defect, key components of the ER stress response were upregulated on the transcriptional level that depicts a common mechanism linked to retinal degeneration in BBS syndromes and LCA, the Bbs1 $^{M390R/M390R}$ mice, Bbs10$^{-/-}$ mice and Cep290$^{-/-}$ mice models used herein; although further studies are required to verify this impact on the posttranscriptional level. These mechanisms were also present in Bbs12$^{-/-}$ mice model, in the Rd16 mouse model; a LCA mice model (Mockel et al., 2012; Starr et al., 2018). In Bbs4$^{-/-}$ mice models ER stress has not been

reported to date even though a Rhodopsin trafficking is already known (Abd-El-Barr et al., 2007). Moreover, the Cep290$^{-/-}$ mouse model of LCA was also shown to present ER stress similar to the BBS models showing a possible common mechanism for the RD. Bbs10$^{-/-}$ and Cep290$^{-/-}$ show a decrease of the different retinal layers at 14 days depicting nuclei loss; with a more significant decrease in Bbs10$^{-/-}$ compared to Cep290$^{-/-}$. This more aggressive BBS phenotype correlates with a significant drop in nuclear count compared to a smaller drop in Cep290. On the other hand, the related phenotype in ALMS model seems UPR unrelated as no upregulation of key players for UPR was observed. Other recent studies suggested that retinopathy in the Alström syndrome might be linked to a defect in the phototransduction cascade (Hostelley et al., 2016). Indeed the related genes were upregulated in embryos of Alms1 mutant zebrafish, while this was not significant in BBS1 mutant zebrafish (Hostelley et al., 2016). We also showed that while all retina layers are decreased

in the 14-day-old Bbs10$^{-/-}$ and Cep290$^{-/-}$ mice, the INL is not decreased in the Alms1$^{foz/foz}$ mice. It could be caused by a delay in the retinal degeneration and we may hypothesize that the INL will be decrease at a later stage on the disease.

The results above further indicate that retinopathy in ciliopathies may be caused by different mechanisms albeit they exhibit similarity and overlap of retinal phenotypes, and clinical intervention in the future should be given based on precise mechanism dissection. It is known that the retinal phenotypes of ciliopathies show large heterogeneity within the same diseases (Scheidecker et al., 2015). For example, it is well known that the BBS syndrome is a genetically heterogeneous disease. Clinical observation showed that BBS1 patients display a milder and a relatively slower rate of retinal degeneration than that caused by other BBS gene mutations (Daniels et al., 2012); an hypothesis that is supported by the fact that Bbs1$^{M390R/M390R}$ knock-in mice exhibit a relatively slow rate of retinal degeneration compared to other BBS mice models (Cognard et al., 2015; Davis et al., 2007; Mockel et al., 2012). For the LCA, the retinal phenotypes of mouse models of LCA caused by different mutations in different genes (not all associated with ciliopathies) showed large variability in the onset and the courses of diseases, the manifestations of retinal fundus, the pattern of dystrophy (cone-rod dystrophy or rod-cone dystrophy).

The major findings here suggest that it is likely to develop a common therapeutic strategy for retinal dystrophy when ER stress is present, regardless of the causing mutation. In our previous research we demonstrated that treatment targeted at ER stress using GIVin could rescue retinal function and retinal morphology in Bbs12$^{-/-}$ mice (Mockel et al., 2012). Other studies have also aimed at developing treatment options for common processes instead of targeting directly the defective gene, this is the case of tauroursodeoxycholic acid (TUDCA) or antioxidants (Drack et al., 2012; Komeima et al., 2007). The vast heterogeneity of the mutations causing RP coupled with the fact that there is not always a proper genetic diagnostic for all the patients make targeted gene therapy a difficult approach. Therefore, the study and development of drugs that can be used in several RP causing situations might be the best option for maintaining PR function for as long as possible, creating a wider therapeutic window for the use of specific treatments for the causing mutations or allowing a better genetic diagnosis in patients with uncommon mutations where the causing defect has not been determined.

Conflicts of interest

All authors declare no conflict of interest.

Acknowledgements

Appendix A. Supplementary data

Supplementary data to this article can be found online at https://doi.org/10.1016/j.exer.2019.107721.

References

Abd-El-Barr, M.M., Sykoudis, K., Andrabi, S., Eichers, E.R., Pennesi, M.E., Tan, P.L., et al., 2007. Impaired photoreceptor protein transport and synaptic transmission in a mouse model of Bardet-Biedl syndrome. Vis. Res. 47 (27), 3394–3407. https://doi.org/10.1016/j.visres.2007.09.016.

Adams, N.A., Awadein, A., Toma, H.S., 2007. The retinal ciliopathies. Ophthalmic Genet. 28 (3), 113–125. https://doi.org/10.1080/13816810701537424.

Arsov, T., Silva, D.G., O'Bryan, M.K., Sainsbury, A., Lee, N.J., Kennedy, C., et al., 2006. Fat aussie–a new Alstrom syndrome mouse showing a critical role for ALMS1 in obesity, diabetes, and spermatogenesis. Mol. Endocrinol. 20 (7), 1610–1622. https://doi.org/10.1210/me.2005-0494.

Bujakowska, K.M., Liu, Q., Pierce, E.A., 2017. Photoreceptor cilia and retinal ciliopathies. Cold Spring Harb. Perspect. Biol. https://doi.org/10.1101/cshperspect.a028274.

Cognard, N., Scerbo, M.J., Obringer, C., Yu, X., Costa, F., Haser, E., et al., 2015. Comparing the Bbs10 complete knockout phenotype with a specific renal epithelial knockout one highlights the link between renal defects and systemic inactivation in mice. Cilia 4, 10. https://doi.org/10.1186/s13630-015-0019-8.

Cui, C., Chatterjee, B., Lozito, T.P., Zhang, Z., Francis, R.J., Yagi, H., et al., 2013. Wdpcp, a PCP protein required for ciliogenesis, regulates directional cell migration and cell polarity by direct modulation of the actin cytoskeleton. PLoS Biol. 11 (11), e1001720. https://doi.org/10.1371/journal.pbio.1001720. PBIOLOGY-D-13-03195 [pii].

Daniels, A.B., Sandberg, M.A., Chen, J., Weigel-DiFranco, C., Fielding Hejtmancic, J., Berson, E.L., 2012. Genotype-phenotype correlations in Bardet-Biedl syndrome. Arch. Ophthalmol. 130 (7), 901–907. https://doi.org/10.1001/archophthalmol.2012.89 archophthalmol.2012.89.

Davis, R.E., Swiderski, R.E., Rahmouni, K., Nishimura, D.Y., Mullins, R.F., Agassandian, K., et al., 2007. A knockin mouse model of the Bardet-Biedl syndrome 1 M390R mutation has cilia defects, ventriculomegaly, retinopathy, and obesity. Proc. Natl. Acad. Sci. U. S. A. 104 (49), 19422–19427. https://doi.org/10.1073/pnas.0708571104.

Dilan, T.L., Singh, R.K., Saravanan, T., Moye, A., Goldberg, A.F.X., Stoilov, P., Ramamurthy, V., 2018. Bardet-Biedl syndrome-8 (BBS8) protein is crucial for the development of outer segments in photoreceptor neurons. Hum. Mol. Genet. 27 (2), 283–294. https://doi.org/10.1093/hmg/ddx399.

Drack, A.V., Dumitrescu, A.V., Bhattarai, S., Gratie, D., Stone, E.M., Mullins, R., Sheffield, V.C., 2012. TUDCA slows retinal degeneration in two different mouse models of retinitis pigmentosa and prevents obesity in Bardet-Biedl syndrome type 1 mice. Investig. Ophthalmol. Vis. Sci. 53 (1), 100–106. https://doi.org/10.1167/iovs.118544.

Estrada-Cuzcano, A., Roepman, R., Cremers, F.P., den Hollander, A.I., Mans, D.A., 2012. Non-syndromic retinal ciliopathies: translating gene discovery into therapy. Hum. Mol. Genet. 21 (R1), R111–R124 dds298 [pii] 10.1093/hmg/dds298.

Garanto, A., Duijkers, L., Collin, R.W., 2015. Species-dependent splice recognition of a cryptic exon resulting from a recurrent intronic CEP290 mutation that causes congenital blindness. Int. J. Mol. Sci. 16 (3), 5285–5298. https://doi.org/10.3390/ijms16035285.

Hamel, C., 2006. Retinitis pigmentosa. Orphanet J. Rare Dis. 1, 40 1750-1172-1-40 [pii] 10.1186/1750-1172-1-40.

Heon, E., Kim, G., Qin, S., Garrison, J.E., Tavares, E., Vincent, A., et al., 2016. Mutations in C8ORF37 cause Bardet-Biedl syndrome (BBS21). Hum. Mol. Genet. 25 (11), 2283–2294. https://doi.org/10.1093/hmg/ddw096.

Hostelley, T.L., Lodh, S., Zaghloul, N.A., 2016. Whole organism transcriptome analysis of zebrafish models of Bardet-Biedl Syndrome and Alstrom Syndrome provides mechanistic insight into shared and divergent phenotypes. BMC Genomics 17, 318. https://doi.org/10.1186/s12864-016-2679-1.

Hsu, Y., Garrison, J.E., Kim, G., Schmitz, A.R., Searby, C.C., Zhang, Q., et al., 2017. BBSome function is required for both the morphogenesis and maintenance of the photoreceptor outer segment. PLoS Genet. 13 (10), e1007057. https://doi.org/10.1371/journal.pgen.1007057.

Knorz, V.J., Spalluto, C., Lessard, M., Purvis, T.L., Adigun, F.F., Collin, G.B., et al., 2010. Centriolar association of ALMS1 and likely centrosomal functions of the ALMS motifcontaining proteins C10orf90 and KIAA1731. Mol. Biol. Cell 21 (21), 3617–3629. https://doi.org/10.1091/mbc.E10-03-0246 E10-03-0246. ([pii]).

Komeima, K., Rogers, B.S., Campochiaro, P.A., 2007. Antioxidants slow photoreceptor cell death in mouse models of retinitis pigmentosa. J. Cell. Physiol. 213 (3), 809–815. https://doi.org/10.1002/jcp.21152.

Marshall, J.D., Beck, S., Maffei, P., Naggert, J.K., 2007. Alstrom syndrome. Eur. J. Hum. Genet. 15 (12), 1193–1202. https://doi.org/10.1038/sj.ejhg.5201933.

Mattapallil, M.J., Wawrousek, E.F., Chan, C.C., Zhao, H., Roychoudhury, J., Ferguson, T.A., Caspi, R.R., 2012. The Rd8 mutation of the Crb1 gene is present in vendor lines of C57BL/6N mice and embryonic stem cells, and confounds ocular induced mutant phenotypes. Investig. Ophthalmol. Vis. Sci. 53 (6), 2921–2927. https://doi.org/10.1167/iovs.12-9662.

May-Simera, H., Nagel-Wolfrum, K., Wolfrum, U., 2017. Cilia - the sensory antennae in the eye. Prog. Retin. Eye Res. https://doi.org/10.1016/j.preteyeres.2017.05.001.

Mockel, A., Obringer, C., Hakvoort, T.B., Seeliger, M., Lamers, W.H., Stoetzel, C., et al., 2012. Pharmacological modulation of the retinal unfolded protein response in Bardet-Biedl syndrome reduces apoptosis and preserves light detection ability. J. Biol. Chem. 287 (44), 37483–37494. https://doi.org/10.1074/jbc.M112.386821.

Mockel, A., Perdomo, Y., Stutzmann, F., Letsch, J., Marion, V., Dollfus, H., 2011. Retinal dystrophy in Bardet-Biedl syndrome and related syndromic ciliopathies. Prog. Retin. Eye Res. 30 (4), 258–274. https://doi.org/10.1016/j.preteyeres.2011.03.001.

Nachury, M.V., Loktev, A.V., Zhang, Q., Westlake, C.J., Peranen, J., Merdes, A., et al., 2007. A core complex of BBS proteins cooperates with the GTPase Rab8 to promote ciliary membrane biogenesis. Cell 129 (6), 1201–1213 S0092-8674(07)00534-X [pii] 10.1016/j.cell.2007.03.053.

Reiter, J.F., Leroux, M.R., 2017. Genes and molecular pathways underpinning ciliopathies. Nat. Rev. Mol. Cell Biol. https://doi.org/10.1038/nrm.2017.60.

Russell, S., Bennett, J., Wellman, J.A., Chung, D.C., Yu, Z.F., Tillman, A., et al., 2017. Efficacy and safety of voretigene neparvovec (AAV2-hRPE65v2) in patients with RPE65-mediated inherited retinal dystrophy: a randomised, controlled, open-label, phase 3 trial. Lancet 390 (10097), 849–860. https://doi.org/10.1016/S01406736(17)31868-8.

Scheidecker, S., Hull, S., Perdomo, Y., Studer, F., Pelletier, V., Muller, J., et al., 2015. Predominantly cone-system dysfunction as rare form of retinal degeneration in patients with molecularly confirmed bardet-biedl syndrome. Am. J. Ophthalmol. 160 (2), 364–372. https://doi.org/10.1016/j.ajo.2015.05.007. e361.

Seo, S., Baye, L.M., Schulz, N.P., Beck, J.S., Zhang, Q., Slusarski, D.C., Sheffield, V.C., 2010. BBS6, BBS10, and BBS12 form a complex with CCT/TRiC family chaperonins and mediate

BBSome assembly. Proc. Natl. Acad. Sci. U. S. A. 107 (4), 1488–1493. https://doi.org/10.1073/pnas.0910268107 0910268107. ([pii]).

Sjostrand, F.S., 1953. The ultrastructure of the outer segments of rods and cones of the eye as revealed by the electron microscope. J. Cell. Physiol. 42 (1), 15–44. Retrieved from http://www.ncbi.nlm.nih.gov/pubmed/13084705.

Starr, C.R., Pitale, P.M., Gorbatyuk, M., 2018. Translational attenuation and retinal degeneration in mice with an active integrated stress response. Cell Death Dis. 9 (5), 484. https://doi.org/10.1038/s41419-018-0513-1.

Waters, A.M., Beales, P.L., 2011. Ciliopathies: an expanding disease spectrum. Pediatr. Nephrol. 26 (7), 1039–1056. https://doi.org/10.1007/s00467-010-1731-7.

Wright, A.F., Chakarova, C.F., Abd El-Aziz, M.M., Bhattacharya, S.S., 2010. Photoreceptor degeneration: genetic and mechanistic dissection of a complex trait. Nat. Rev. Genet. 11 (4), 273–284. https://doi.org/10.1038/nrg2717.

3.2. Results 2: MNPs for drug delivery to the retinal tissues

Some of the results shown here will be published on the paper "MNPs for drug delivery to the retinal tissues" that is currently in writing process. It will be submitted to the Journal of Biological Chemistry (JBC). This paper will contain my work as well as that of another PhD Student, Marco Bassetto whose thesis and work was carried on in OZ Bioscience.

3.2.1. Synopsis:

Previous studies in our laboratory have shown the possibility of modulating apoptosis caused by the UPR in $Bbs^{-/-}$ mice models. In order to improve the delivery of the compounds already studied by our group we have, in collaboration with OZ Bioscience in the frame of the Ocuther project, tested the use of MNPs guided by a magnet for the delivery of our compounds to the retina after topical application in the form of eyedrops. One single application of our treatment in 14-days old mice was enough to achieve significant increase of the ERG response in our treated mice 2 weeks after the application of the treatment. In addition to the increase in ERG response we were able to observe an improvement on the retinal structure of the treated mice as well as a modulation in the proteins targeted by our treatment, although for now we were only able to show a tendency. We also report the possible pathway followed by the MNPs after topical application with the magnet as observed by MRI and the distribution in the retinal tissues observed by TEM.

3.2.2. Magnetic nanoparticles formulation and characterization:

To understand how our treatment works it is necessary to know the characteristic of our MNPs such as size or surface charge as they define how the MNPS should behave as they cross the ocular tissues. We will briefly summarize part of the data obtained by Marco Basetto regarding the characterization of the MNPs.

2.2.1 Magnetic nanoparticles formulation

With the coprecipitation of iron salts in alkaline medium we were able to obtain two colloids with high iron content. These colloids respond to magnetic fields as we can observe that after magnet application there is a separation of the iron content of the colloid (Figure 10 A). To characterize the colloidal characteristics of the MNPs DLS was one of the methods used showing an average hydrodynamic diameter of less than 140 nm for both MNPs (Figure 10 C). The zeta potential of our MNPs was also studied in order to know if the surface coating was able to produce the desired electric charges. These experiments showed that NP01 is indeed anionic and NP02 is as expected, cationic.

2.2.2. Magnetic nanoparticles characterization

The chemical composition of the MNPs was investigated using X-Ray, both MNPs present the characteristic X-ray diffraction pattern of magnetite (Figure 10 B). In the case of NP02 we can also observe a minor contribution of ghoetite, another iron oxide salt. MNPs crystal size was derived from the X-Ray diffraction patterns and they correspond to 9-10 nm for both MNPs. This size was also observed in TEM experiments, where the MNPs were observed to be round shaped objects.
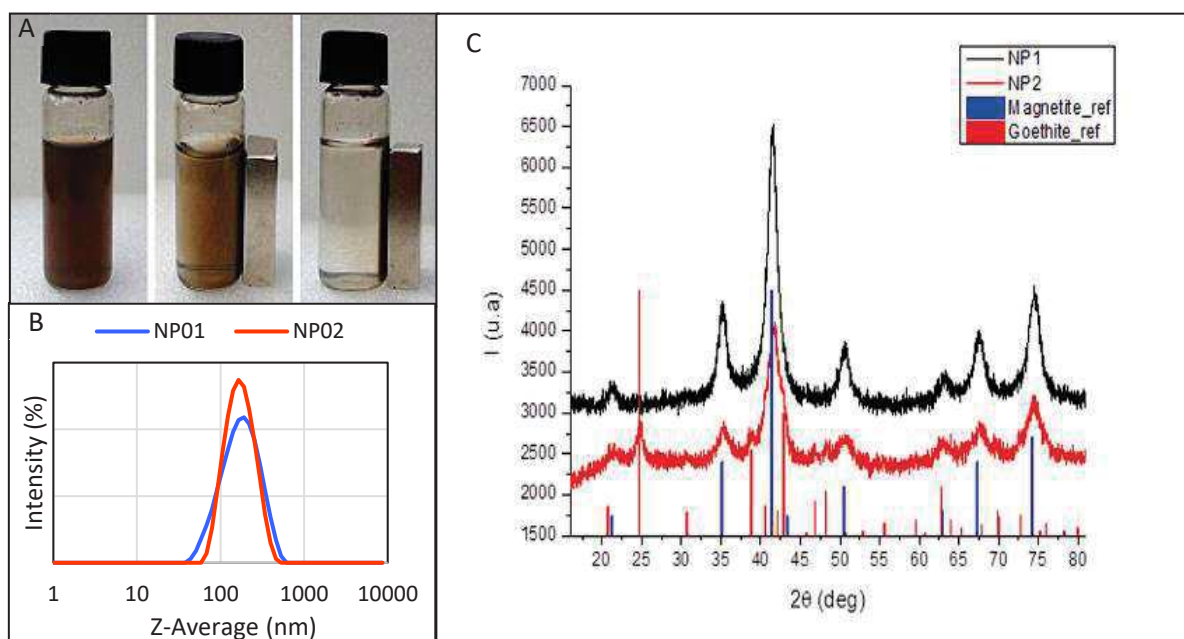
Figure 10: MNPs physico-chemical characterization. A shows horizontal magnetic separation of NP01 from the supernatant while exposed to a permanent magnetic field. B shows MNP's powder X-ray diffraction patterns. Both NP01 (black line) and NP02 (red line) have a crystalline core corresponding to magnetite (blue marks). In the case of NP02 (red line), it has been recorded also a minor presence of ghoetite (red marks). C shows the hydrodynamic diameter distribution of NP01 (Blue) and NP02 (orange) by DLS. Both MNPs are monodisperse with sizes (Z-average) under 140nm. Note that the horizontal axis is expressed in logarithmic scale.

The stability of the loaded MNPs in different buffers, each one alone and in a mix was studied using DLS. The mix of the anionic NP01 and the cationic NP02 was shown to be stable with only a minimum aggregation observed (Figure 11). Drug loading of the MNPs did not show any difference in the hydrodynamic size distribution, meaning that the loading of our compounds does not affect the colloidal properties of the MNPs.
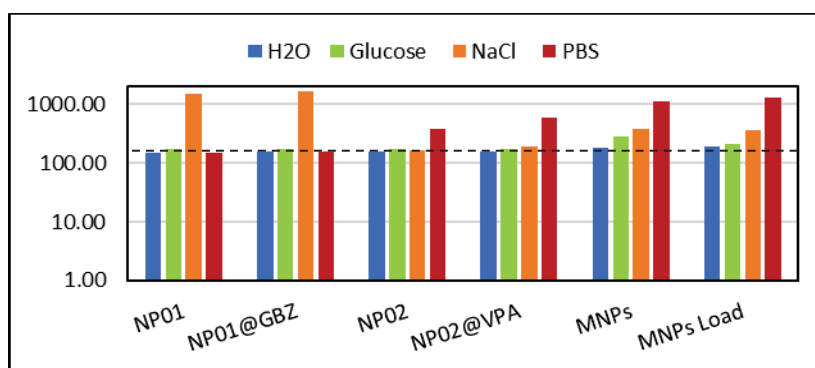
Figure 11: MNPs stability in the major physiological buffers. Comparison of MNPs hydrodynamic diameter in water (blue), glucose 5% (green), NaCl 0.9% (orange) and PBS (red). The black dashed line has been set at NP01 and NP02 size values in water. Note that the vertical axis is expressed in logarithmic scale.

Drug loading was measured using HPLC. This method shown that the MNPs at a concentration of 1 mg Fe/ml were able to load 4.5 µM of GBZ (on NP01) and 1.2 mM of VPA (On NP02) with a loading efficiency of 30% and 10% respectively (Figure 12).
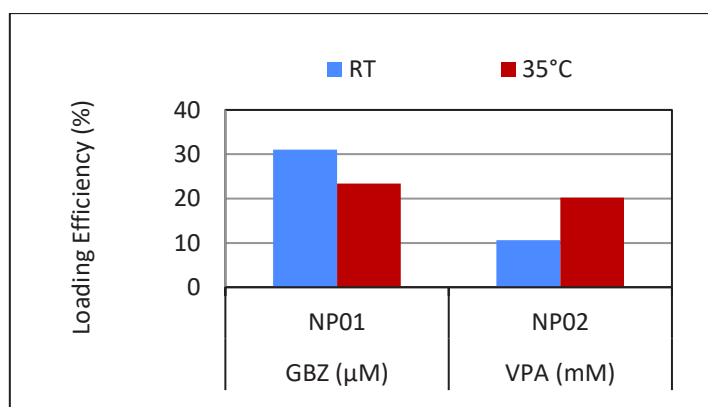

Figure 12: Drug Loading Efficiency. Effect of temperature on GBZ and VPA loading on NP01 and NP02 respectively.

3.3. *In vivo* MNPs testing:

3.2.3.1 Mobility and behaviour of the magnetic nanoparticles:

As we have mentioned before one of the most important question regarding our delivery route is: how would the MNPs behave and the pathway they follow through the tissues after topical application. While some publications study the movement of the MNPs inside the vitreous there is not much information regarding the movement in topical application and the possible effects of magnetic fields in the movement of the MNPs in general. In Figure 13 we can observe a representation of the planes we have used for MRI imaging.
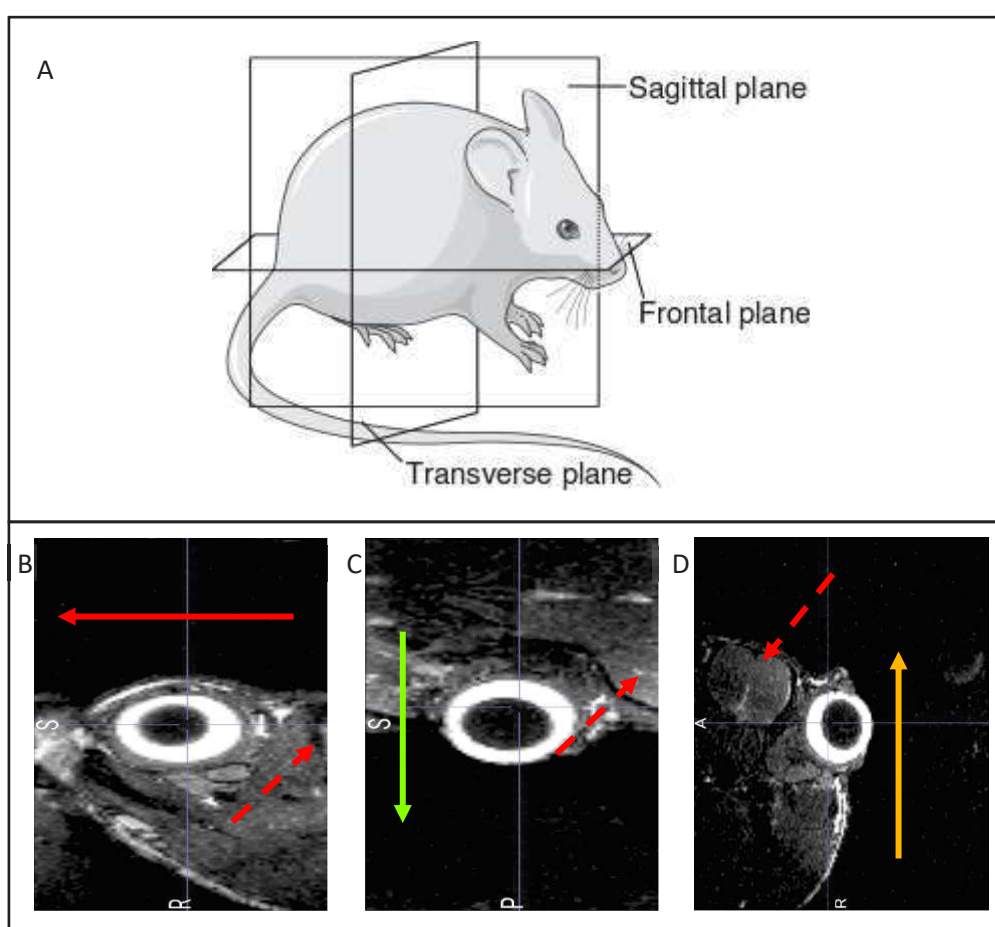

Figure 13. MRI acquisition planes. Representation of the different planes of the MRI images. A) Scheme of the planes used for the representation of our MRI images (image from Shahrokni et al. 2012). B) Sagittal plane. Red arrow shows the direction from the posterior portion to the anterior portion of the mice heads. C) Frontal plane. Green Arrow shows the direction from the medial portion of the head of the mice to the lateral portion. D) Transverse plane. Yellow arrow shows the direction from the inferior portion of the head of the mice to the superior portion. Red dashed arrow shows the brain of the mice.

3.2.3.2. Mobility of the MNPs after topical application:

After topical application of the MNPs we were able to see the MNPs using MRI. Due to the characteristics of the imaging technique and our MNPs we observe the MNPs as a black signal coming from the tissue (which is shown as white and grey). We compared the mobility between both of our MNPs and also the mobility of the mix of MNPs. In all the cases we observed the signal in a similar position, in a superior and anterior part of the eye globe (Figure 14) and closer to the midline of the mice. Our results seem to show that the surface charge of the MNPs does not influence the mobility of the MNPs as we can see similar distribution between all the treatment groups.
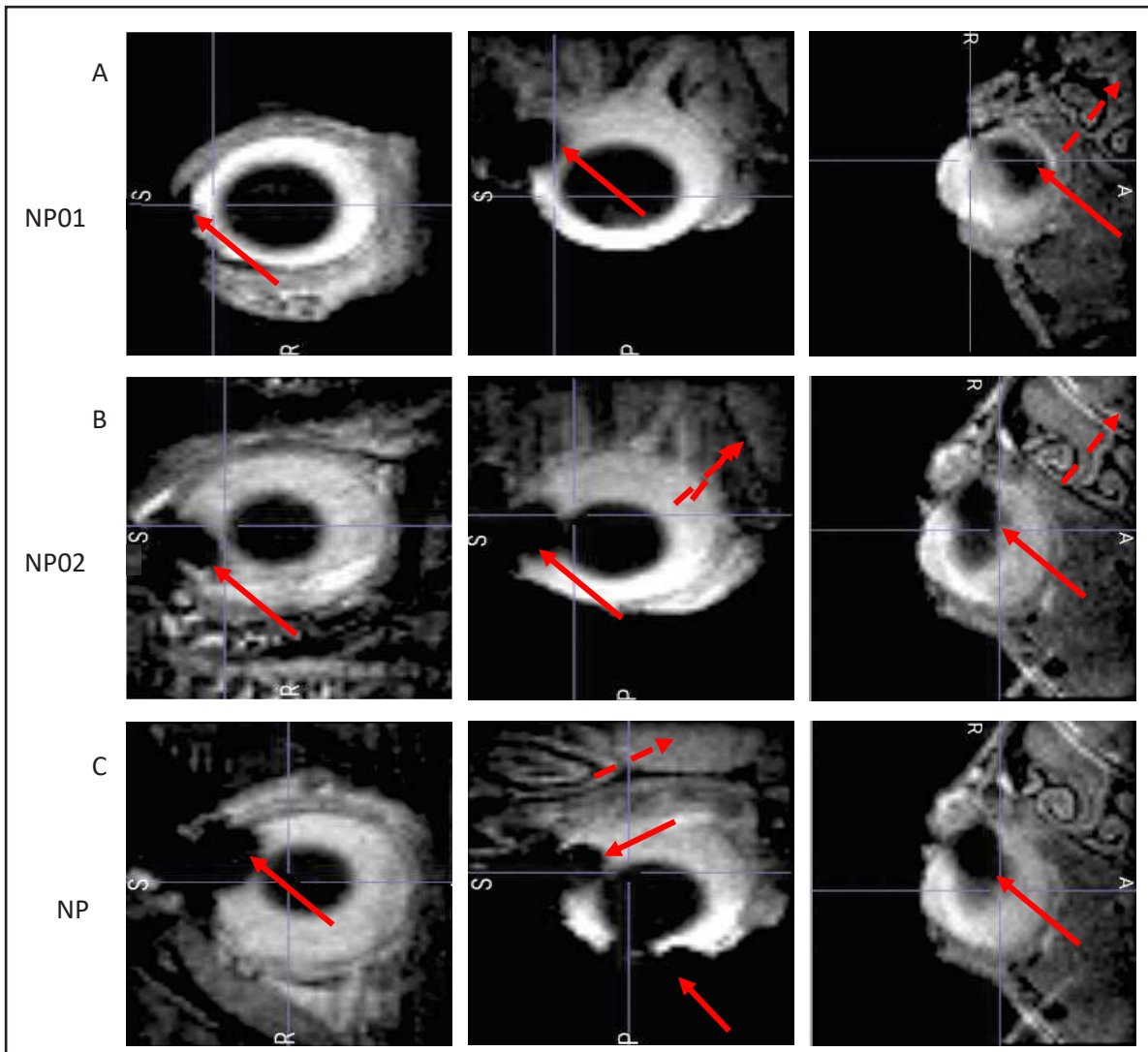
Figure. 14. Distribution of the topical treatment with MNPs*. MRI images of the different topical treatments applied. The order of the planes (from left to right) is sagittal, transvers and coronal. A) Different planes of the mice treated with NP01. B) Different planes of the mice treated with NP02. C) Different planes of the mice treated with the mixture of NP01 and NP02. Red arrow shows the MNPs. All the images were acquired using the RARE sequence of the MRI. Dashed arrow shows the position of the brain of the mice. Mice used were 2 months old.*

While most of the MNPs are on the same position, we have also noted that in some of the mice we could also see signal coming from what could be a position around the cornea of the eyes, meaning that not all the MNPs were moved along the surface of the eye but some of them seem to penetrate the tissue in this portion (Figure 15). We observed this secondary position for all our treated groups. Thus, neither the magnet nor the surface charge of the MNPs seem to affect the ability of the MNPs to cross to the anterior chamber.
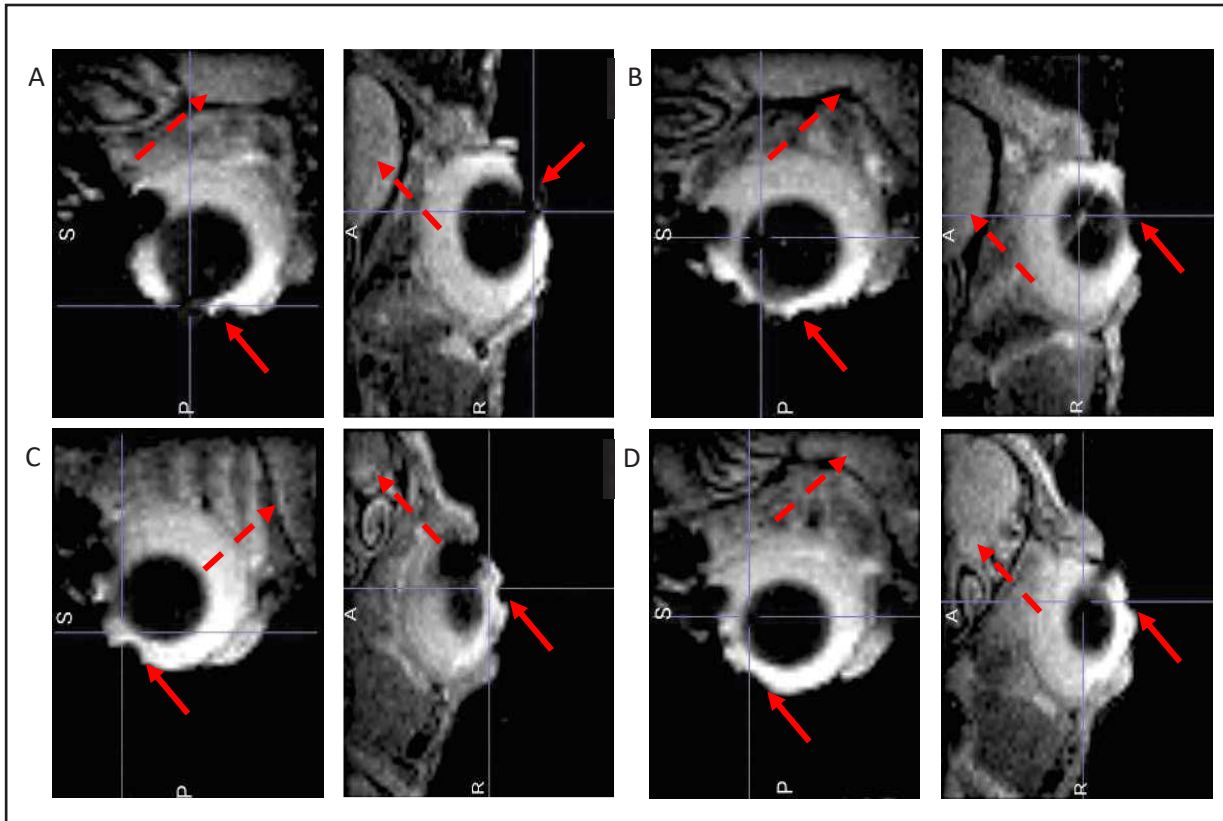

Figure 15. Presence of the MNPs in the anterior chamber. RARE sequence. Image showing the presence of MNPs on the portion corresponding to the cornea and the anterior chamber. Red arrows show the position of the MNPs. A) Shows the image from a mouse treated with the mix of MNPs and the magnet. B) Shows the images from a mouse treated with the mix of MNPs and no magnet. C) Shows the images from a mouse treated with NP01 and the magnet. D) shows the image from a mouse treated with NP02 and the magnet.

As part of our study of the mobility of the MNPs we tried to observe for how long would the MNPs stay in the ocular tissues or the tissues surrounding them. in this perspective, we also performed MRI one day after the topical application of the MNPs. Interestingly, we did not observe any signal the day after the application of the magnet (Figure 16). This was the case for all the applied MNPs and for the mice treated with or without the magnet. This was observed if the MNPs were washed away from the tissue

or distributed in the tissue meaning that the signal emitted by the MNPs could be lower than the threshold of for the MRI.

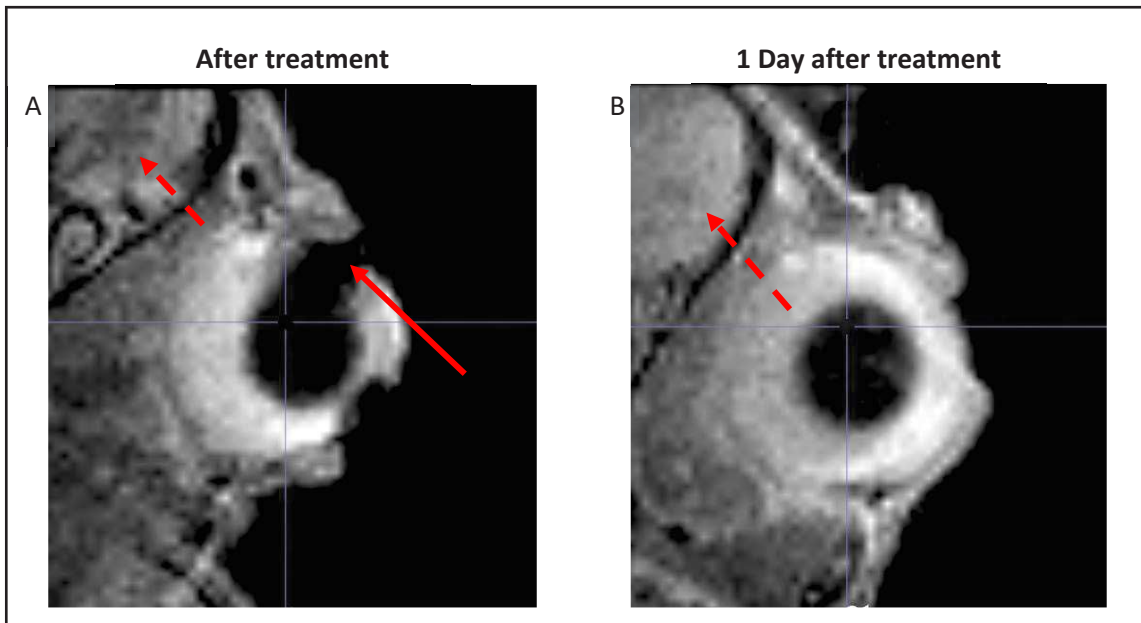
Figure 16. MRI images 24h post treatment. MRI imaging of mice treated with topical MNPs. RARE sequence. A) Image acquired immediately after topical application of the MNPs, the arrow points the signal coming from the MNPs present in the ocular tissues. B) The same eye as in A is shown 1 day after topical application of the MNPs. We can observe that the signal pointed out before has banished.

Finally, we were also interested in the possible effect of the magnetic field application in the mobility of the MNPs. We observed on our images that the signal was stronger in the mice that were treated under the influence of the magnetic field. Moreover, we did not only observe an overall increase in the signal with MRI but we could also observe that the increase of the signal was not only located around the eyeball but also inside the ocular tissues. (Figure 17). These differences between the mice treated with or without the application of the magnet seem to show that the magnet improve the mobility of the MNPs and their capability to penetrate the tissues.
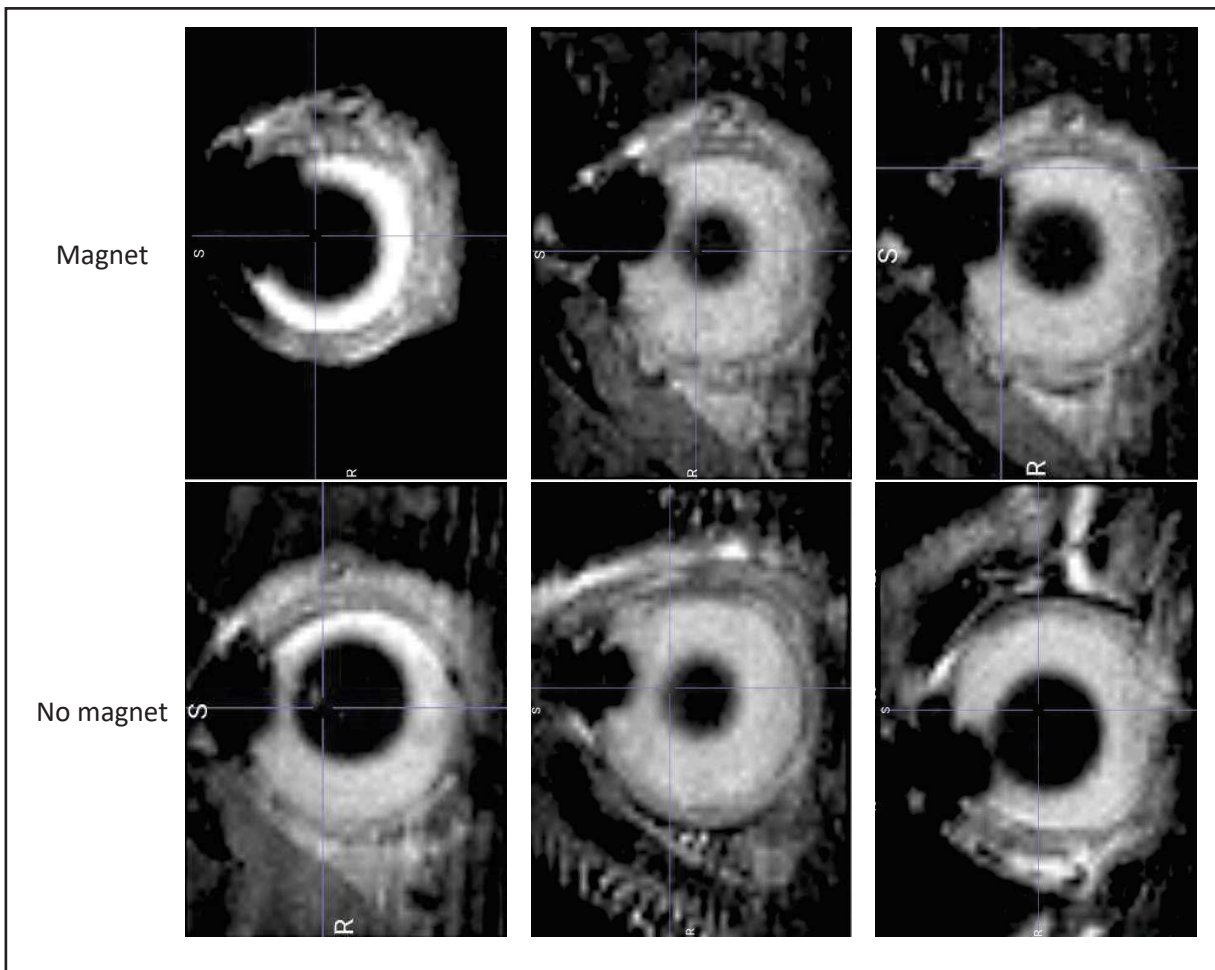

Figure 17. Effect of the magnet on MNPs migration. Sagittal planes RARE sequences. Comparation of the presence of signal coming from MNPs inside the ocular tissue with and without the application of the magnet during treatment

3.2.3.3. Mobility of the MNPs after IVT:

We also observed the MNPs inside the vitreous after IVT, in this set of experiment rats were used instead of mice. The rat eye presents an axial length of 6.29 mm and a vitreous volume of 54.4 µl (Hughes, 1979) while the eye of the mice present an axial length of 3.37 mm and a vitreous volume of 5.3 µl (Remtulla & Hallett, 1985). These differences in vitreous volume and size of the eyes facilitate the observation of the MNPs after IVT in the vitreous and MRI acquisition. In our preliminary trials we tested several concentrations of MNP. The aim of testing these different concentrations was to obtain an image with a clear signal but where the strength of the signal would not mask small changes in the distribution of the MNPs. We could see the signal of the MNPs in all the concentrations tested (Figure 18). However, while we could see the signal on the animals injected with 0,0625 mg/ml of MNPs it was decided that the signal coming from these images was very low to get reliable images of the movement of the MNPs. As mentioned in the methods section these are preliminary studies that will be continued by our collaborators in the University of Eastern Finland.
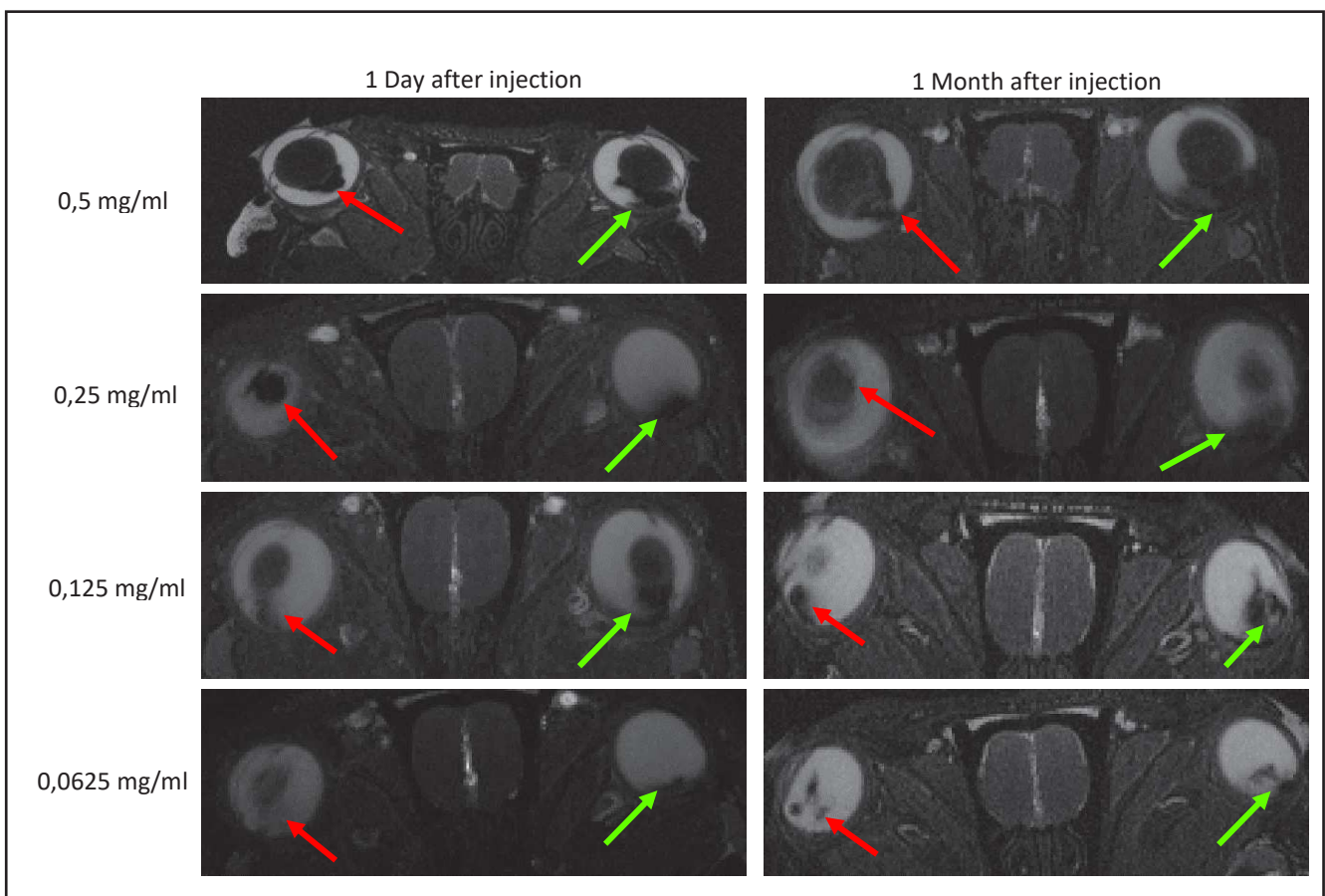

Figure 18. Distribution of MNPs after IVT. FISP sequences from rats treated with different concentrations of MNPs. Red arrow points to the NP02 and green arrow point to the NP01 injected eye. The left column shows the eye globes one day after injection while the right one shows the same animals one month after injection. Images obtained in 3-month-old rats.

We also used these preliminary tests for the concentration analysis in order to assess the movement of the MNPs inside the vitreous after IVT. In this case we observed that nor the distribution nor the amount of MNPs seem to vary significantly up to one month after the injection. This was the case for both of our MNPs indicating that MNPs charge is not related to their ability to stay in the vitreous after IVT. Nonetheless, our preliminary data showed that the positive MNPs (red arrow in Figure 18) seem to stay in a more compact/localized position after injection than the negatively charged MNPs (green arrow in Figure 18). More information is needed to completely assess if there is any difference between both MNPs in terms of distribution inside the vitreous. These experiments are still ongoing and the results will be obtained by the Ocular pharmacology group from the University of Eastern Finland as part of our collaboration. The experiments will be carried on by another PhD student from the Ocuther project, Amir Sadeghi Boroujeni. Finally, once we have assessed that there was no change in the distribution of the MNPs we wanted to know if it was possible to move the MNPs inside the vitreous using the magnet. After 30 minutes of application of the magnet we proceeded to MRI imaging and we were indeed able to observe that the distribution of the MNPs had changed (Figure 19). We were interested by the fact that not all the bulk of the MNPs seemed to move as we can observe two different signals. Moreover, it is interesting that we only see two different signals and no connection between them as we would expect, possibly meaning that the MNPs found in between these two spots are in a concentration below the threshold of the MRI imaging.
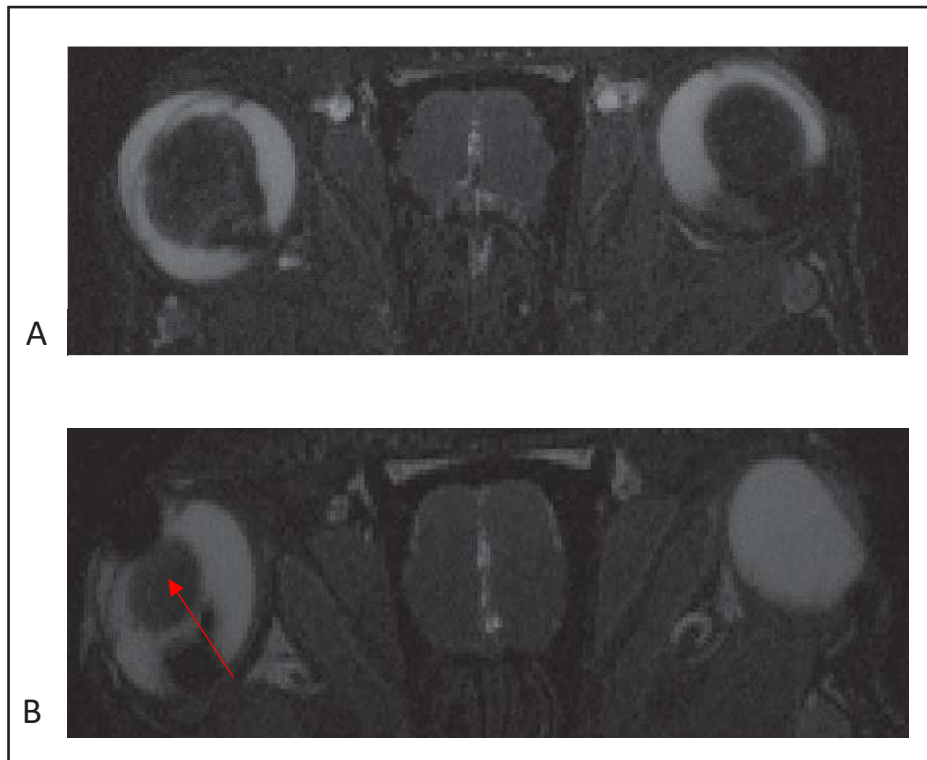
Figure 19. Effect of the magnet in MNPs inside the vitreous. A shows the treated animal one month after injection. B shows the same animal after application of the magnet for 30. The red arrow points to the cluster of displaced MNPs after the application of the external magnetic field

We were also able to observe our MNPs in a more direct manner using TEM. We could observe the MNPs in the PR layer of the retina of 14 days old mice eyes (Figure 20). MNPs were observed in the PR cells as soon as 15 minutes after the treatment and in all other time points studied (20 and 30 minutes).
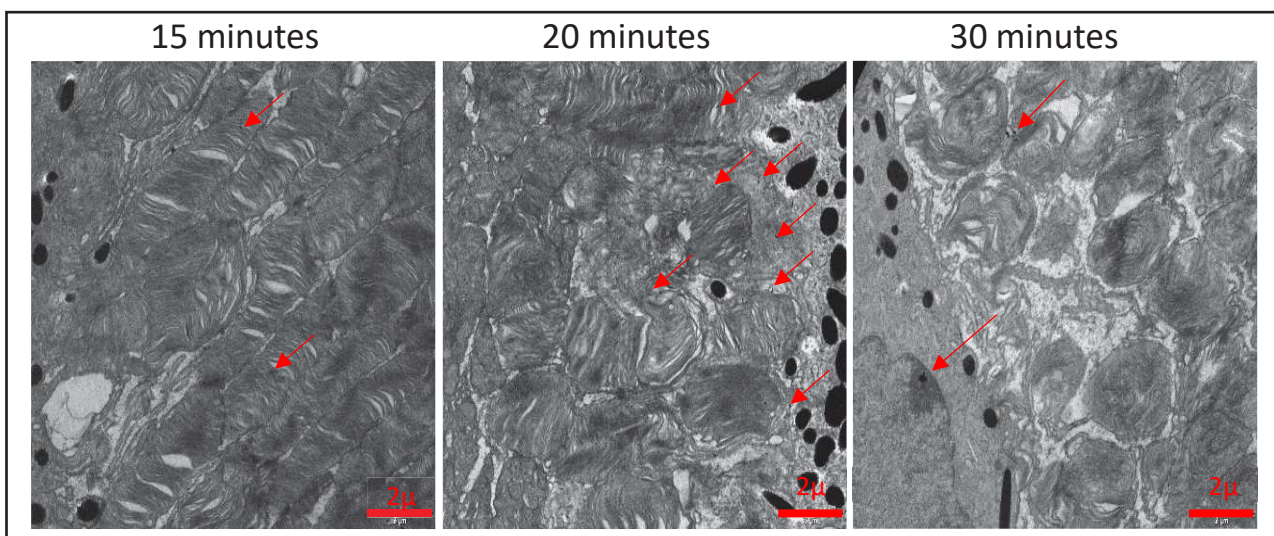
Figure 20. Localization of MNPs after topical application. TEM images of three animals treated with the MNPs and the application of the magnetic field. The eyes were analysed at different timepoints to assess the movement of the MNPs at different times.

69

We were able to observe the MNPs not only in the PR layer but it was also visible in other layers such as the INL. The image acquired was obtained before the experiments to assess the stability of the MNPs in different media and the treatment was done using NaCl 0.9% which explains the high accumulation of MNPs in one area when compared to other pictures (Figure 21). We changed the vehicle to 5% glucose for the rest of the treatments.

Figure 21. MNPs outside the PR layer. TEM image. Mice treated with topical application of the MNPs and the application of the magnetic field. The mice were treated using NaCl 0.9% as vehicle explaining the high aggregation observed.

3.2.4. Toxicity of the MNPs:

Our MNPs are made with an iron oxide core. One of the concerns using this type of material is the fact that iron can interact in the cellular environment and produce ROS via the Fenton reaction (Song & Dunaief, 2013):
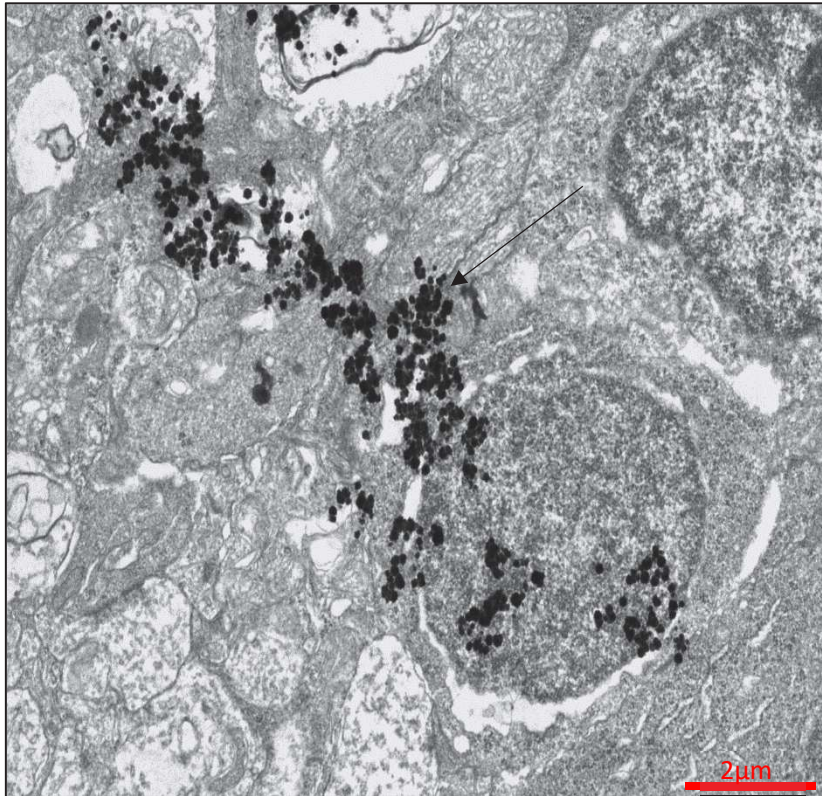
$$Fe^{2+} + H2O2 \rightarrow Fe^{3+} + OH\cdot + OH-$$

3.2.4.1. Toxicity in vitro:

As a previous step for the testing of the MNPs *in vivo*, Marco Basetto analysed their potential toxicity in two cell models. One is hTERT-RPE1 cells (ATCC® CRL-400) cell line of retinal pigmented epithelium cells and the other is a photoreceptor cell precursor called 661-W (The university of Oklahoma, Health Sciences centre, Department of Cell biology). The effect of our different MNPs on these cell types was studied showing toxicity only at high iron concentrations.
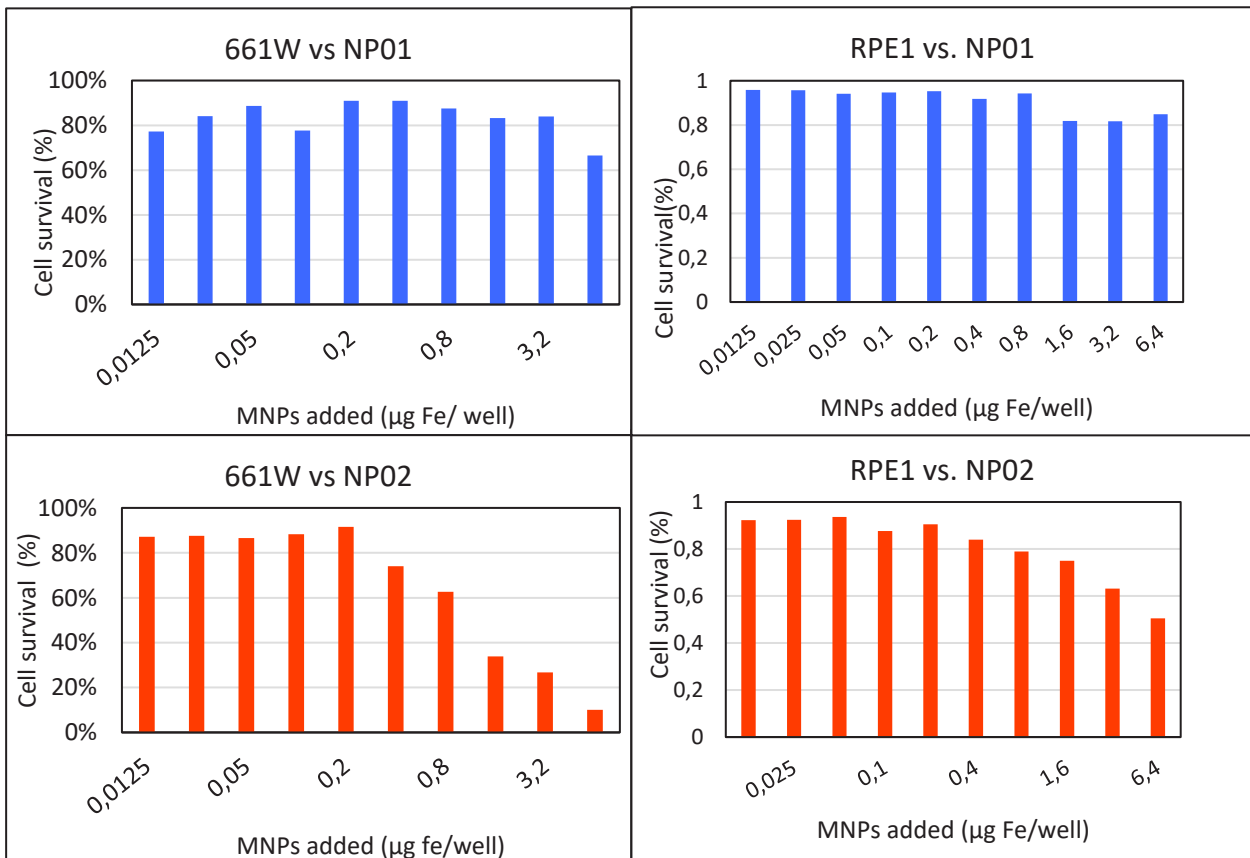
Figure 22. Effect of the MNPs on cell viability. The effect of increasing iron concentrations on cell survival was studied. Showing that only very high iron concentrations could affect cell survival.

3.2.4.2. Toxicity i*n vivo*:

After topical application of the unloaded MNPs in *Bbs^{+/+}* mice the Scotopic ERG recording showed no significant decrease in the a-wave measures. This was observed in all the dilutions used (Figure 23).

Therefore, we can conclude that are no negative side effects from our MNPs on the retinal function in the period of time of our study. Moreover, no sign of irritation or discomfort was observed in the animals post-MNPs application or in the following days.
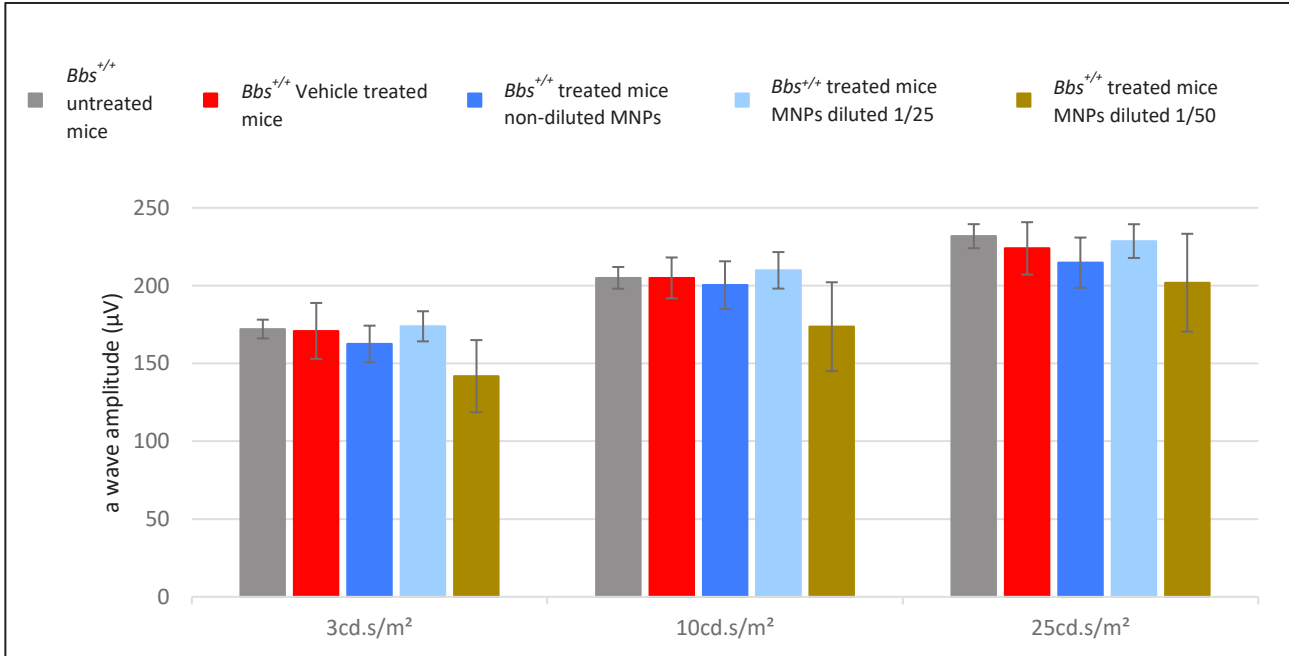
Figure 23. In vivo toxicity of the MNPs. Scotopic a-wave recording Bbs+/+ *mice treated with unloaded MNPs. No significant difference in the ERG recording was observed between the different groups. Results are shown as average and error bars correspond to the SEM.*

All of our treatments were done with only one application of MNPs as the possible iron toxicity was a concern. Nonetheless, we also have some preliminary data on the effect of multiple MNPs application on the ERG recording of *Bbs*+/+ mice. Up to three treatment sessions with loaded MNPs and the magnet were carried on for these experiments.

3.2.5 Biological effect of the MNPs:

Once we verified the safety profile of our MNPs the next step is to assess if the loaded MNPs are able to carry our compounds to the tissue. For this, we analysed the effect the MNPs have in our treated mice to see how it affects several disease markers that have already been validated as targets for our treatment. Our main goal is to preserve the retinal function with our treatment. Thus, ERG is our main tool to assess the efficacy of the MNPs. Coupled with the improve on ERG recording we would expect changes in the retinal degeneration markers such as ER dilatation and ONL thickness making them secondary markers of the efficacy.

3.2.5.1. Effect of the MNPs in the ERG recording:

Effect of the loaded MNPs in Bbs$^{+/+}$ mice ERG recording:

After testing our unloaded MNPs in the *Bbs*$^{+/+}$ mice we analysed the effect the loaded MNPs could have in the retinal function of the *Bbs*$^{+/+}$ mice (Figure 24). We could not observe any effect of our MNPs on the retinal function of our *Bbs*$^{+/+}$ mice.

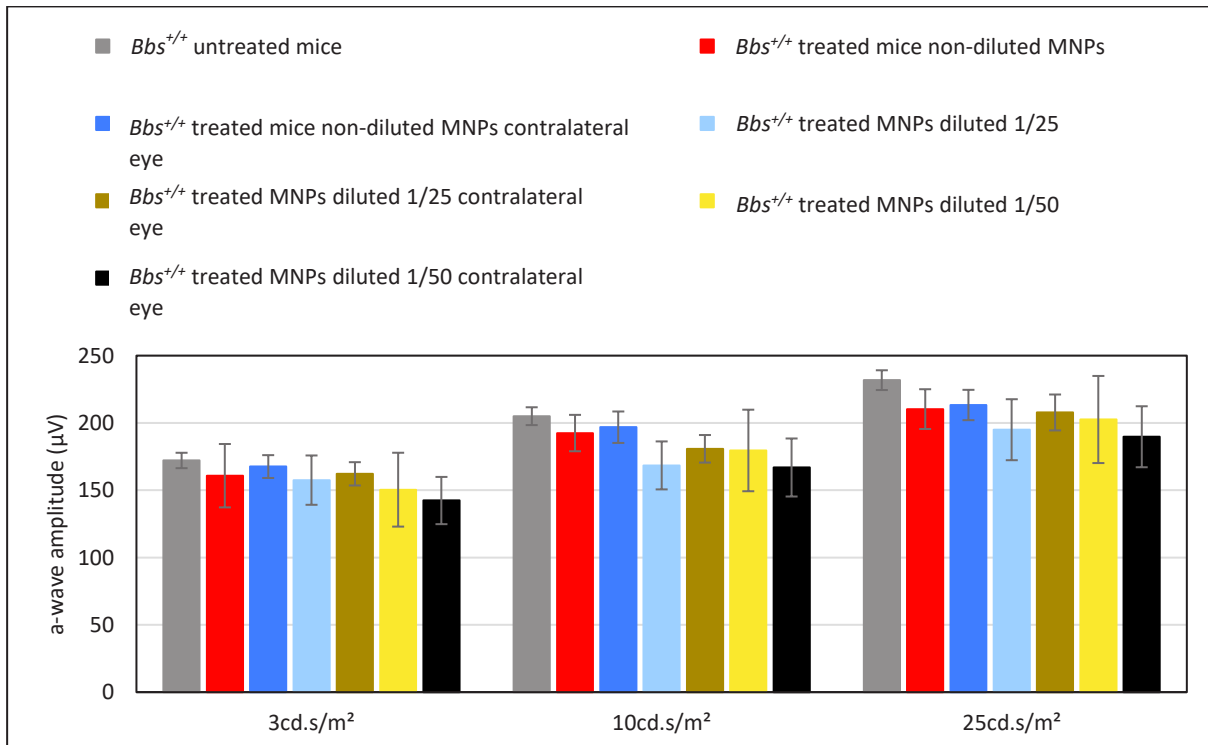**Figure 24. Effect of treatment with the loaded MNPs on ERG recording. Scotopic a-wave recording Bbs$^{+/+}$ mice treated with loaded MNPs. No significant difference in the ERG recording was observed between the different groups. Results are shown as average and error bars correspond to the SEM.**

Effect of the loaded MNPs in *Bbs*^{-/-} mice ERG recording

Once we assessed that the MNPs had no effect on the ERG recording of the *Bbs*^{+/+} we investigated if the treatment was able to restore the retinal function of these mice. As with the other treatment groups we tested different concentration of the MNPs. In this case we were able to observe a slight increase in the Scotopic ERG only in one of the concentrations used (Figure 25). The increase is significant when compared to the untreated *Bbs*^{-/-} mice. However, the response from the treated mice was still lower than that of the control group.
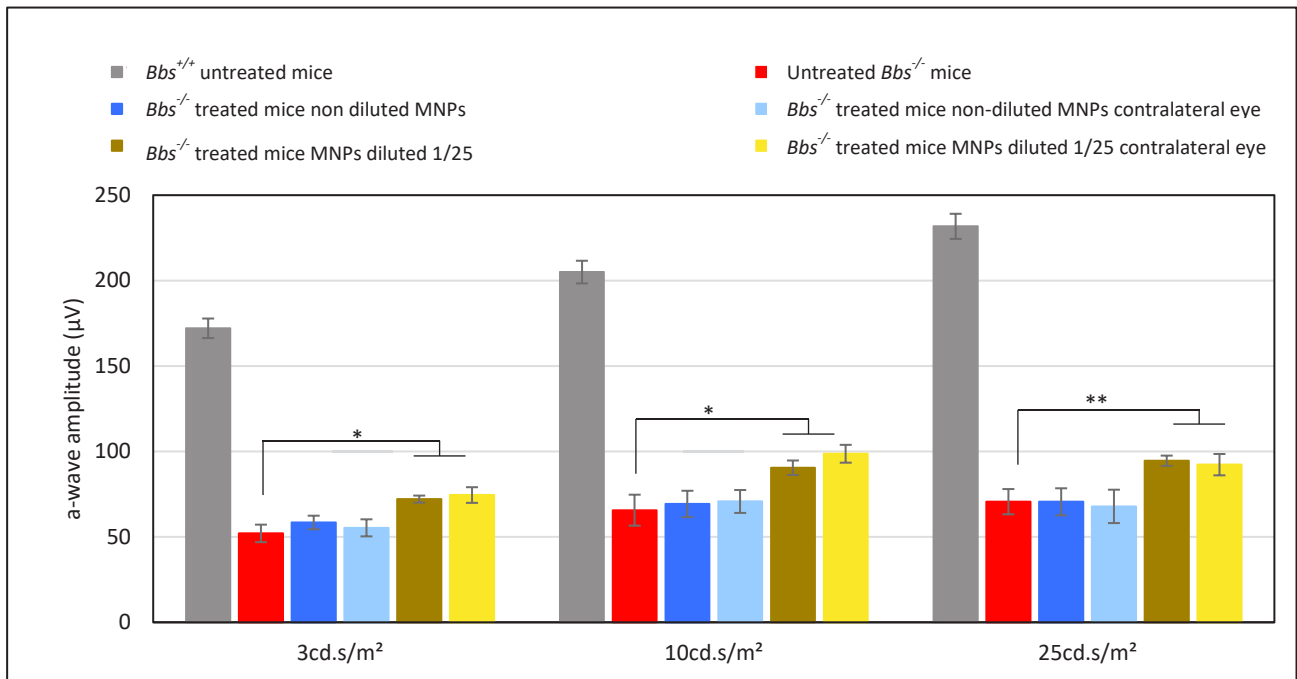
Figure 25. Effect of treatment with the loaded MNPs on ERG recording. Scotopic a-wave recording Bbs^{-/-} mice treated with loaded MNPs. Only the ERG of the Bbs^{-/-} mice treated with the 1/25 dilution of MNPs showed a significant increase in the ERG response. Results are shown as average and error bars correspond to the SEM.

As we have explained in the material and methods section, for diluting our MNPs we use two solutions containing both VPA and GBZ, this means that for the mice treated with a more diluted solution of MNPs, more solution was added to the eyedrop. This raises the question whether the solution itself is responsible for the improvement in ERG. Thus, scotopic ERG recordings were acquired from mice treated only with our vehicle and the solution containing both drugs. We treated these mice with an eyedrop containing the same amount of solution containing VPA and GBZ as the eyedrop of the mice treated with the 1/25 dilution of MNPs. We could observe that in these mice no improvement on the ERG recording was observed (Figure 26). Meaning that our compounds alone as eyedrops are not able to replicate this positive effect in the ERG recording.
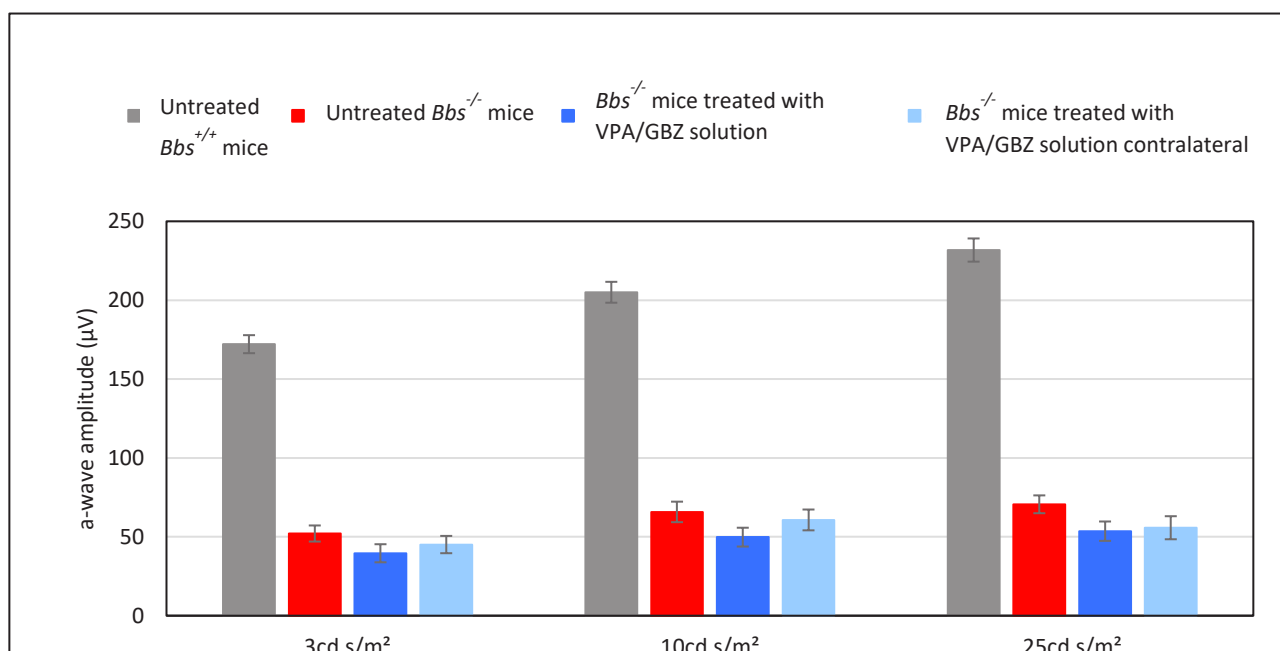
Figure 26. Effect of treatment with VPA and GBZ solutions on ERG recording. Scotopic a-wave recording Bbs^{-/-} mice treated *with eyedrops containing both VPA and GBZ. No significant difference in the ERG recording was observed between the* *different groups. Results are shown as average and error bars correspond to the SEM.*

Once we discarded that the beneficial effect observed in the ERG response was not due to the solution containing our compounds we decided to test if the beneficial effect could come from only one of our MNPs. Since we have two different type of MNPs it is possible that they do not behave similarly in their path from the ocular surface to the tissues, meaning there could be differences between our MNPs n term of their capacity to bring their load to the target. As we were able to see, the scotopic ERG recording of mice treated with only one loaded MNPs did not show any improvement (Figure 27).
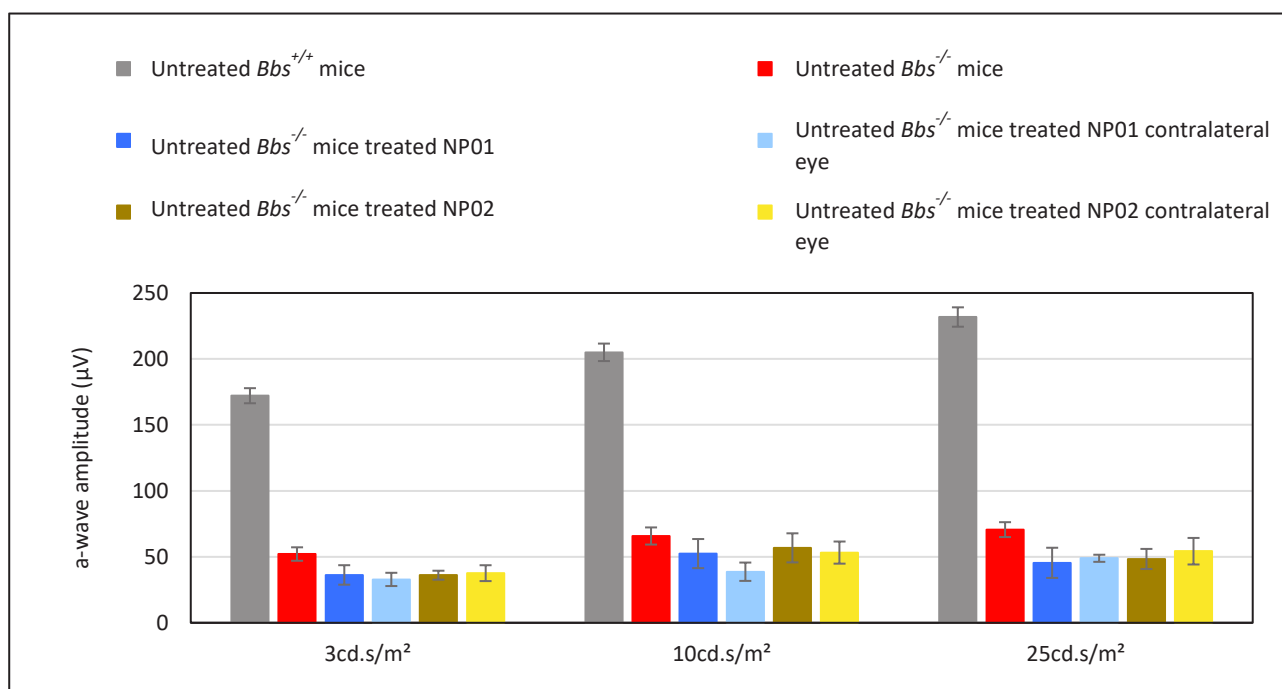
Figure 27. Effect of treatment either loaded NP01 or NP02 on ERG recording. No significant difference in the ERG recording was observed between the different groups. Results are shown as average and error bars correspond to the SEM.

3.2.5.2. Effect of the MNPs on the ER dilatation and ONL thickness

After studying the effect of our treatment on the ERG recording, we continued to assess the effects our treatment has on the *Bbs*$^{-/-}$ mice. We continued analysing different markers related to our mice model and our compounds. In this case the next marker we measured was the ER dilatation. Our treated mice presented overall less ER cisternae dilatation when compared to our untreated *Bbs*$^{-/-}$ mice (Figure 28). However, the difference is not statistically significant, it is possible that this is related to the number of samples analysed (n=3 per group).
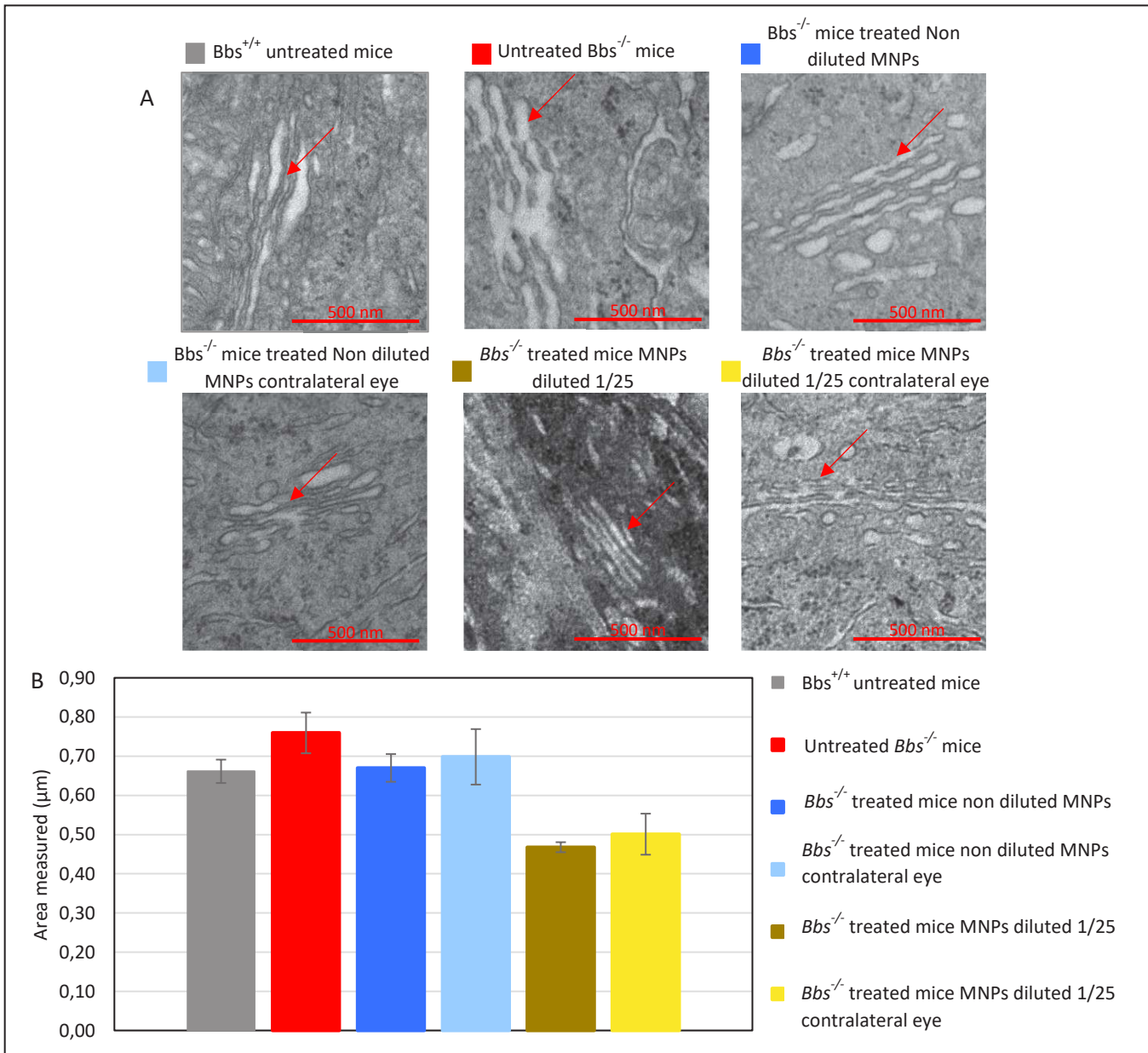
Figure 28. Effect of treatment with the loaded MNPs on ER dilatation. A show representative TEM images, the arrows point to the ER. B shows the results average measures for the different groups analysed. Error bars correspond to the SEM.

Another one of the markers analysed was the thickness of the ONL, photoreceptor cell death leads to a loss of ONL thickness, followed by a reduction of the thickness of the layer. We measured the ONL thickness in toluidine blue ultra-thin sections. Our measures showed an increase in the ONL thickness in our treated $Bbs^{-/-}$ mice when compared with our untreated mice (Figure 29).
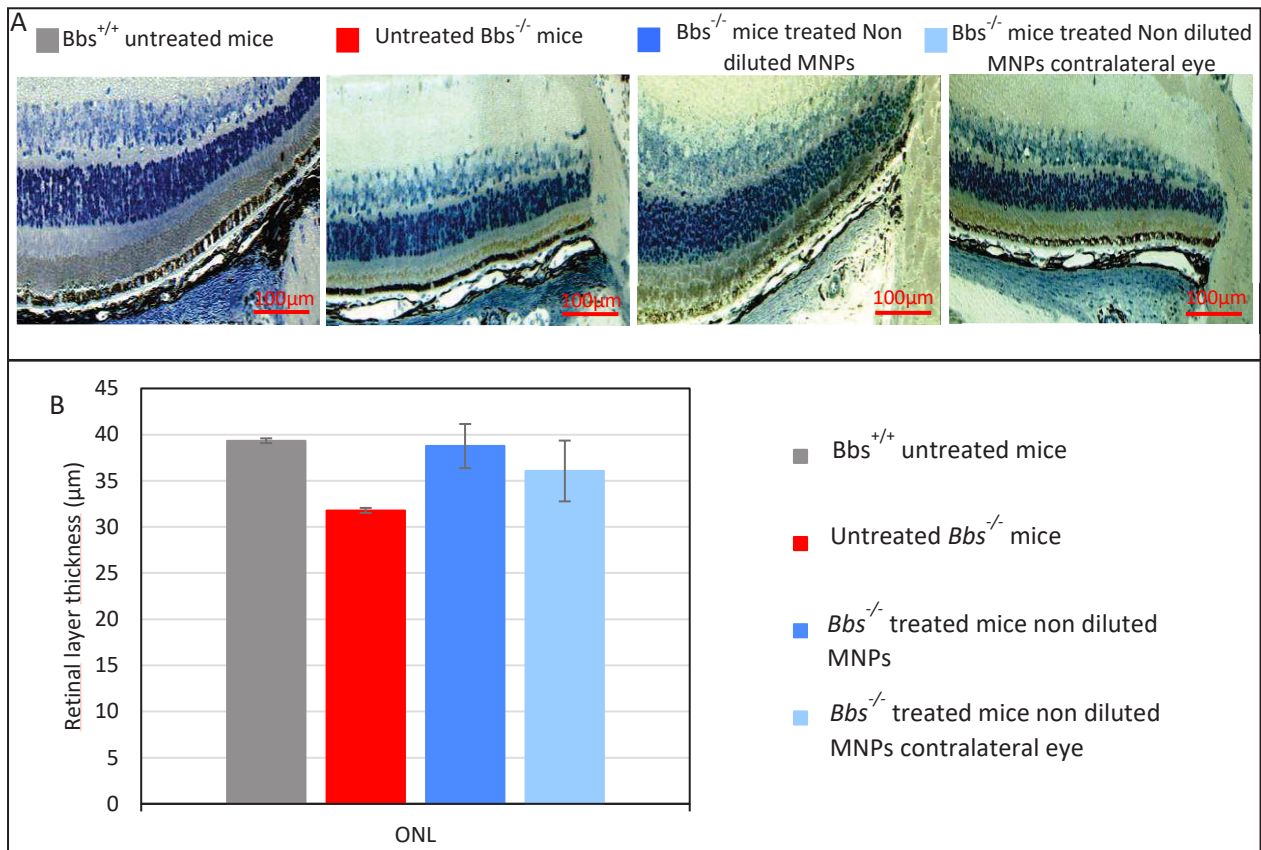
Figure 29. Effect of treatment with the loaded MNPs on ONL thickness. A show representative tolouidin blue image. B shows the results average measures for the different groups analysed. Error bars correspond to the SEM.

3.2.5.3. Effect of the MNPs on the target UPR proteins

In order to assess if the topical treatment with the MNPs was able to produce the desired effect we assessed the quantity of our target proteins using WB (Figure 30). If our MNPs are able to bring both VPA and GBZ to the retina we would expect an increase in Bip chaperone quantity and in the ratio of p-eIF2α/eIF2α. We measured the quantity of p-eIF2α, eIF2α and Bip chaperone in tissues from our Bbs$^{-/-}$ mice treated with the 1/25 dilution of MNPs and compared it with our untreated Bbs$^{-/-}$ and Bbs$^{+/+}$ mice.

While the results show the expected effects both in the measure of retina there is no statistically significant result. A possible explanation is that the number of samples studied for each set of experiment is still low and thus no statistically significancy is observed.

A

B

C

D

Ratio p-eIF2α/eIF2α

Legend

1. Molecular weight
2. Molecular weight unstained
3. $Bbs^{+/+}$ untreated mice
4. $Bbs^{-/-}$ untreated mice
5. $Bbs^{-/-}$ treated mice MNPs diluted 1/25
6. $Bbs^{-/-}$ treated mice MNPs diluted 1/25 contralateral eye

Figure 30. Effect of treatment with the loaded MNPs on target UPR protein quantification. A shows the total protein load on the membrane used for normalization. B shows the detected bands for each protein. C shows the quantification obtained for each protein normalized by the total protein using BioRad Stainfree technology. D shows the p-eIF2α/eIF2α ratio.

IV. Discussion

4. Discussion

In this thesis I report the results obtained regarding the potential use of MNPs loaded with drugs and guided by external magnetic fields as drug delivery systems targeted at the retinal tissues.

Up to this date, dug delivery to the retina remains a challenge due to the different anatomical and physiological barriers. Especially when topical administration of treatments is involved, as th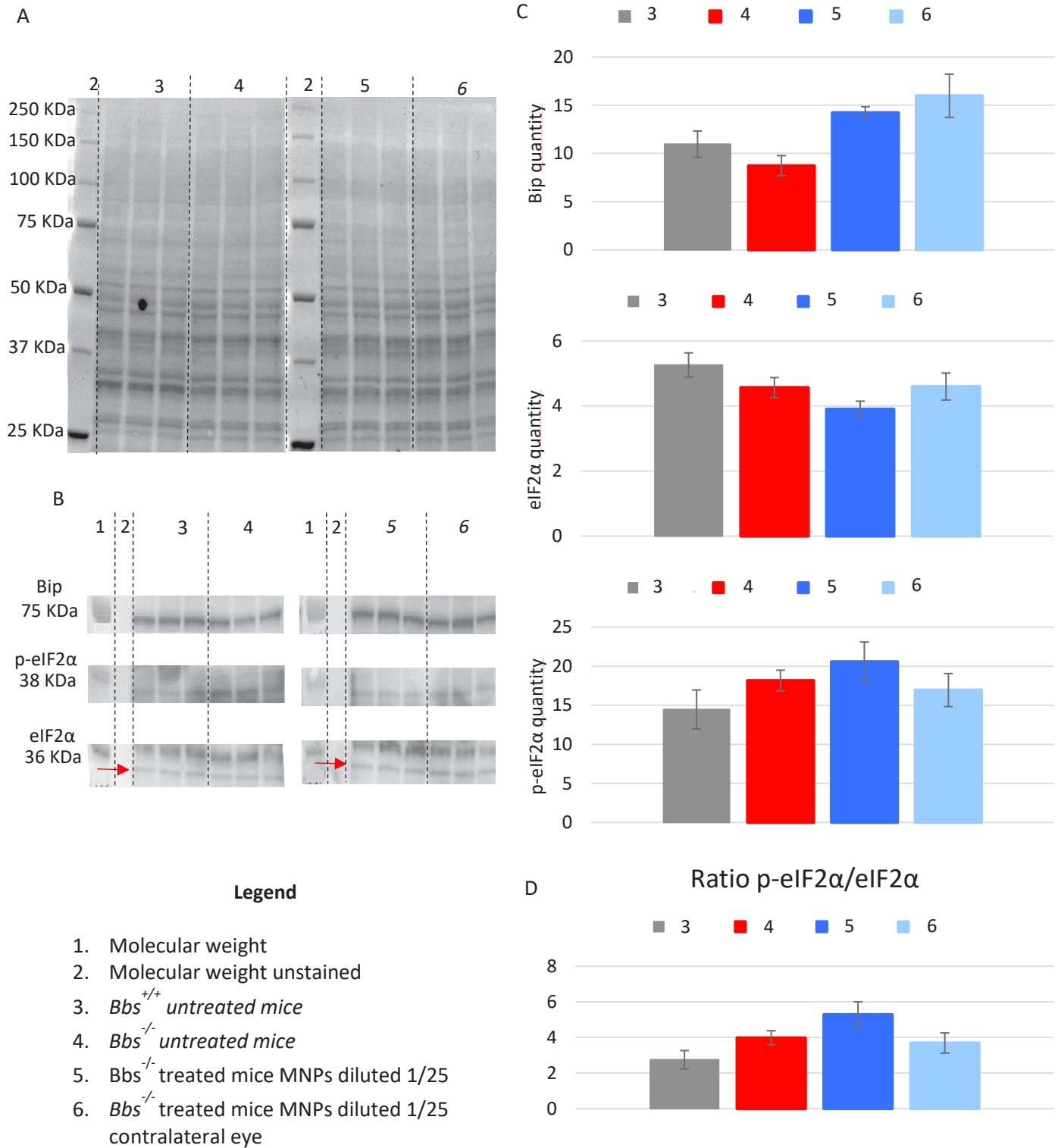e compound would need to face most of these barriers. While different solutions have been studied ranging from the use of physical forces such as electrophoresis to new formulations such as liposomes no clear solution has been achieved. Ideally the solution to overcome these barriers would be one that can be used in a wide range of compounds in term of size, lipophilicity/hydrophilicity, superficial charge and so on. This is needed as the different barriers blocks the passage of different type of drugs, for example cornea limits both hydrophilic and lipophilic drugs (Bucolo et al., 2012). The characteristics of the MNPs and the possibility of further functionalizing them in terms of loading or targeting with different coatings opens up the possibility of designing MNPs for a wide range of drugs. Moreover, the optimization of the guidance of the MNPs with magnetic fields make them a very potent tool for drug delivery. This is the reason MNPs as drug delivery system have been proposed to overcome the ocular barriers. While most of the studies using MNPs in the ocular tissues are related to cell transplants there are few that have used MNPs as drug delivery system (Prow et al., 2008; Mousavikhamene et al., 2017; Giannaccini et al., 2018; Amato et al., 2020). This leads to a lack of information regarding the potential difficulties and advantages derived from the use of MNPs as drug delivery systems. Moreover, comparison between the studies that have used MNPs for ocular use can be complicated as different type of particles, magnets and approaches have been used.

4.1. MNPs as topical drug delivery system for targeted drug delivery to the retina

4.1.1. Distribution of the MNPs

One of the main problems of using eyedrops for retinal drug delivery is the fact that most of the drugs applied will not be able to reach the retina due to several anatomical and physiological factors. In our case in our collaboration with OZ Bioscience within the Ocuther project it was theorized that the magnetic pull from an external magnet could potentially help overcome these barriers and thus increase the amount of drug delivered to the posterior segment. It is interesting that most of the studies where MNPs have been studied as drug delivery system for ocular tissues no external magnetic field was used (Prow et al., 2008; Giannaccini et al., 2018;

Amato et al., 2020). The explanation behind this is the fact that these studies rely on the presumed capability of the MNPs of migrating to the PR and the RPE layer but it also means that there is a lack information about the use of magnetic fields in ocular drug delivery and the effects on the movement of the MNPs once inside the tissues.

In our study, we used magnetite core particles with two different coatings as we were trying to achieve electrostatic binding of two differently charged compounds. In this case we did not attempt further functionalization of the coating. This means that we are analysing only the effect of the magnetic pull and not the possible effect of targeting specific tissues by adding certain molecules on the coating as we have seen in other studies (Giannaccini et al., 2017). The first step we took was to assess if our MNPs could really reach the retina after topical application, for this we used TEM. We could indeed observe the MNPs in the retina, while we could not observe them in the vitreous and it is interesting to note that we did not only observe the MNPs in the PR and RPE layers but also in other layers such as the INL. Comparing this information with studies that have also analysed the distribution of MNPs we can see that when MNPs are injected outside the tissue they only appear to be able to cross as far as to the ONL ((Tzameret et al., 2019). in the study done by Dengler et al, while they did not assess the localization of the MNPs it seemed that they were found in all the retinal layers after systemic administration of the MNPs based on the images they presented in their paper (Dengler et al., 2010). It is possible that this is the only study that present this distribution of the MNPs due to the way they positioned their magnet as it was placed on top of the eyelids and the magnetic pull would pull the MNPs in the direction of the eyelids. Thus, it would seem that in our experiments MNPs indeed arrive to the retina from the vitreous and not from the choroid. While we know the MNPs do reach the retina and possibly not from the choroid, the information gathered from TEM is not sufficient to properly describe the pathway they follow. MRI has been used in different studies to observe the localization of MNPs inside the eye (Harrison et al., 2012; Raju et al., 2012; Tzameret et al., 2019). While this technique does not give any insight in the localization inside the different tissues it has the advantage of being able to track the movement of the MNPs without needing to sacrifice the animals, allowing for the follow-up of the MNPs in the same animals for longer periods. Nonetheless, the technique itself present some complications when used with mice. This is caused by the small size of the eyeballs making the observation of this tissues a complicated matter, in this case, in order to be able to observe the MNPs and achieve enough sensitivity to observe the MNPs we decided to acquire image of one eye alone. Our results suggest that the main way of absorption for the MNPs is the non-corneal route as we can see that most of our MNPs do not seem to go across the cornea but they accumulate in a position

around the corneal limbus. This information coupled with what we have seen in the TEM images could probably point that the MNPs move to the conjunctiva and sclera and then are able to diffuse from there to the vitreous and then they could be able to reach the different layers of the retina. Another possibility is that after the conjunctiva and sclera they could reach the retina instead and move inside the retinal tissue from this point. However, with the MRI we were able to observe the MNPs highly concentrated in a position just at the end of the cornea with no signal in other parts of the retina such as close to the optic nerve. This is important since our TEM images are taken in the surroundings of the optic nerve. This could indicate that while most of the MNPs do accumulate in the localization of the MNPs there could be a small flux from this portion to the back of the eye. The fact that the MNPs could accumulate in this position could be related to some sort of funnel effect. As they would need to move through narrow intercellular spaces meaning that the bulk of the MNPs could reach the position observed in MRI but from there the movement could be restricted by the space available for movement and only a smaller flow of MNPs would move through the tissues. The clustering of MNPs after crossing tissues have also been observed before, for example for MNPs crossing the retina (Amato et al., 2020; Giannaccini et al., 2017). This theory could also explain why we are not able to see MNPs closer to the optic nerve or in other portions of the retina as this reduced flow would potentially not be concentrated enough to produce a signal that can be detected with MRI. In this regard, we have to highlight the fact that the concentrations used for the topical application of MNPs for MRI was higher than the concentrations used in our treatments to assess the effect of the MNPS. This was needed in order to be sure that the MNPs would be in a concentration high enough to be detected with the MRI. However, this difference in concentration could mean that the movement of the MNPs in each group is slightly different as this accumulation we observed could be less in mice treated with lower concentration of MNPs.

Another interesting point gathered from the MRI information is the fact that 24 hours after the application of the treatment the signal of the MNPs disappears. There are some possible explanations for this, one likely explanation is that the MNPs do not reach the retina and the vitreous but stay on the conjunctiva or around it and are cleared from there to the systemic circulation due to the high vascularization of this area (Ahmed & Patton, 1985). It is also possible that the MNPs distribute on the tissue and the signal is lost as the concentration of the MNPs would be below the sensitivity threshold. But it is also likely that there is a combination of these two events and part of the applied MNPs are lost through systemic application. While potentially a problem when attempting the treatment of retinal diseases this can be interesting for

treatment of diseases such as uveitis as this could increase the amount of MNPs that reach the choroid after topical administration.

Since there are no attempts published of studies that used external magnetic fields to the guidance of topical treatment with MNPs on the eye the effect of the magnetic fields on the MNPs and its movement is unknown. In this case we could observe that more MNPs could be observed inside the tissues in the animals that were treated with the application of the external field. While most of the MNPs were observed in what would be the conjunctiva there were nonetheless some animals where we could see the presence of MNPs attached to and potentially penetrating in the cornea and anterior chamber. Interestingly, this was observed for our MNPs separately and in a mix, showing that this localization was not dependent on the charge. It has been described that the cornea is negatively charged (Liaw et al., 1992) meaning that usually only the positively charged MNPs bind to the surface and permeate through the tissue but since we saw both negatively and positively charged MNPs in this position it is possible that the effect of the magnetic field influenced the movement of the MNPs to the cornea. While this was not observed in all the treated animals it would still be something to study further as enhancing drug delivery to the anterior chamber with the use of MNPs is also needed.

4.1.2. Toxicity of the MNPs

Since the term nanoparticles encompasses all the particles with a diameter of under 100 nm, there are several different types of materials that are used for the core of the particles as well as different coatings that can be added to these cores. These different combinations also bring the possibilities of toxic effect on the cells depending on the characteristic of the particles. In the case of the MNPs they have been tested in a large amount of cell types such as PR precursors (Ma et al., 2019), RPE cells (Grottone et al., 2014) or corneal endothelium cells (Bi et al., 2013). Most of the studies we have mentioned have shown no significant alteration to the ocular tissues that could indicate toxicity of the particles used. Only one study showed signs of inflammatory cells infiltration after the injection of MNPs (Harrison et al., 2012) but these cells did not phagocyte the MNPs. However, the fact that the MNPs we used contain iron in the core, could potentially lead to toxicity, thus the importance of the coating of MNPs is highlighted. While the main use of our coating is to give our MNPs the surface charge needed for the electrostatic binding of our compounds, they serve a secondary role as the cover the surface of the iron core of the MNPs. The production of hydroxyl radicals has been shown to be produced on the surface of the MNPs (Voinov et al., 2011) hence the need of coatings to avoid direct exposure of the iron core surface to the cells. The toxicity of the MNPs becomes a bigger concern in the light of our preliminary results in the behaviour of the MNPs after IVT. In this case we

were able to observe the MNPs inside the vitreous for longer than 6 weeks. While we did not assess directly the toxicity of the MNPs in terms of inflammation of the tissue or cell infiltration we did not observe any sign of discomfort or inflammation on the ocular surface of the animals between the application of the treatment and the sacrifice of the animals. In the TEM images and toluidine blue ultra-thin sections used for the measure of the ER dilatation and the ONL thickness no gross changes were observed in the tissue, meaning that the pass of the MNPs did not induced significant inflammation or alteration of the tissue. On the other hand, the ERG did not show loss of PR response to flash as there was no decrease in the ERG a-wave amplitudes of the mice treated with the MNPs. While other studies have analysed the possible toxicity of MNPs for a period of up to 5 months (Raju et al., 2011) our study only lasted for two weeks after the application of the MNPs, potentially more studies could be done in order to assess if the coating of the MNPs degrade overtime and at what rate as the loss of the coating would potentially increase the risk of a toxic effect. Overall, for the period of our treatment no toxic effect was observed for the MNPs used which is coherent with previous studies that have assessed the toxicity of MNPs on different cellular types over different periods of time and with different types MNPs.

4.1.3. Biological effects of the MNPs

For the test of the MNPs as drug delivery system we have used two drugs that we have already tested in our lab (Mockel et al., 2012). In the previous studies the treatment was applied in two different ways, VPA was given systemically with the drinking water and GBZ was applied as eyedrops. In this case we decided to use only two of the three compounds that were used in this previous study as using three different compounds and having three different type of MNPs would potentially complicate the application of the treatment. In this case, we do have three components in our treatment, the MNPs themselves (core and coating), the compounds used (VPA and GBZ) and finally the solutions used for the dilution of the MNPs for our different treatment groups. In order to fully assess the effect of our treatment we have measured the effect of all these components separately on the ERG response. We were only able to observe an increase in the ERG response of our mice treated with our MNPs in a dilution 1/25. We could not observe any changes in the ERG of the mice treated with the unloaded MNPs, the solution containing our compounds or when the treatment contained only one leaded MNP. This shows that the effect observed was indeed due to the treatment containing both MNPs and that application of our compounds in form of eyedrops alone is not enough to achieve any improvement on ERG response after a single application. While the improvement of the a-wave we recorded was statistically significant it was still not at the levels of the $Bbs^{+/+}$ mice. It is

interesting that in this case the results were obtained when we diluted the MNPs 25 times. There are several reasons that could explain this. Ideally, the use of MNPs would increase the amount of compounds reaching the tissues as observed in other studies that used MNPs as drug delivery system (Amato et al., 2020). This increase in the amount of drug reaching the tissue could mean that the amount of drug is outside the therapeutical window of the compounds and thus, toxic effects could appear. In our study, we did not observe any alteration of the ERG response with the non-diluted MNPs so this would not seem to be the case. However, we saw in MRI that the MNPs seem to accumulate in a portion of the eye and this potentially could slow the flow of MNPs from the ocular tissue to inside the eye due to a funnel effect. If this is the case this would explain the positive effect obtained with the lower concentration used as it is possible that the lesser amount of MNPs present a less restricted movement inside the tissue. Moreover, we were able to measure the effect of our treatment in the retinal structure of the retina. In this case, the differences in the markers observed (ER dilatation and ONL thickness) is not statistically significant but shows a tendency to a positive effect derived of our treatment. It is interesting to note that we observed no improve on the retinal function in our mice treated with non-diluted MNPs while we were able to observe an improvement on the retinal structure. There have been reports where, for example, improve on PR cell survival was not followed by an increase on ERG recordings(Liang et al., 2001). In our case, the reason behind this could be the time elapsed between the treatment and the analyse of the ERG. We used only a single application of a topical treatment and analysed the results 2 weeks after, meaning that while there was a positive effect of our treatment it is possible that this positive effect is starting to wear off. Another explanation, could be related to the distribution of the MNPs after topical application, in this case it could be possible that most of the MNPs move through a similar area, thus the treatment would not reach the whole retina and this improvement on the retinal anatomy would not necessarily be followed by an improvement on the retinal function. Our treatment using MNPs was also able to modulate their target proteins from UPR. These results show that our treatment is indeed acting on our molecular targets. When comparing our results with the previous results obtained in our laboratory (Mockel et al., 2012) it is interesting to note the difference in application of the treatments. In the study by Mockel et al. both VPA and GBZ were given at different times but both were given over a period of 2 weeks while our experiments applied the both drugs at once one single time.

4.2. Feasibility of treatment with MNPs as eyedrops guided by magnetic fields

Mice and rodent models in general are widely used in research. They present several advantages such as the possibility to create genetic models or the relatively easy management for treatment and husbandry makes them suitable for different uses in research. However, for the study of pharmacokinetic of the eye, mice models are not as used as for other areas of research. This means that there is less information regarding several factors that could affect the ocular pharmacokinetics. Nonetheless, some characteristics of mice have been described as potentially giving over-optimistic results regarding the use of topical application of treatments that target the retina. While many factors such as aqueous humour flow or irideal and ciliary body blood flow might affect the pharmacokinetic in the most critical factor affecting the delivery of MNPs using magnetic field will be the distance. One clear difference between mice and humans is the distance between the ocular surface and the retina. In mice the axial length is of 3.37 mm (Remtulla & Hallett, 1985) while the axial distance in humans is of around 24 mm (Oyster, n.d.). The size of the head would also affect the distance between the eye and where the magnet would be positioned. In the case of our mice the distance between the back of the head and the eye is around 1.5 cm for the *Bbs*$^{+/+}$ mice and around 0.9 cm for the *Bbs*$^{-/-}$ mice while the diameter of the head of a three year old child would be around 15 cm (*Growth Charts - Data Table of Infant Head Circumference-for-Age Charts*, n.d.). These two size differences would be critical as they determine the distance between the eyedrop and the magnet. The movement of the MNPs is not determined by the strength of the magnet but rather by the gradient in the magnetic field, this is, the difference in strength on the magnetic field for each point in the space. However, the gradient decrease with the distance, thus the further away from the magnet, the lower the magnetic field gradient will be and the MNPs will be less attracted by the magnet. The axial length of the eye on the other hand will determine the distance the MNPs need to move to reach the retina, the lesser distance in the mice also means that during their movement the magnetic field gradient that affect the MNPs would vary less than the magnetic field gradient that could affect the movement if we try to use the MNPs in humans for example. This would influence the design of the set-up for treatment of bigger animals as the magnetic field gradient would need to be clearly determined for designing effectively the set up for topical treatment. In these regards, the study from Zahn et al have studied the feasibility of drug delivery to the ocular tissues using the magnetic field (Zahn et al., 2020). They theorized that a magnetic field of 20 T m^{-1} is promising for the penetration of MNPs inside the ocular tissues. In our case, if we observe the magnetic field gradient of our magnet (Figure 31) we can observe that while the eyedrop

would be subjected to that gradient in the *Bbs*$^{-/-}$ mice (at a distance of 0.9 cm) this would not the be case for the *Bbs*$^{+/+}$mice (at a distance of 1.5 cm) that would be subjected to a magnetic gradient field of around 6 T m^{-1}.
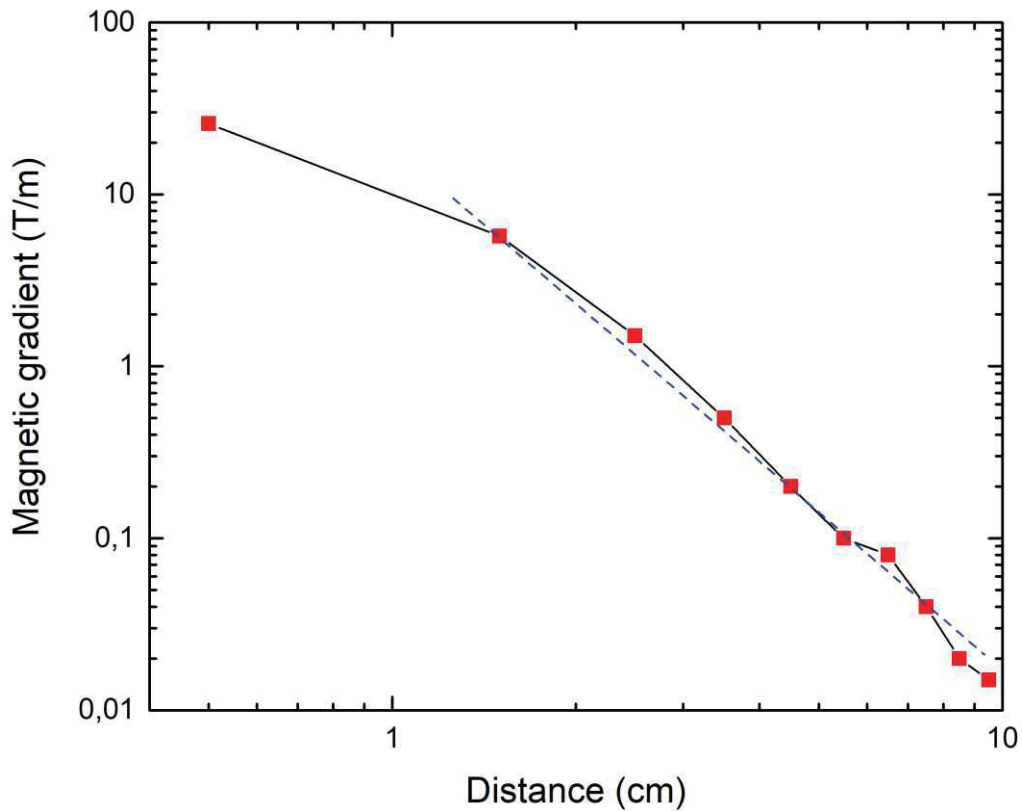

Figure 31. Magnetic field gradient. Table shows the decrease in the magnetic field gradient with the distance for the magnet used in our treatment. The dash line shows the expected decrease of the magnetic field gradient with the distance while the red squares shows the actual magnetic field gradient. The axes are shown in logarithmic scale.

When comparing our results with this study we were able to achieve the passage of MNPs with seemingly lower magnetic fields gradients (at least in the case of the *Bbs*$^{+/+}$mice). While one of the reasons for this could be the fact that the barriers of the eye such as the cornea, sclera and conjunctiva are smaller in the mice (del Amo et al., 2017; Henriksson et al., 2009, 2013) the difference in the magnetic field gradient is 4-fold for these mice. While mice model could over-estimate the results obtained with the topical application of the MNPs there is a lack of information regarding the use of magnetic fields for drug delivery to the retina. For example, the results obtained in our experiments could still indicate that the simulations obtained by Zahn et al. need to be confirmed using lower magnetic field gradients as this would mean the need of less potent magnet set-ups and would potentially simplify the design of the set-ups. In general, our data is relevant as the first *in vivo* study that attempt the use of MNPs for retinal drug delivery and can be the starting point in order to further develop them as drug delivery system.

V. Conclusions and perspectives

5. Conclusions and perspectives

We have been able to show the feasibility of the use of MNPs for topical application of eyedrops for drug delivery to the retina. A single application of the treatment in 14-days old mice was enough to induce a positive response as shown for an increase in the ERG response of the mice two weeks after the treatment. While the a-wave amplitude was still lower than the amplitudes recorded in the $Bbs^{+/+}$ mice it was also accompanied by an improvement on the retinal degeneration as shown by the modulation of disease markers such as the ONL thickness and the ER dilatation. Basic information on the movement of the MNPs was obtained and the probable pathway of the MNPs has been theorized based on MRI and TEM images obtained. While potentially the use of rodent models could overestimate the effect of topically applied MNPs the fact that only one dose was used during our studies and that the effect was both assessed two weeks after the treatment are still encouraging. This study can be a starting point to understand how the MNPs behave after topical application, one critical aspect to study is the movement of the MNPs when under the influence of the magnetic field. By observing different concentration of MNPs applied and different time of magnet exposure we could better understand how they behave. We have contributed to the information available regarding the potential use of MNPs guided with magnetic fields for drug delivery to the retina. However, the design of future experiments in larger animals such as rabbits, will be marked by the need of stronger magnets capable of producing the same magnetic field gradient in distances greater than the ones studied in our project.

VI. Bibliography

6. Bibliography

Agarwal, R., Iezhitsa, I., Agarwal, P., Nasir, N. A. A., Razali, N., Alyautdin, R., & Ismail, N. M.

(2016). Liposomes in topical ophthalmic drug delivery: An update. *Drug Delivery*, *23*(4),

1075–1091. https://doi.org/10.3109/10717544.2014.943336

Agrahari, V., Mandal, A., Agrahari, V., Trinh, H. M., Joseph, M., Ray, A., Hadji, H., Mitra, R., Pal,

D., & Mitra, A. K. (2016). A comprehensive insight on ocular pharmacokinetics. *Drug*

Delivery and Translational Research, *6*(6), 735–754. https://doi.org/10.1007/s13346-

016-0339-2

Ahmed, I., & Patton, T. F. (1985). Importance of the noncorneal absorption route in topical

ophthalmic drug delivery. *Investigative Ophthalmology & Visual Science*, *26*(4), 584–

587.

Amato, R., Dal Monte, M., Lulli, M., Raffa, V., & Casini, G. (2018). Nanoparticle-Mediated

Delivery of Neuroprotective Substances for the Treatment of Diabetic Retinopathy.

Current Neuropharmacology, *16*(7), 993–1003.

https://doi.org/10.2174/1570159X15666170717115654

Amato, R., Giannaccini, M., Dal Monte, M., Cammalleri, M., Pini, A., Raffa, V., Lulli, M., &

Casini, G. (2020). Association of the Somatostatin Analog Octreotide With Magnetic

Nanoparticles for Intraocular Delivery: A Possible Approach for the Treatment of

Diabetic Retinopathy. *Frontiers in Bioengineering and Biotechnology*, *8*.

https://doi.org/10.3389/fbioe.2020.00144

Ames, P., & Galor, A. (2015). Cyclosporine ophthalmic emulsions for the treatment of dry eye:

A review of the clinical evidence. *Clinical Investigation*, *5*(3), 267–285.

https://doi.org/10.4155/cli.14.135

Arya, G., Vandana, M., Acharya, S., & Sahoo, S. K. (2011). Enhanced antiproliferative activity of

Herceptin (HER2)-conjugated gemcitabine-loaded chitosan nanoparticle in pancreatic

cancer therapy. *Nanomedicine: Nanotechnology, Biology and Medicine*, *7*(6), 859–870.

https://doi.org/10.1016/j.nano.2011.03.009

Banga, A. K., Bose, S., & Ghosh, T. K. (1999). Iontophoresis and electroporation: Comparisons

and contrasts. *International Journal of Pharmaceutics*, *179*(1), 1–19.

https://doi.org/10.1016/S0378-5173(98)00360-3

Barar, J., Javadzadeh, A. R., & Omidi, Y. (2008). Ocular novel drug delivery: Impacts of

membranes and barriers. *Expert Opinion on Drug Delivery*, *5*(5), 567–581.

https://doi.org/10.1517/17425247.5.5.567

Barraud, L., Merle, P., Soma, E., Lefrançois, L., Guerret, S., Chevallier, M., Dubernet, C.,

Couvreur, P., Trépo, C., & Vitvitski, L. (2005). Increase of doxorubicin sensitivity by

doxorubicin-loading into nanoparticles for hepatocellular carcinoma cells in vitro and

in vivo. *Journal of Hepatology*, *42*(5), 736–743.

https://doi.org/10.1016/j.jhep.2004.12.035

Beales, P. L., Elcioglu, N., Woolf, A. S., Parker, D., & Flinter, F. A. (1999). New criteria for

improved diagnosis of Bardet-Biedl syndrome: Results of a population survey. *Journal

of Medical Genetics*, *36*(6), 437–446. https://doi.org/10.1136/jmg.36.6.437

Bertens, C. J. F., Gijs, M., van den Biggelaar, F. J. H. M., & Nuijts, R. M. M. A. (2018). Topical

drug delivery devices: A review. *Experimental Eye Research*, *168*, 149–160.

https://doi.org/10.1016/j.exer.2018.01.010

Bertolotti, A., Zhang, Y., Hendershot, L. M., Harding, H. P., & Ron, D. (2000). Dynamic

interaction of BiP and ER stress transducers in the unfolded-protein response. *Nature

Cell Biology*, *2*(6), 326–332. https://doi.org/10.1038/35014014

Bi, Y.-L., Wu, M.-F., Lu, L.-X., Zhou, Q., Du, F., Sun, X.-T., Tang, S.-F., & Xu, G.-T. (2013).

Functions of corneal endothelial cells do not change after uptake of

superparamagnetic iron oxide nanoparticles. *Molecular Medicine Reports*, *7*(6), 1767–

1772. https://doi.org/10.3892/mmr.2013.1418

Bill, A., Törnquist, P., & Alm, A. (1980). Permeability of the intraocular blood vessels. *Transactions of the Ophthalmological Societies of the United Kingdom*, *100*(3), 332–336.

Brun, A., Yu, X., Obringer, C., Ajoy, D., Haser, E., Stoetzel, C., Roux, M. J., Messaddeq, N., Dollfus, H., & Marion, V. (2019). In vivo phenotypic and molecular characterization of retinal degeneration in mouse models of three ciliopathies. *Experimental Eye Research*, *186*, 107721. https://doi.org/10.1016/j.exer.2019.107721

Bucolo, C., Drago, F., & Salomone, S. (2012). Ocular drug delivery: A clue from nanotechnology. *Frontiers in Pharmacology*, *3*. https://doi.org/10.3389/fphar.2012.00188

Cardoso, V. F., Francesko, A., Ribeiro, C., Bañobre-López, M., Martins, P., & Lanceros-Mendez, S. (2018). Advances in Magnetic Nanoparticles for Biomedical Applications. *Advanced Healthcare Materials*, *7*(5), 1700845. https://doi.org/10.1002/adhm.201700845

Cheruvu, N. P. S., & Kompella, U. B. (2006). Bovine and Porcine Transscleral Solute Transport: Influence of Lipophilicity and the Choroid–Bruch's Layer. *Investigative Ophthalmology & Visual Science*, *47*(10), 4513–4522. https://doi.org/10.1167/iovs.06-0404

Chopra, P., Hao, J., & Li, S. K. (2010). Iontophoretic transport of charged macromolecules across human sclera. *International Journal of Pharmaceutics*, *388*(1), 107–113. https://doi.org/10.1016/j.ijpharm.2009.12.046

Cognard, N., Scerbo, M. J., Obringer, C., Yu, X., Costa, F., Haser, E., Le, D., Stoetzel, C., Roux, M. J., Moulin, B., Dollfus, H., & Marion, V. (2015). Comparing the Bbs10 complete knockout phenotype with a specific renal epithelial knockout one highlights the link between renal defects and systemic inactivation in mice. *Cilia*, *4*. https://doi.org/10.1186/s13630-015-0019-8

Cooper, R. C., & Yang, H. (2019). Hydrogel-based ocular drug delivery systems: Emerging fabrication strategies, applications, and bench-to-bedside manufacturing

considerations. *Journal of Controlled Release*, *306*, 29–39.

https://doi.org/10.1016/j.jconrel.2019.05.034

Datta, P., Allamargot, C., Hudson, J. S., Andersen, E. K., Bhattarai, S., Drack, A. V., Sheffield, V.

C., & Seo, S. (2015). Accumulation of non-outer segment proteins in the outer segment

underlies photoreceptor degeneration in Bardet–Biedl syndrome. *Proceedings of the*

National Academy of Sciences, *112*(32), E4400–E4409.

https://doi.org/10.1073/pnas.1510111112

Davies, N. M. (2000). Biopharmaceutical Considerations In Topical Ocular Drug Delivery.

Clinical and Experimental Pharmacology and Physiology, *27*(7), 558–562.

https://doi.org/10.1046/j.1440-1681.2000.03288.x

Davis, B. M., Normando, E. M., Guo, L., Turner, L. A., Nizari, S., O'Shea, P., Moss, S. E.,

Somavarapu, S., & Cordeiro, M. F. (2014). Topical Delivery of Avastin to the Posterior

Segment of the Eye In Vivo Using Annexin A5-associated Liposomes. *Small*, *10*(8),

1575–1584. https://doi.org/10.1002/smll.201303433

Davis, R. E., Swiderski, R. E., Rahmouni, K., Nishimura, D. Y., Mullins, R. F., Agassandian, K.,

Philp, A. R., Searby, C. C., Andrews, M. P., Thompson, S., Berry, C. J., Thedens, D. R.,

Yang, B., Weiss, R. M., Cassell, M. D., Stone, E. M., & Sheffield, V. C. (2007). A knockin

mouse model of the Bardet–Biedl syndrome 1 M390R mutation has cilia defects,

ventriculomegaly, retinopathy, and obesity. *Proceedings of the National Academy of*

Sciences, *104*(49), 19422–19427. https://doi.org/10.1073/pnas.0708571104

de Melo, J., & Blackshaw, S. (2018). In Vivo Electroporation of Developing Mouse Retina. In C.

J. F. Boon & J. Wijnholds (Eds.), *Retinal Gene Therapy: Methods and Protocols* (pp.

101–111). Springer. https://doi.org/10.1007/978-1-4939-7522-8_8

del Amo, E. M., Rimpelä, A.-K., Heikkinen, E., Kari, O. K., Ramsay, E., Lajunen, T., Schmitt, M.,

Pelkonen, L., Bhattacharya, M., Richardson, D., Subrizi, A., Turunen, T., Reinisalo, M.,

Itkonen, J., Toropainen, E., Casteleijn, M., Kidron, H., Antopolsky, M., Vellonen, K.-S., …

Urtti, A. (2017). Pharmacokinetic aspects of retinal drug delivery. *Progress in Retinal and Eye Research*, *57*, 134–185. https://doi.org/10.1016/j.preteyeres.2016.12.001

Dengler, M., Saatchi, K., Dailey, J. P., Matsubara, J., Mikelberg, F. S., Häfeli, U. O., & Yeung, S. N. (2010). Targeted Delivery of Magnetic Cobalt Nanoparticles to the Eye Following Systemic Administration. *AIP Conference Proceedings*, *1311*(1), 329–336. https://doi.org/10.1063/1.3530034

Doughty, M. J., & Zaman, M. L. (2000). Human Corneal Thickness and Its Impact on Intraocular Pressure Measures: A Review and Meta-analysis Approach. *Survey of Ophthalmology*, *44*(5), 367–408. https://doi.org/10.1016/S0039-6257(00)00110-7

Eljarrat-Binstock, E., Pe'er, J., & Domb, A. J. (2010). New Techniques for Drug Delivery to the Posterior Eye Segment. *Pharmaceutical Research*, *27*(4), 530–543. https://doi.org/10.1007/s11095-009-0042-9

Evertsson, M., Kjellman, P., Cinthio, M., Andersson, R., Tran, T. A., In't Zandt, R., Grafström, G., Toftevall, H., Fredriksson, S., Ingvar, C., Strand, S.-E., & Jansson, T. (2017). Combined Magnetomotive ultrasound, PET/CT, and MR imaging of 68Ga-labelled superparamagnetic iron oxide nanoparticles in rat sentinel lymph nodes in vivo. *Scientific Reports*, *7*(1), 4824. https://doi.org/10.1038/s41598-017-04396-z

Fatima, H., & Kim, K.-S. (2018). Iron-based magnetic nanoparticles for magnetic resonance imaging. *Advanced Powder Technology*, *29*(11), 2678–2685. https://doi.org/10.1016/j.apt.2018.07.017

Forsythe, E., Kenny, J., Bacchelli, C., & Beales, P. L. (2018). Managing Bardet–Biedl Syndrome—Now and in the Future. *Frontiers in Pediatrics*, *6*. https://doi.org/10.3389/fped.2018.00023

Gardeniers, H. J. G. E., Luttge, R., Berenschot, E. J. W., Boer, M. J. de, Yeshurun, S. Y., Hefetz, M., Oever, R. van't, & Berg, A. van den. (2003). Silicon micromachined hollow

microneedles for transdermal liquid transport. *Journal of Microelectromechanical Systems*, *12*(6), 855–862. https://doi.org/10.1109/JMEMS.2003.820293

Garrigue, J.-S., Amrane, M., Faure, M.-O., Holopainen, J. M., & Tong, L. (2017). Relevance of Lipid-Based Products in the Management of Dry Eye Disease. *Journal of Ocular Pharmacology and Therapeutics*, *33*(9), 647–661. https://doi.org/10.1089/jop.2017.0052

Giannaccini, M., Giannini, M., Calatayud, M. P., Goya, G. F., Cuschieri, A., Dente, L., & Raffa, V. (2014). Magnetic Nanoparticles as Intraocular Drug Delivery System to Target Retinal Pigmented Epithelium (RPE). *International Journal of Molecular Sciences*, *15*(1), 1590–1605. https://doi.org/10.3390/ijms15011590

Giannaccini, M., Pedicini, L., De Matienzo, G., Chiellini, F., Dente, L., & Raffa, V. (2017). Magnetic nanoparticles: A strategy to target the choroidal layer in the posterior segment of the eye. *Scientific Reports*, *7*(1), 43092. https://doi.org/10.1038/srep43092

Giannaccini, M., Usai, A., Chiellini, F., Guadagni, V., Andreazzoli, M., Ori, M., Pasqualetti, M., Dente, L., & Raffa, V. (2018). Neurotrophin-conjugated nanoparticles prevent retina damage induced by oxidative stress. *Cellular and Molecular Life Sciences*, *75*(7), 1255–1267. https://doi.org/10.1007/s00018-017-2691-x

Gorbatyuk, M. S., Starr, C. R., & Gorbatyuk, O. S. (2020). Endoplasmic reticulum stress: New insights into the pathogenesis and treatment of retinal degenerative diseases. *Progress in Retinal and Eye Research*, 100860. https://doi.org/10.1016/j.preteyeres.2020.100860

Gote, V., Sikder, S., Sicotte, J., & Pal, D. (2019). Ocular Drug Delivery: Present Innovations and Future Challenges. *Journal of Pharmacology and Experimental Therapeutics*, *370*(3), 602–624. https://doi.org/10.1124/jpet.119.256933

Gouronc, A., Zilliox, V., Jacquemont, M.-L., Darcel, F., Leuvrey, A.-S., Nourisson, E., Antin, M., Alessandri, J.-L., Doray, B., Gueguen, P., Payet, F., Randrianaivo, H., Stoetzel, C.,

Scheidecker, S., Flodrops, H., Dollfus, H., & Muller, J. (2020). High prevalence of

Bardet-Biedl syndrome in La Réunion Island is due to a founder variant in ARL6/BBS3.

Clinical Genetics, *98*(2), 166–171. https://doi.org/10.1111/cge.13768

Grottone, G. T., Loureiro, R. R., Covre, J., Rodrigues, E. B., & Gomes, J. Á. P. (2014). ARPE-19

Cell Uptake of Small and Ultrasmall Superparamagnetic Iron Oxide. *Current Eye*

Research, *39*(4), 403–410. https://doi.org/10.3109/02713683.2013.845228

Growth Charts—Data Table of Infant Head Circumference-for-age Charts. (n.d.). Retrieved 26

October 2020, from https://www.cdc.gov/growthcharts/html_charts/hcageinf.htm

Guo, T., Lin, M., Huang, J., Zhou, C., Tian, W., Yu, H., Jiang, X., Ye, J., Shi, Y., Xiao, Y., Bian, X., &

Feng, X. (2018, April 29). *The Recent Advances of Magnetic Nanoparticles in Medicine*

[Review Article]. Journal of Nanomaterials; Hindawi.

https://doi.org/10.1155/2018/7805147

Guy, R. H., Kalia, Y. N., Delgado-Charro, M. B., Merino, V., López, A., & Marro, D. (2000).

Iontophoresis: Electrorepulsion and electroosmosis. *Journal of Controlled Release*,

64(1), 129–132. https://doi.org/10.1016/S0168-3659(99)00132-7

Hämäläinen, K. M., Kananen, K., Auriola, S., Kontturi, K., & Urtti, A. (1997). Characterization of

paracellular and aqueous penetration routes in cornea, conjunctiva, and sclera.

Investigative Ophthalmology & Visual Science, *38*(3), 627–634.

Han, H. D., Mangala, L. S., Lee, J. W., Shahzad, M. M. K., Kim, H. S., Shen, D., Nam, E. J., Mora,

E. M., Stone, R. L., Lu, C., Lee, S. J., Roh, J. W., Nick, A. M., Lopez-Berestein, G., & Sood,

A. K. (2010). Targeted Gene Silencing Using RGD-Labeled Chitosan Nanoparticles.

Clinical Cancer Research, *16*(15), 3910–3922. https://doi.org/10.1158/1078-0432.CCR-

10-0005

Hao, J., Li, S. K., Liu, C.-Y., & Kao, W. W. Y. (2009). Electrically assisted delivery of

macromolecules into the corneal epithelium. *Experimental Eye Research*, *89*(6), 934–

941. https://doi.org/10.1016/j.exer.2009.08.001

VI. Bibliography

Harrison, J., Bartlett, C. A., Cowin, G., Nicholls, P. K., Evans, C. W., Clemons, T. D., Zdyrko, B., Luzinov, I. A., Harvey, A. R., Iyer, K. S., Dunlop, S. A., & Fitzgerald, M. (2012). In vivo Imaging and Biodistribution of Multimodal Polymeric Nanoparticles Delivered to the Optic Nerve. *Small*, *8*(10), 1579–1589. https://doi.org/10.1002/smll.201102648

Hedayatnasab, Z., Abnisa, F., & Daud, W. M. A. W. (2017). Review on magnetic nanoparticles for magnetic nanofluid hyperthermia application. *Materials & Design*, *123*, 174–196. https://doi.org/10.1016/j.matdes.2017.03.036

Henriksson, J. T., De Paiva, C. S., Farley, W., Pflugfelder, S. C., Burns, A. R., & Bergmanson, J. P. G. (2013). Morphological Alterations of the Palpebral Conjunctival Epithelium in a Dry Eye Model. *Cornea*, *32*(4), 483–490. https://doi.org/10.1097/ICO.0b013e318265682c

Henriksson, J. T., McDermott, A. M., & Bergmanson, J. P. G. (2009). Dimensions and Morphology of the Cornea in Three Strains of Mice. *Investigative Ophthalmology & Visual Science*, *50*(8), 3648–3654. https://doi.org/10.1167/iovs.08-2941

Hetz, C., Zhang, K., & Kaufman, R. J. (2020). Mechanisms, regulation and functions of the unfolded protein response. *Nature Reviews Molecular Cell Biology*, *21*(8), 421–438. https://doi.org/10.1038/s41580-020-0250-z

Himawan, E., Ekström, P., Buzgo, M., Gaillard, P., Stefánsson, E., Marigo, V., Loftsson, T., & Paquet-Durand, F. (2019). Drug delivery to retinal photoreceptors. *Drug Discovery Today*, *24*(8), 1637–1643. https://doi.org/10.1016/j.drudis.2019.03.004

Hosoya, K., Lee, V. H. L., & Kim, K.-J. (2005). Roles of the conjunctiva in ocular drug delivery: A review of conjunctival transport mechanisms and their regulation. *European Journal of Pharmaceutics and Biopharmaceutics*, *60*(2), 227–240. https://doi.org/10.1016/j.ejpb.2004.12.007

Huang, D., Chen, Y.-S., & Rupenthal, I. D. (2018). Overcoming ocular drug delivery barriers through the use of physical forces. *Advanced Drug Delivery Reviews*, *126*, 96–112. https://doi.org/10.1016/j.addr.2017.09.008

VI. Bibliography

Hughes, A. (1979). A schematic eye for the rat. *Vision Research*, *19*(5), 569–588.

https://doi.org/10.1016/0042-6989(79)90143-3

Ito, A., Hibino, E., Kobayashi, C., Terasaki, H., Kagami, H., Ueda, M., Kobayashi, T., & Honda, H.

(2005). Construction and Delivery of Tissue-Engineered Human Retinal Pigment

Epithelial Cell Sheets, Using Magnetite Nanoparticles and Magnetic Force. *Tissue*

Engineering, *11*(3–4), 489–496. https://doi.org/10.1089/ten.2005.11.489

Jackson, T. L., Antcliff, R. J., Hillenkamp, J., & Marshall, J. (2003). Human Retinal Molecular

Weight Exclusion Limit and Estimate of Species Variation. *Investigative Ophthalmology*

& Visual Science, *44*(5), 2141–2146. https://doi.org/10.1167/iovs.02-1027

Jager, R. D., Aiello, L. P., Patel, S. C., & Cunningham, E. T. J. (2004). RISKS OF INTRAVITREOUS

INJECTION: A COMPREHENSIVE REVIEW. *RETINA*, *24*(5), 676–698.

Jiang, J., Gill, H. S., Ghate, D., McCarey, B. E., Patel, S. R., Edelhauser, H. F., & Prausnitz, M. R.

(2007). Coated Microneedles for Drug Delivery to the Eye. *Investigative*

Ophthalmology & Visual Science, *48*(9), 4038–4043. https://doi.org/10.1167/iovs.07-

0066

Joyce, N. C. (2003). Proliferative capacity of the corneal endothelium. *Progress in Retinal and*

Eye Research, *22*(3), 359–389. https://doi.org/10.1016/S1350-9462(02)00065-4

Kalia, Y. N., Naik, A., Garrison, J., & Guy, R. H. (2004). Iontophoretic drug delivery. *Advanced*

Drug Delivery Reviews, *56*(5), 619–658. https://doi.org/10.1016/j.addr.2003.10.026

Ke, Y.-N., & Yang, W.-X. (2014). Primary cilium: An elaborate structure that blocks cell division?

Gene, *547*(2), 175–185. https://doi.org/10.1016/j.gene.2014.06.050

Kim, S. H., Lutz, R. J., Wang, N. S., & Robinson, M. R. (2007). Transport Barriers in Transscleral

Drug Delivery for Retinal Diseases. *Ophthalmic Research*, *39*(5), 244–254.

https://doi.org/10.1159/000108117

Kim, Y. C., Grossniklaus, H. E., Edelhauser, H. F., & Prausnitz, M. R. (2014). Intrastromal Delivery

of Bevacizumab Using Microneedles to Treat Corneal Neovascularization. *Investigative*

Ophthalmology & Visual Science, *55*(11), 7376–7386. https://doi.org/10.1167/iovs.14-15257

Korenfeld, M. S., Silverstein, S. M., Cooke, D. L., Vogel, R., & Crockett, R. S. (2009). Difluprednate ophthalmic emulsion 0.05% for postoperative inflammation and pain. *Journal of Cataract & Refractive Surgery*, *35*(1), 26–34. https://doi.org/10.1016/j.jcrs.2008.09.024

Lamb, T., & Burns, M. E. (2004). *Visual transduction by rod and cone photoreceptors*. MIT Press. https://openresearch-repository.anu.edu.au/handle/1885/77227

Le Goff, M. M., & Bishop, P. N. (2008). Adult vitreous structure and postnatal changes. *Eye*, *22*(10), 1214–1222. https://doi.org/10.1038/eye.2008.21

Lentacker, I., De Cock, I., Deckers, R., De Smedt, S. C., & Moonen, C. T. W. (2014). Understanding ultrasound induced sonoporation: Definitions and underlying mechanisms. *Advanced Drug Delivery Reviews*, *72*, 49–64. https://doi.org/10.1016/j.addr.2013.11.008

Liang, F.-Q., Aleman, T. S., Dejneka, N. S., Dudus, L., Fisher, K. J., Maguire, A. M., Jacobson, S. G., & Bennett, J. (2001). Long-Term Protection of Retinal Structure but Not Function Using RAAV.CNTF in Animal Models of Retinitis Pigmentosa. *Molecular Therapy*, *4*(5), 461–472. https://doi.org/10.1006/mthe.2001.0473

Liaw, J., Rojanasakul, Y., & Robinson, J. R. (1992). The effect of drug charge type and charge density on corneal transport. *International Journal of Pharmaceutics*, *88*(1), 111–124. https://doi.org/10.1016/0378-5173(92)90308-O

L. Lim, H., Hwang, Y., Kar, M., & Varghese, S. (2014). Smart hydrogels as functional biomimetic systems. *Biomaterials Science*, *2*(5), 603–618. https://doi.org/10.1039/C3BM60288E

Lu, M., Cohen, M. H., Rieves, D., & Pazdur, R. (2010). FDA report: Ferumoxytol for intravenous iron therapy in adult patients with chronic kidney disease. *American Journal of Hematology*, *85*(5), 315–319. https://doi.org/10.1002/ajh.21656

Ma, D. J., Lim, M.-S., Park, U. C., Park, J.-B., Ji, S. Y., & Yu, H. G. (2019). Magnetic Iron Oxide

Nanoparticle Labeling of Photoreceptor Precursors for Magnetic Resonance Imaging.

Tissue Engineering Part C: Methods, *25*(9), 532–542.

https://doi.org/10.1089/ten.tec.2019.0136

Malicki, J. J., & Johnson, C. A. (2017). The Cilium: Cellular Antenna and Central Processing Unit.

Trends in Cell Biology, *27*(2), 126–140. https://doi.org/10.1016/j.tcb.2016.08.002

Marro, D., Kalia, Y. N., Begoña Delgado-Charro, M., & Guy, R. H. (2001). Contributions of

Electromigration and Electroosmosis to Iontophoretic Drug Delivery. *Pharmaceutical*

Research, *18*(12), 1701–1708. https://doi.org/10.1023/A:1013318412527

Matsuda, T., & Cepko, C. L. (2004). Electroporation and RNA interference in the rodent retina

in vivo and in vitro. *Proceedings of the National Academy of Sciences*, *101*(1), 16–22.

https://doi.org/10.1073/pnas.2235688100

Matsuda, Takahiko, & Cepko, C. L. (2007). Controlled expression of transgenes introduced by in

vivo electroporation. *Proceedings of the National Academy of Sciences*, *104*(3), 1027–

1032. https://doi.org/10.1073/pnas.0610155104

May-Simera, H., Nagel-Wolfrum, K., & Wolfrum, U. (2017). Cilia—The sensory antennae in the

eye. *Progress in Retinal and Eye Research*, *60*, 144–180.

https://doi.org/10.1016/j.preteyeres.2017.05.001

Meng, T., Kulkarni, V., Simmers, R., Brar, V., & Xu, Q. (2019). Therapeutic implications of

nanomedicine for ocular drug delivery. *Drug Discovery Today*, *24*(8), 1524–1538.

https://doi.org/10.1016/j.drudis.2019.05.006

Mimura, T., Yamagami, S., Usui, T., Ishii, Y., Ono, K., Yokoo, S., Funatsu, H., Araie, M., & Amano,

S. (2005). Long-term outcome of iron-endocytosing cultured corneal endothelial cell

transplantation with magnetic attraction. *Experimental Eye Research*, *80*(2), 149–157.

https://doi.org/10.1016/j.exer.2004.08.021

VI. Bibliography

Mirza, S., Ahmad, M. S., Shah, M. I. A., & Ateeq, M. (2020). Chapter 11 - Magnetic

nanoparticles: Drug delivery and bioimaging applications. In M. R. Shah, M. Imran, & S.

Ullah (Eds.), *Metal Nanoparticles for Drug Delivery and Diagnostic Applications* (pp.

189–213). Elsevier. https://doi.org/10.1016/B978-0-12-816960-5.00011-2

Mitragotri, S., Edwards, D. A., Blankschtein, D., & Langer, R. (1995). A Mechanistic Study of

Ultrasonically-Enhanced Transdermal Drug Delivery. *Journal of Pharmaceutical

Sciences*, *84*(6), 697–706. https://doi.org/10.1002/jps.2600840607

Mockel, A., Obringer, C., Hakvoort, T. B. M., Seeliger, M., Lamers, W. H., Stoetzel, C., Dollfus,

H., & Marion, V. (2012). Pharmacological Modulation of the Retinal Unfolded Protein

Response in Bardet-Biedl Syndrome Reduces Apoptosis and Preserves Light Detection

Ability. *The Journal of Biological Chemistry*, *287*(44), 37483–37494.

https://doi.org/10.1074/jbc.M112.386821

Moosa, R. M., Choonara, Y. E., Toit, L. C. du, Kumar, P., Carmichael, T., Tomar, L. K., Tyagi, C., &

Pillay, V. (2014). A review of topically administered mini-tablets for drug delivery to the

anterior segment of the eye. *Journal of Pharmacy and Pharmacology*, *66*(4), 490–506.

https://doi.org/10.1111/jphp.12131

Mousavikhamene, Z., Abdekhodaie, M. J., & Ahmadieh, H. (2017). Facilitation of transscleral

drug delivery by drug loaded magnetic polymeric particles. *Materials Science and

Engineering: C*, *79*, 812–820. https://doi.org/10.1016/j.msec.2017.05.015

Moysidis, S. N., Alvarez-Delfin, K., Peschansky, V. J., Salero, E., Weisman, A. D., Bartakova, A.,

Raffa, G. A., Merkhofer, R. M., Kador, K. E., Kunzevitzky, N. J., & Goldberg, J. L. (2015).

Magnetic field-guided cell delivery with nanoparticle-loaded human corneal

endothelial cells. *Nanomedicine: Nanotechnology, Biology and Medicine*, *11*(3), 499–

509. https://doi.org/10.1016/j.nano.2014.12.002

Naha, P. C., Zaki, A. A., Hecht, E., Chorny, M., Chhour, P., Blankemeyer, E., Yates, D. M.,

Witschey, W. R. T., Litt, H. I., Tsourkas, A., & Cormode, D. P. (2014). Dextran coated

bismuth–iron oxide nanohybrid contrast agents for computed tomography and

magnetic resonance imaging. *Journal of Materials Chemistry B*, *2*(46), 8239–8248.

https://doi.org/10.1039/C4TB01159G

Neumann, E., & Rosenheck, K. (1972). Permeability changes induced by electric impulses in

vesicular membranes. *The Journal of Membrane Biology*, *10*(1), 279–290.

https://doi.org/10.1007/BF01867861

O'Neil, E. C., Huang, J., Suhler, E. B., Jr, J. P. D., Perez, V. L., Gritz, D. C., McWilliams, K., Peskin,

E., Ying, G., Bunya, V. Y., Maguire, M. G., & Kempen, J. H. (2018). Iontophoretic

delivery of dexamethasone phosphate for non-infectious, non-necrotising anterior

scleritis, dose-finding clinical trial. *British Journal of Ophthalmology*, *102*(8), 1011–

1013. https://doi.org/10.1136/bjophthalmol-2017-311610

Oyster, C. W. (n.d.). *The Human Eye: Structure and Function*. 16.

Park, J., Zhang, Y., Vykhodtseva, N., Akula, J. D., & McDannold, N. J. (2012). Targeted and

Reversible Blood-Retinal Barrier Disruption via Focused Ultrasound and Microbubbles.

PLOS ONE, *7*(8), e42754. https://doi.org/10.1371/journal.pone.0042754

Park, J.-H., Allen, M. G., & Prausnitz, M. R. (2005). Biodegradable polymer microneedles:

Fabrication, mechanics and transdermal drug delivery. *Journal of Controlled Release*,

104(1), 51–66. https://doi.org/10.1016/j.jconrel.2005.02.002

Patane, M. A., Cohen, A., Sugarman, J., & From, S. (2010). Randomized, Double-Masked Study

of Four Iontophoresis Dose Levels of EGP-437 in Non-Infectious Anterior Segment

Uveitis Subjects. *Investigative Ophthalmology & Visual Science*, *51*(13), 5263–5263.

Patane, Michael A., Cohen, A., From, S., Torkildsen, G., Welch, D., & Ousler, G. W. (2011).

Ocular iontophoresis of EGP-437 (dexamethasone phosphate) in dry eye patients:

Results of a randomized clinical trial. *Clinical Ophthalmology (Auckland, N.Z.)*, *5*, 633–

643. https://doi.org/10.2147/OPTH.S19349

VI. Bibliography

Patel, S. R., Lin, A. S. P., Edelhauser, H. F., & Prausnitz, M. R. (2011). Suprachoroidal Drug

Delivery to the Back of the Eye Using Hollow Microneedles. *Pharmaceutical Research*,

28(1), 166–176. https://doi.org/10.1007/s11095-010-0271-y

Patel, S. V., Bachman, L. A., Hann, C. R., Bahler, C. K., & Fautsch, M. P. (2009). Human Corneal

Endothelial Cell Transplantation in a Human Ex Vivo Model. *Investigative*

Ophthalmology & Visual Science, *50*(5), 2123–2131. https://doi.org/10.1167/iovs.08-

2653

Peng, Y., Tang, L., & Zhou, Y. (2017). Subretinal Injection: A Review on the Novel Route of

Therapeutic Delivery for Vitreoretinal Diseases. *Ophthalmic Research*, *58*(4), 217–226.

https://doi.org/10.1159/000479157

Pitkänen, L., Ranta, V.-P., Moilanen, H., & Urtti, A. (2005). Permeability of Retinal Pigment

Epithelium: Effects of Permeant Molecular Weight and Lipophilicity. *Investigative*

Ophthalmology & Visual Science, *46*(2), 641–646. https://doi.org/10.1167/iovs.04-

1051

Prow, T. W., Bhutto, I., Kim, S. Y., Grebe, R., Merges, C., McLeod, D. S., Uno, K., Mennon, M.,

Rodriguez, L., Leong, K., & Lutty, G. A. (2008). Ocular Nanoparticle Toxicity and

Transfection of the Retina and Retinal Pigment Epithelium. *Nanomedicine :*

Nanotechnology, Biology, and Medicine, *4*(4), 340–349.

https://doi.org/10.1016/j.nano.2008.06.003

Raju, H. B., Hu, Y., Padgett, K. R., Rodriguez, J. E., & Goldberg, J. L. (2012). Investigation of

nanoparticles using magnetic resonance imaging after intravitreal injection. *Clinical &*

Experimental Ophthalmology, *40*(1), 100–107. https://doi.org/10.1111/j.1442-

9071.2011.02651.x

Raju, H. B., Hu, Y., Vedula, A., Dubovy, S. R., & Goldberg, J. L. (2011). Evaluation of Magnetic

Micro- and Nanoparticle Toxicity to Ocular Tissues. *PLOS ONE*, *6*(5), e17452.

https://doi.org/10.1371/journal.pone.0017452

Ranta, V.-P., & Urtti, A. (2006). Transscleral drug delivery to the posterior eye: Prospects of
pharmacokinetic modeling. *Advanced Drug Delivery Reviews*, *58*(11), 1164–1181.
https://doi.org/10.1016/j.addr.2006.07.025

Raviola, G. (1974). Effects of Paracentesis on The Blood-Aqueous Barrier: An Electron
Microscope Study on Macaca Mulatto, Using Horseradish Peroxidase as a Tracer.
Investigative Ophthalmology & Visual Science, *13*(11), 828–858.

Raviola, G. (1977). The structural basis of the blood-ocular barriers. *Experimental Eye Research*,
25, 27–63. https://doi.org/10.1016/S0014-4835(77)80009-2

Reguera, J., Aberasturi, D. J. de, Henriksen-Lacey, M., Langer, J., Espinosa, A., Szczupak, B.,
Wilhelm, C., & M. Liz-Marzán, L. (2017). Janus plasmonic–magnetic gold–iron oxide
nanoparticles as contrast agents for multimodal imaging. *Nanoscale*, *9*(27), 9467–
9480. https://doi.org/10.1039/C7NR01406F

Reiter, J. F., & Leroux, M. R. (2017). Genes and molecular pathways underpinning ciliopathies.
Nature Reviews Molecular Cell Biology, *18*(9), 533–547.
https://doi.org/10.1038/nrm.2017.60

Remtulla, S., & Hallett, P. E. (1985). A schematic eye for the mouse, and comparisons with the
rat. *Vision Research*, *25*(1), 21–31. https://doi.org/10.1016/0042-6989(85)90076-8

ROBINSON, J. C. (1993). Ocular anatomy and physiology relevant to ocular drug delivery.
Ocular Anatomy and Physiology Relevant to Ocular Drug Delivery, *58*, 29–57.

Ron, D., & Walter, P. (2007). Signal integration in the endoplasmic reticulum unfolded protein
response. *Nature Reviews. Molecular Cell Biology*, *8*(7), 519–529.
https://doi.org/10.1038/nrm2199

Salamanca, A. E. de, Diebold, Y., Calonge, M., García-Vazquez, C., Callejo, S., Vila, A., & Alonso,
M. J. (2006). Chitosan Nanoparticles as a Potential Drug Delivery System for the Ocular
Surface: Toxicity, Uptake Mechanism and In Vivo Tolerance. *Investigative*

Ophthalmology & Visual Science, *47*(4), 1416–1425. https://doi.org/10.1167/iovs.05-0495

Singh, V., & Ahmad, R. (2011). The Challenges of Ophthalmic drug Delivery: A Review. *International Journal of Drug Delivery*, *3*, 56–62.

Smith, R. S., & Rudt, L. A. (1975). Ocular vascular and epithelial barriers to microperoxidase. *Investigative Ophthalmology & Visual Science*, *14*(7), 556–560.

Snider, E. J., Kubelick, K. P., Tweed, K., Kim, R. K., Li, Y., Gao, K., Read, A. T., Emelianov, S., & Ethier, C. R. (2018). Improving Stem Cell Delivery to the Trabecular Meshwork Using Magnetic Nanoparticles. *Scientific Reports*, *8*(1), 12251. https://doi.org/10.1038/s41598-018-30834-7

Song, D., & Dunaief, J. L. (2013). Retinal iron homeostasis in health and disease. *Frontiers in Aging Neuroscience*, *5*. https://doi.org/10.3389/fnagi.2013.00024

Sonoda, S., Tachibana, K., Uchino, E., Okubo, A., Yamamoto, M., Sakoda, K., Hisatomi, T., Sonoda, K.-H., Negishi, Y., Izumi, Y., Takao, S., & Sakamoto, T. (2006). Gene Transfer to Corneal Epithelium and Keratocytes Mediated by Ultrasound with Microbubbles. *Investigative Ophthalmology & Visual Science*, *47*(2), 558–564. https://doi.org/10.1167/iovs.05-0889

Starr, C. R., Pitale, P. M., & Gorbatyuk, M. (2018). Translational attenuation and retinal degeneration in mice with an active integrated stress response. *Cell Death & Disease*, *9*(5), 1–9. https://doi.org/10.1038/s41419-018-0513-1

Sun, C., Veiseh, O., Gunn, J., Fang, C., Hansen, S., Lee, D., Sze, R., Ellenbogen, R. G., Olson, J., & Zhang, M. (2008). In Vivo MRI Detection of Gliomas by Chlorotoxin-Conjugated Superparamagnetic Nanoprobes. *Small*, *4*(3), 372–379. https://doi.org/10.1002/smll.200700784

VI. Bibliography

Tatham, A. J., Sarodia, U., Gatrad, F., & Awan, A. (2013). Eye drop instillation technique in patients with glaucoma. *Eye*, *27*(11), 1293–1298. https://doi.org/10.1038/eye.2013.187

Thakur, R. R. S., Fallows, S. J., McMillan, H. L., Donnelly, R. F., & Jones, D. S. (2014). Microneedle-mediated intrascleral delivery of in situ forming thermoresponsive implants for sustained ocular drug delivery. *Journal of Pharmacy and Pharmacology*, *66*(4), 584–595. https://doi.org/10.1111/jphp.12152

Thornit, D. N., Vinten, C. M., Sander, B., Lund-Andersen, H., & Cour, M. la. (2010). Blood–Retinal Barrier Glycerol Permeability in Diabetic Macular Edema and Healthy Eyes: Estimations from Macular Volume Changes after Peroral Glycerol. *Investigative Ophthalmology & Visual Science*, *51*(6), 2827–2834. https://doi.org/10.1167/iovs.09-4172

Tieleman, D. P. (2004). The molecular basis of electroporation. *BMC Biochemistry*, *5*(1), 10. https://doi.org/10.1186/1471-2091-5-10

Touchard, E., Berdugo, M., Bigey, P., El Sanharawi, M., Savoldelli, M., Naud, M.-C., Jeanny, J.-C., & Behar-Cohen, F. (2012). Suprachoroidal Electrotransfer: A Nonviral Gene Delivery Method to Transfect the Choroid and the Retina Without Detaching the Retina. *Molecular Therapy*, *20*(8), 1559–1570. https://doi.org/10.1038/mt.2011.304

Tzameret, A., Ketter-Katz, H., Edelshtain, V., Sher, I., Corem-Salkmon, E., Levy, I., Last, D., Guez, D., Mardor, Y., Margel, S., & Rotenstrich, Y. (2019). In vivo MRI assessment of bioactive magnetic iron oxide/human serum albumin nanoparticle delivery into the posterior segment of the eye in a rat model of retinal degeneration. *Journal of Nanobiotechnology*, *17*(1), 3. https://doi.org/10.1186/s12951-018-0438-y

Urtti, A. (2006). Challenges and obstacles of ocular pharmacokinetics and drug delivery. *Advanced Drug Delivery Reviews*, *58*(11), 1131–1135. https://doi.org/10.1016/j.addr.2006.07.027

VI. Bibliography

Urtti, A., Pipkin, J. D., Rork, G., Sendo, T., Finne, U., & Repta, A. J. (1990). Controlled drug

delivery devices for experimental ocular studies with timolol 2. Ocular and systemic

absorption in rabbits. *International Journal of Pharmaceutics*, *61*(3), 241–249.

https://doi.org/10.1016/0378-5173(90)90215-P

Vighi, E., Trifunović, D., Veiga-Crespo, P., Rentsch, A., Hoffmann, D., Sahaboglu, A., Strasser, T.,

Kulkarni, M., Bertolotti, E., Heuvel, A. van den, Peters, T., Reijerkerk, A., Euler, T.,

Ueffing, M., Schwede, F., Genieser, H.-G., Gaillard, P., Marigo, V., Ekström, P., &

Paquet-Durand, F. (2018). Combination of cGMP analogue and drug delivery system

provides functional protection in hereditary retinal degeneration. *Proceedings of the*

National Academy of Sciences, *115*(13), E2997–E3006.

https://doi.org/10.1073/pnas.1718792115

Voinov, M. A., Sosa Pagán, J. O., Morrison, E., Smirnova, T. I., & Smirnov, A. I. (2011). Surface-

mediated production of hydroxyl radicals as a mechanism of iron oxide nanoparticle

biotoxicity. *Journal of the American Chemical Society*, *133*(1), 35–41.

https://doi.org/10.1021/ja104683w

Wang, M., & Kaufman, R. J. (2016). Protein misfolding in the endoplasmic reticulum as a

conduit to human disease. *Nature*, *529*(7586), 326–335.

https://doi.org/10.1038/nature17041

Wang, Y., Xu, X., Gu, Y., Cheng, Y., & Cao, F. (2018). Recent advance of nanoparticle-based

topical drug delivery to the posterior segment of the eye. *Expert Opinion on Drug*

Delivery, *15*(7), 687–701. https://doi.org/10.1080/17425247.2018.1496080

Waters, A. M., & Beales, P. L. (2011). Ciliopathies: An expanding disease spectrum. *Pediatric*

Nephrology, *26*(7), 1039–1056. https://doi.org/10.1007/s00467-010-1731-7

Wirostko, B. M., Assang, C. M., Mann, B., From, S., & Raizman, M. (2017). Efficacy and safety of

an Iontophoresis platform to control post cataract inflammation and pain.

Investigative Ophthalmology & Visual Science, *58*(8), 1081–1081.

VI. Bibliography

Wright, A. F., Chakarova, C. F., Abd El-Aziz, M. M., & Bhattacharya, S. S. (2010). Photoreceptor degeneration: Genetic and mechanistic dissection of a complex trait. *Nature Reviews Genetics*, *11*(4), 273–284. https://doi.org/10.1038/nrg2717

Wu, K., Su, D., Liu, J., Saha, R., & Wang, J.-P. (2019). Magnetic nanoparticles in nanomedicine: A review of recent advances. *Nanotechnology*, *30*(50), 502003. https://doi.org/10.1088/1361-6528/ab4241

Wu, Y., Liu, Y., Li, X., Kebebe, D., Zhang, B., Ren, J., Lu, J., Li, J., Du, S., & Liu, Z. (2019). Research progress of in-situ gelling ophthalmic drug delivery system. *Asian Journal of Pharmaceutical Sciences*, *14*(1), 1–15. https://doi.org/10.1016/j.ajps.2018.04.008

Xia, X., Atkins, M., Dalal, R., Kuzmenko, O., Chang, K.-C., Sun, C. B., Benatti, C. A., Rak, D. J., Nahmou, M., Kunzevitzky, N. J., & Goldberg, J. L. (2019). Magnetic Human Corneal Endothelial Cell Transplant: Delivery, Retention, and Short-Term Efficacy. *Investigative Ophthalmology & Visual Science*, *60*(7), 2438–2448. https://doi.org/10.1167/iovs.18-26001

Yanai, A., Häfeli, U. O., Metcalfe, A. L., Soema, P., Addo, L., Gregory-Evans, C. Y., Po, K., Shan, X., Moritz, O. L., & Gregory-Evans, K. (2012). Focused Magnetic Stem Cell Targeting to the Retina Using Superparamagnetic Iron Oxide Nanoparticles. *Cell Transplantation*, *21*(6), 1137–1148. https://doi.org/10.3727/096368911X627435

Zahn, D., Klein, K., Radon, P., Berkov, D., Erokhin, S., Nagel, E., Eichhorn, M., Wiekhorst, F., & Dutz, S. (2020). Investigation of magnetically driven passage of magnetic nanoparticles through eye tissues for magnetic drug targeting. *Nanotechnology*, *31*(49), 495101. https://doi.org/10.1088/1361-6528/abb0b4

Zhang, H., Liu, X. L., Zhang, Y. F., Gao, F., Li, G. L., He, Y., Peng, M. L., & Fan, H. M. (2018). Magnetic nanoparticles based cancer therapy: Current status and applications. *Science China Life Sciences*, *61*(4), 400–414. https://doi.org/10.1007/s11427-017-9271-1

Résumé en Français

Ce résumé français résume brièvement le contexte scientifique, l'objectif de la thèse, la stratégie expérimentale et les résultats obtenus.

Non-invasive pharmacological treatment of retinal degeneration in the Bardet-Biedl Syndrome and related ciliopathies

Introduction :

Les dégénérescences rétiniennes héréditaires sont caractérisées par une dégénérescence progressive des cellules photoréceptrices et sont parmi les principales causes de cécité infantile en Europe. Alors que de multiples approches thérapeutiques sont étudiées et développées, l'une des préoccupations majeures et de longue date concernant le traitement des maladies rétiniennes héréditaires reste le ciblage efficace des cellules photoréceptrices touchées. L'adressage efficace de médicaments à la rétine reste un défi, l'injection intravitréenne (Figure 1.) étant l'une des méthodes les plus utilisées à ce jour.

Néanmoins, cette méthode présente une faible compliance du patient et les effets secondaires délétères potentiels. Une autre voie d'administration pour le traitement des maladies rétiniennes est l'administration systémique. Alors qu'il est possible d'atteindre le tissu rétinien avec des médicaments oraux, la concentration nécessaire à administrer est élevée et l'accès à la rétine est limitée en raison de l'existence d'une barrière serrée appelée barrière hémato-rétine.
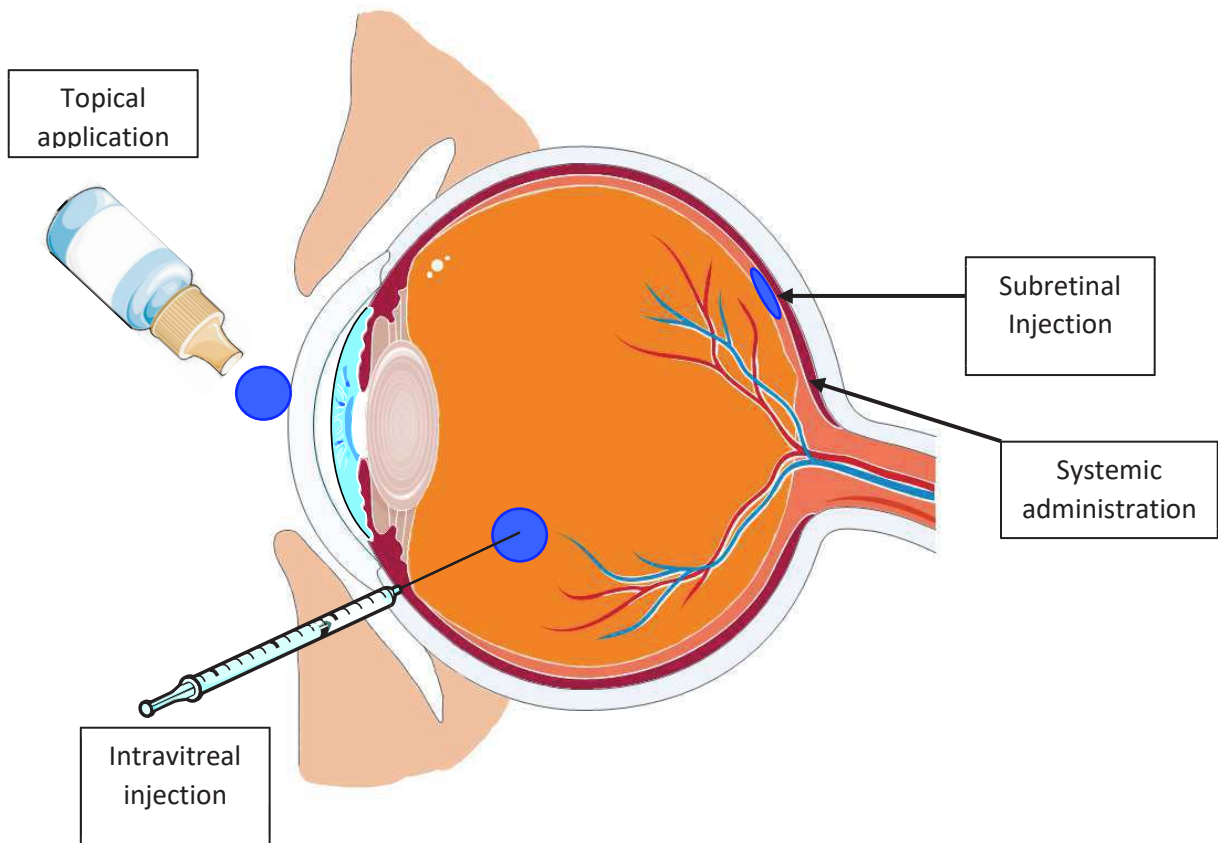
Figure 1. Représentation de l'oïl et les méthodes les plus commun pour l'administration de traitements pour les maladies ophtalmologiques.

Enfin, l'application topique de médicaments pour le traitement des maladies rétiniennes est considérée comme non efficace, certaines des limites de cette approche étant :

1. Les drogues appliquées topiquement sont lavées par les larmes, le clignotement et la circulation locale sur le point d'application.

2. La cornée agit une barrière serrée pour les composés qui sont appliqués de manière topique.

3. Si le médicament pénètre dans la chambre antérieure, le renouvellement de l'humeur aqueuse risque d'éloigner la drogue de sa cible.

4. La diffusion à travers la conjonctive et la sclérotique est limitée, la circulation systémique à travers le vaisseau local étant un facteur limitant important.

5. La quantité de drogue atteignant la chambre postérieure représente habituellement moins de 1% de la totalité du médicament appliqué topiquement. Une fois dans le corps vitré, les drogues peuvent être éliminés par le flux vers la chambre antérieure ou par clairance par les barrières sang-aqueuses et sang-rétiniennes.

6. La rétine présente une barrière physique sous la forme de la membrane limite interne qui peut limiter l'accès des molécules.

L'objectif de ce projet est de développer un système d'administration topique de médicaments ciblant les cellules photoréceptrices de la rétine, pouvant surmonter ces limitations. À cet effet, nous proposons l'utilisation de nanoparticules à noyau de fer superparamagnétiques (MNPs) comme gouttes oculaires guidées par un champ magnétique pour atteindre les tissus rétiniens.

Le protocole d'application de nos MNPs est le suivant : une goutte composée des MNPs est appliquée sur l'œil de la souris. Après l'application de la goutte, un aimant d'une puissance de 1 Tesla est placé à l'arrière de la tête de la souris pendant une durée de 30 minutes, comme indiqué dans la figure 2 :
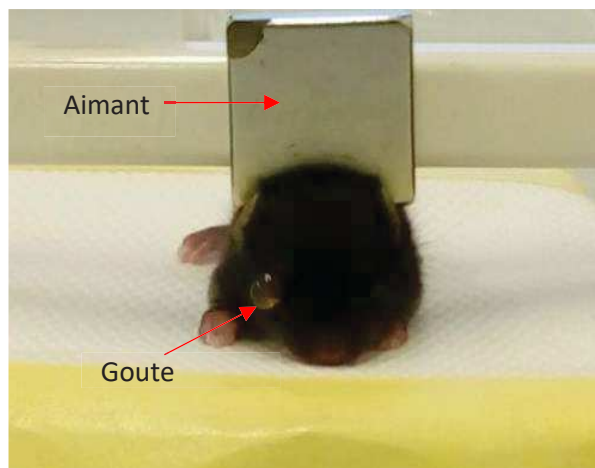

Figure 2. Set-up pour l'application de collyre contenant des MNPs. La figure montre la position de souris, l'aimant derrière la tête de souris et la goute avec des MNPs.

La raison en est que le champ magnétique peut améliorer le mouvement des MNPs en évitant, par exemple, l'absorption par la circulation locale tout en augmentant leur pénétration à travers les barrières biologiques de l'œil. Pour tester les MNPs, nous avons utilisé un modèle de souris mimant une Ciliopathie, à savoir les modèles KO du syndrome de Bardet-Biedl (BBS) que le laboratoire a étudié en profondeur. Des travaux antérieurs dans notre laboratoire ont montré que les modèles murins tels que le Bbs ($Bbs12^{-/-}$, $Bbs10^{-/-}$ et $Bbs1^{-/-}$) ou $Cep290^{-/-}$ (lié à l'amaurose congénitale Leber (LCA)) semblent partager un mécanisme commun d'apoptose dans les photorécepteurs [1]. La perturbation du transport des protéines du segment interne vers le segment externe des photorécepteurs, due à un dysfonctionnement des cils, entraîne une

accumulation de protéines dans le réticulum endoplasmique (RE) du segment interne des photorécepteurs (IS). Cette accumulation de protéines active à son tour un mécanisme appelé l'Unfolded Protein Response (UPR). L'activation prolongée de l'URP conduit à l'apoptose des photorécepteurs, à la diminution de l'épaisseur de la rétine et la dilatation du RE due à l'accumulation de protéines. L'utilisation de l'acide valproïque (VPA) et du guanabenz (GBZ) pour contrecarrer ces effets a déjà été démontrée par notre groupe : ces deux médicaments, déjà commercialisés, affecte l'UPR par la modulation des composants clés de cette voie. Le VPA augmente la concentration de la protéine chaperonne Bip, augmentant le pliage des protéines mal repliées présentes dans le RE ; le GBZ inhibera quant à lui la phosphatase GADD34, cette enzyme déphosphorylant Eif2 alpha, agissant dans l'UPR par diminution de la traduction des protéines. L'effet de ces deux médicaments conduit à la préservation de la fonction rétinienne dans le modèle murin $Bbs12^{-/-}$ [2]. Dans ces cas les deux composés ont été administré chaque jour pour une période de deux semaines.

Pour ce travail de thèse, nous avons utilisé des MNPs chargés avec ces 2 médicaments. Les souris utilisées ont été élevées sous fond génétique C57BL/6J. Les MNPs ont été appliqués sur des souris de 14 jours et les effets de ces composés ont été testés deux semaines après l'application topique. Nous avons utilisé des souris $Bbs^{+/+}$ pour les tests de toxicité et de mobilité et des souris $Bbs^{-/-}$ pour tester l'effet biologique de nos médicaments.

Résultats :

Pour obtenir nos résultats nous avons étudié les effets des nanoparticules sur les marqueurs d'UPR. Dans notre cas nous nous intéressons à la fonction rétinienne avec l'electroretinogram (ERG) (figure 3.), les effets sur la dilatation de réticulum endoplasmique et épaisseur de rétine et finalement les effets sur la concentration de protéines. Pour notre traitements nous avons administré le collyre dans un seule œil mais on a mesuré pour tous les cas aussi l'œil non traité (œil control).
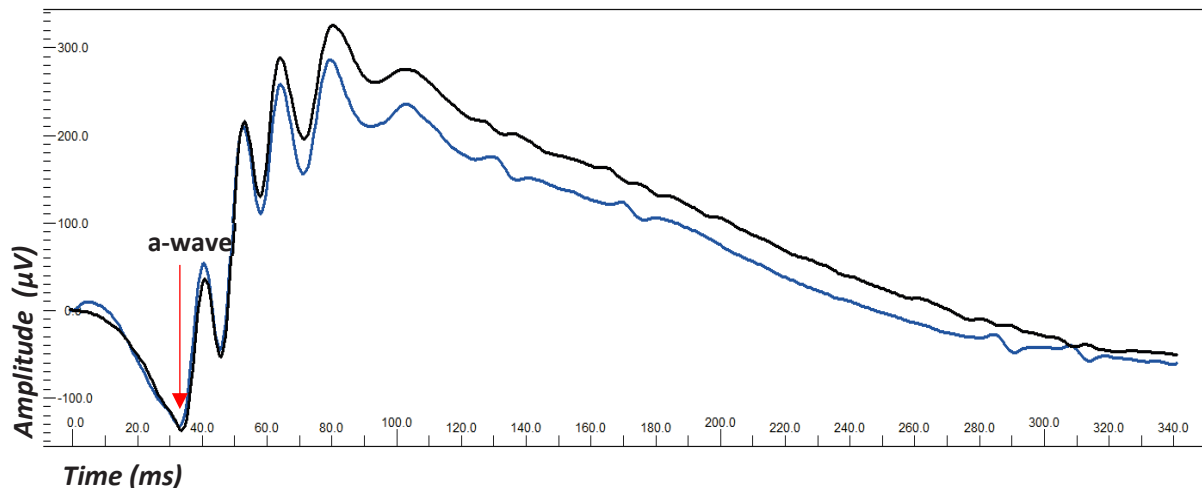
Figure 3. Example de tracé obtenu avec l'ERG. La flèche rouge indique le point mesuré dans notre projet (onde-a).

1-Toxicité des nanoparticules :

Nous abordons le profil d'innocuité des MNPs car le fer peut causer des effets inflammatoires par la formation d'espèces réactives d'oxygène (ROS) dans le tissu. Néanmoins, plusieurs études ont déjà étudié la sécurité des nanoparticules dans les tissus oculaires [3]

1.1-Toxicité *in vitro* :

Pour évaluer la toxicité possible des MNPs dans les tissus rétiniens, nous avons appliqué notre traitement à 2 cultures cellulaires différentes : des cellules hTERT-RPE1 (ATCC® CRL-400) et des cellules précurseurs de photorécepteurs 661W (The University of Oklahoma, Health Sciences centre, Department of Cell biology). Nous n'avons observé aucune augmentation de l'apoptose cellulaire suite à une exposition aux MNPs.

1.2 Toxicité *in vivo* :

Pour évaluer les effets secondaires potentiels des MNPs dans la fonction rétinienne, des souris *Bbs^{+/+}* ont été traitées en utilisant nos MNPs comme expliqué précédemment. L'enregistrement par ERG a été effectué après l'application topique. Différentes dilutions ont été testées : 1 mg / ml de MNP, 0,04 mg / ml de MNP, 0,02 mg / ml de MNP et 0,01 mg / ml de MNP avec 6 souris utilisées par groupe. Aucune diminution significative de l'enregistrement ERG n'a été observée chez nos souris *Bbs^{+/+}* traitées par rapport à nos souris *Bbs^{+/+}* non traitées. Nous pouvons en conclure que l'application des MNPs n'a pas d'impact négatif sur la fonction rétinienne.

2-Mobilité des nanoparticules :

Le principal problème avec l'application de médicaments topiques oculaires est la faible biodisponibilité des composés. Par conséquent, nous nous devions d'évaluer comment les MNPs sont capables d'atteindre la rétine et comment ils peuvent pénétrer à l'intérieur de l'œil. La durée de nos études pour la mobilité des MNPs a été affectée par le confinement dû à la COVID-19, mais d'autres expériences concernant la mobilité et le comportement des MNPs seront menées par le groupe dirigé par le Pr. Arto Urtti, étudiant la délivrance de médicaments oculaires. Les nanoparticules de noyau ferreux peuvent être observées en utilisant l'imagerie par résonance magnétique (IRM) car elles présentent des caractéristiques similaires aux agents de contraste utilisés dans la pratique clinique

2.1- Mouvement des nanoparticules après application en collyre :

En utilisant l'IRM, nous avons pu observer le comportement des MNPs après application topique sur des souris. Après application, nous n'avons pas pu observer de différence dans le mouvement de nos différents MNPs. Ça veut dire que les différent MNPs présent une mobilité similaire tant quand appliqué séparément comme quand appliqué en combinaison. Mais l'ajout de l'aimant améliorait la mobilité des MNPs après application topique (Figure 4.). D'après l'imagerie IRM, après application topique et ajout de l'aimant, il semble que les MNPs soient capables d'accéder à l'intérieur de l'œil, néanmoins, 24 heures après le traitement, nous ne pouvions plus observer les MNPs. Cela pourrait signifier que la plupart des MNPs ont été emportés ou que la concentration restante soit, soit distribuée autour de l'œil, soit présente avec une concentration indétectable très faible.
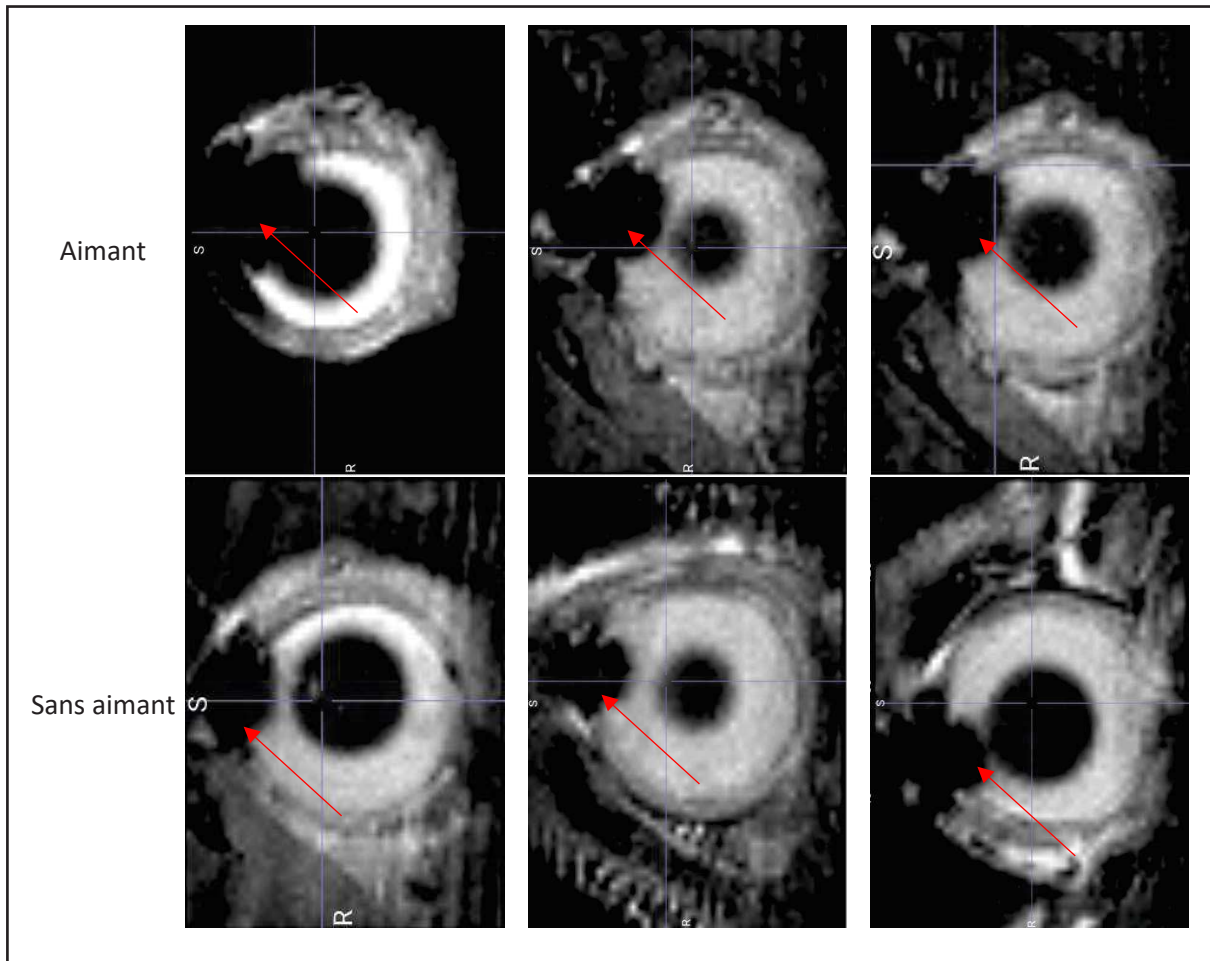
Figure 4. Images obtenues par IRM. Nous pouvons observer la présence plus forte des MNPs à l'intérieur de tissues oculaires quand l'aimant était appliqué pendant le traitement. Les MNPs corresponde a la flèche rouge.

Pour nous assurer que les MNPs arrivent à la rétine nous avons utilisé la microscopie électronique en transmission qui nous permet d'observer directement les MNPs dans les tissus. Avec cette technique il était possible de visualiser les MNPs dans la rétine et la couche de photorécepteurs.

2.2-Comportement des nanoparticules dans le vitrée :

Nous avons également évalué comment les MNPs pouvaient se comporter à l'intérieur du corps vitré. Pour cet ensemble d'expériences, nous avons choisi d'utiliser des rats, car le volume du corps vitré est plus élevé que chez les souris. La méthode utilisée pour cette évaluation était l'injection intravitréenne (IVT). Les MNPs sont restés au même endroit après IVT pendant une

période allant jusqu'à 1 mois sans changer sa distribution de manière significative, mais après l'application de l'aimant, les MNPs ont pu se déplacer à l'intérieur du corps vitré.**3-Effet des nanoparticules sur les modelés animaux :**

Les effets de l'application de nos MNPs chargés avec les 2 composés (VPA et GBZ) ont été évalués chez les souris *Bbs*^{-/-}. Différentes dilutions ont été testées : 1 mg / ml de MNP, 0,04 mg / ml de MNP, 0,02 mg / ml de MNP et 0,01 mg / ml de MNP avec 6 souris étudiées par groupe. Les 6 souris ont subi un enregistrement ERG, puis 3 souris ont été utilisées pour les mesures de dilatation ER et 3 souris ont été utilisées pour les dosages Western Blot.

3.1-ERG :

Nous avons enregistré des ERG scotopiques (adaptés à l'obscurité) et photopiques (adaptés à la lumière). Nous avons observé une légère amélioration de l'enregistrement des ERG scotopiques chez les souris traitées avec les MNPs chargés de VPA et de GBZ. L'amélioration était statistiquement significative seulement pour les souris traitées avec une dilution de particules 1 :25 (Figure 5.). Nous avons également analysé l'ERG chez des souris *Bbs*^{-/-} traitées uniquement avec des solutions VPA et GBZ et avec un seul MNPs chargé (soit avec VPA ou GBZ). Dans tous ces essais, nous n'avons pu observer aucune amélioration de l'enregistrement ERG. Ces résultats indiquent que pour avoir un effet de notre traitement avec des MNPs nous avons besoins de le deux MNPs particules chargés pour avoir une efficacité de notre traitement. Souris non traité
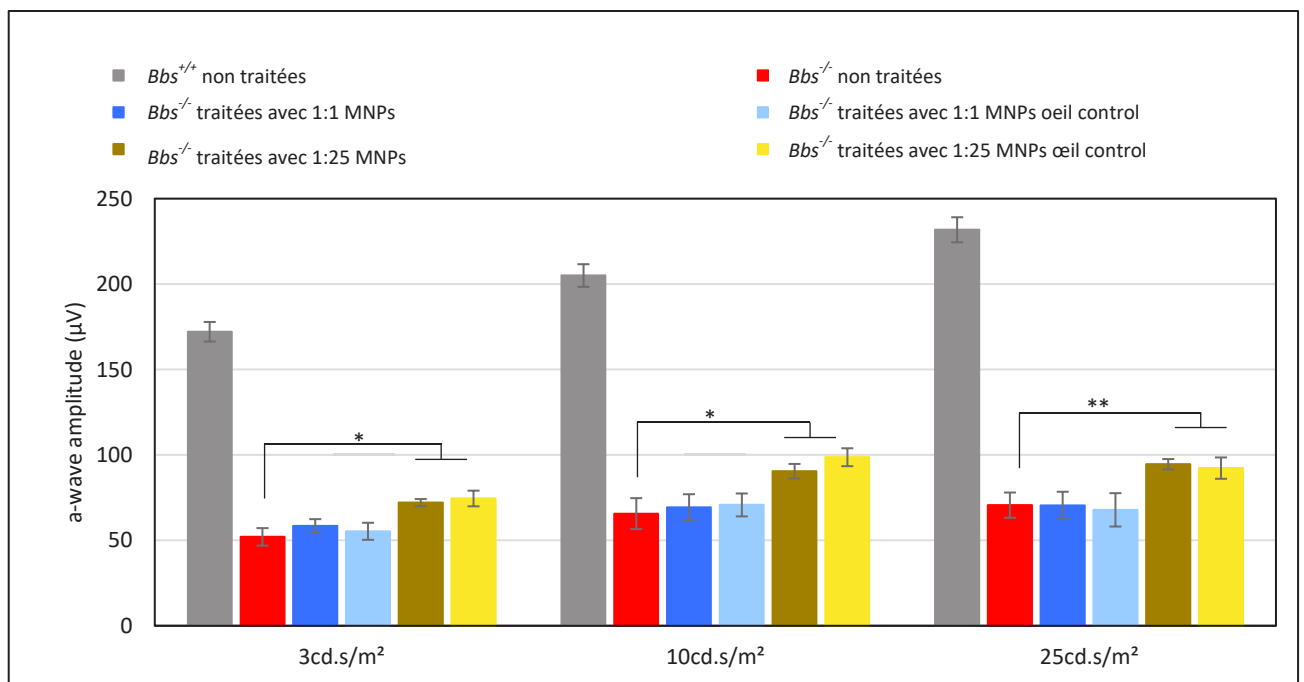
Figure 5. Effet des MNPs sur la fonction rétinienne. L'intensité de l'onde a est montré. Seulement les souris traitées avec des MNPs avec une dilution 1 :25 ont montré une amélioration dans l'ERG.

L'enregistrement photopique ERG n'était pas mesurable car le signal était en dessous du bruit de fond.

3.2-Effet des nanoparticules sur les tissus :

Afin de mesurer la dilatation du réticulum endoplasmique comme marqueur de l'UPR, nous avons utilisé la microscopie électronique en transmission (MET). Nous avons ainsi pu observer d'une part la diminution de la dilatation du RE chez nos souris *Bbs*$^{-/-}$ traitées par rapport aux souris *Bbs*$^{-/-}$ non traitées. Ces résultats ont été observé avec les souris traités avec un dilution de nanoparticules 1 :25 mais pas avec les souris traitées avec des autres dilutions (Figure 6.). Les résultats obtenus ne sont pas statistiquement significatifs. C'est possible que soit le nombre de souris ou soit le période de deux semaines après le traitement sont la cause pour ce manque de signification statistique.

D'autre part les résultats des mesures des souris *Bbs*$^{-/-}$ traitées étaient similaires à ceux obtenus chez nos souris *Bbs*$^{+/+}$. Enfin, pour finir, nous avons observé une tendance à l'augmentation de l'épaisseur de la couche nucléaire externe de la rétine, correspondant à une augmentation possible de la survie des cellules photoréceptrices chez nos souris *Bbs*$^{-/-}$ traitées par rapport aux souris non traitées.
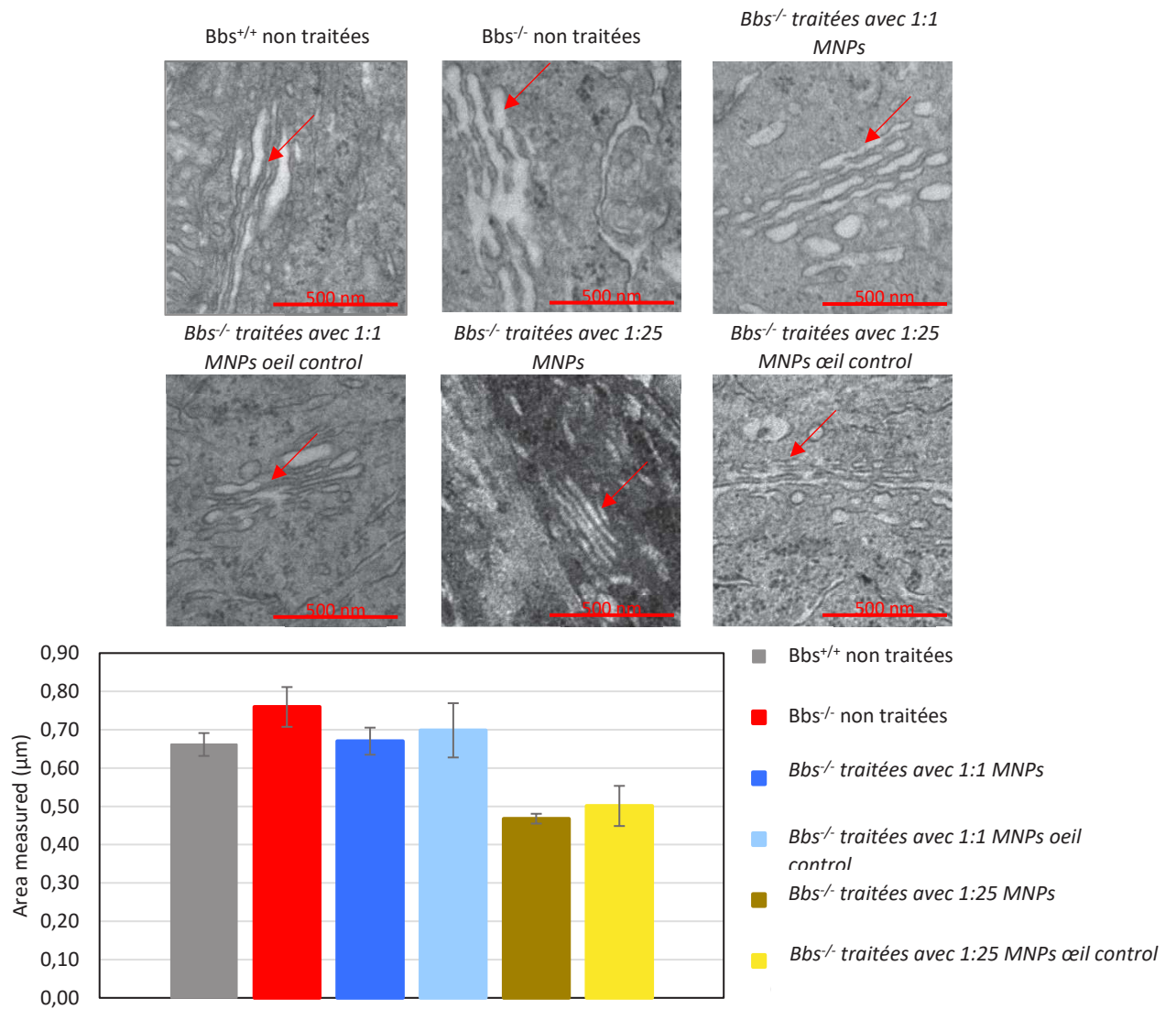
Figure 6. Effet des MNPs sur les tissue rétinienne. Mesure de dilatation de réticulum endoplasmique, marqueur d'UPR. Nous observons une diminution de dilatation des réticulums dans toutes les groupes de souris traitées mais cette diminution est plus forte dans les souris traitées avec les MNPs en dilution 1 :25. Néanmoins, ces résultats ne sont pas statistiquement significatifs.

3.3-Western Blot (WB) :

Pour analyser l'effet de notre traitement dans les tissus rétiniens, nous avons utilisé des tests WB afin d'étudier un ensemble de protéines liées à la voie UPR. Comme nous avons déjà expliqué, l'effet de VPA c'est d'augmenter la quantité de chaperonne Bip. D'une autre part GBZ a comme effet l'inhibition de la déphosphorylation du facteur p-eIF2α. Après les traitements avec les MNPs on a pu observer que dans les souris traités avec les MNPs en dilution 1:25 la concentration de Bip chaperon est incrémenté, donc le VPA est capable de moduler la concentration de protéines dans les tissus oculaires après la application comme collyre. De la même manière la quantité de p- eIF2α observé est majeur dans les tissue des souris traitées. Dans ces cas si nous observons le ratio p-eIF2α/eIF2α l'augmentation de ce ratio dans les souris traitées nous indique que la forme phosphorylée est la forme prédominante. Ce résultat peut montrer que la différence que nous observons c'est à cause de l'effet de GBZ (Figure 7.).

A

B

Legend

7. Poids moléculaire
8. Poids moléculaire unstained
9. *Bbs+/+ non traitées*
10. *Bbs-/- non traitées*
11. Bbs-/- traitées avec 1:25 MNPs
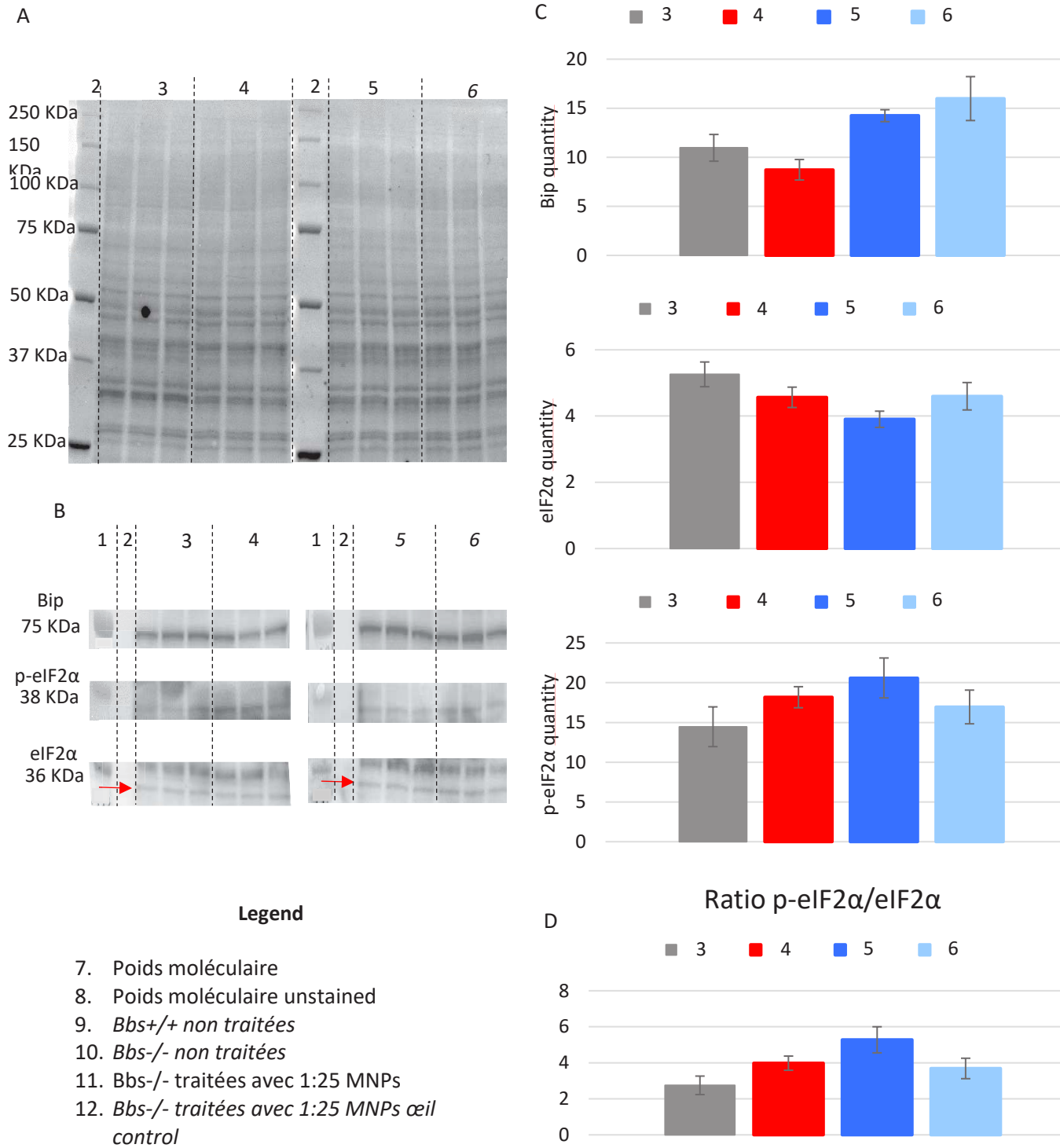12. *Bbs-/- traitées avec 1:25 MNPs œil control*

C

D

Ratio p-eIF2α/eIF2α

Figure 7. Effet des MNPs sur la concentration de protéines cibles. A) Protéines totales sur la membrane. B) Protéines détecté. C) Quantification des protéines ciblées. D) Ratio p-eIF2α/ eIF2α

4-Conclusions :

Nous avons ainsi pu démontrer des effets positifs efficaces et durables à partir d'une seule application de nos MNPs. Deux semaines après notre traitement, nous avons pu observer une amélioration des enregistrements ERG, une diminution de la dilatation du réticulum endoplasmique, ainsi que la modulation des protéines UPR cibles. Notre système s'est également avéré sûr, sans effets négatifs observés dans nos études actuelles. Nous avons essayé de répondre aux questions de base liées à la faisabilité de l'utilisation des MNPs en termes de sécurité et d'efficacité, car, à notre connaissance, très peu d'informations sont disponibles, concernant l'utilisation et l'étude des MNPs en tant qu'approche topique visant à traiter maladies rétiniennes.

Références :

1.   Brun A, Yu X, Obringer C, et al. In vivo phenotypic and molecular characterization of retinal degeneration in mouse models of three ciliopathies. *Exp Eye Res*. 2019;186:107721. doi:10.1016/j.exer.2019.107721

2.   Mockel A, Obringer C, Hakvoort TBM, et al. Pharmacological Modulation of the Retinal Unfolded Protein Response in Bardet-Biedl Syndrome Reduces Apoptosis and Preserves Light Detection Ability. *J Biol Chem*. 2012;287(44):37483-37494. doi:10.1074/jbc.M112.386821

3.   Raju HB, Hu Y, Vedula A, Dubovy SR, Goldberg JL. Evaluation of Magnetic Micro- and Nanoparticle Toxicity to Ocular Tissues. *PLOS ONE*. 2011;6(5):e17452. doi:10.1371/journal.pone.0017452

Université de Strasbourg

Daniel AJOY MORENO

École Doctorale des Sciences de la Vie et de la Santé
STRASBOURG

Non-invasive pharmacological treatment of retinal degeneration in the Bardet-Biedl Syndrome and related ciliopathies

Thesis summary

The delivery of compounds to the ocular tissues presents several challenges due to the physiological and anatomical barriers of the eye. While several methods have been studied to overcome these difficulties none of them has been able to completely overcome them. During these three years I have worked on testing magnetic nanoparticles as drug delivery systems for retinal diseases. For this, we collaborated with OZ Bioscience for the formulation of the particles. We have used a mice model for Bardet-Biedl syndrome to test our delivery system. The results obtained increases the existing knowledge regarding the behaviour of the particles after topical application. Using compounds already studied in our group we were also able to show that a single application of the treatment was able to induce a positive effect in our treated animals.

Keywords: Magnetic nanoparticles, topical application, drug delivery, retinal diseases, mice model.

Résumé de Thèse

L'administration de traitements aux tissus oculaires présente plusieurs défis en raison des barrières physiologiques et anatomiques de l'œil. Si plusieurs méthodes ont été étudiées pour surmonter ces difficultés, aucune d'entre elles n'a pu les surmonter complètement. Au cours de ces trois années, j'ai travaillé sur les tests de nanoparticules magnétiques en tant que systèmes d'administration de médicaments pour les maladies rétiniennes. Pour cela, nous avons collaboré avec OZ Bioscience pour la formulation des particules. Nous avons utilisé un modèle de souris pour le syndrome de Bardet-Biedl pour tester notre système d'administration. Les résultats obtenus enrichissent les connaissances existantes sur le comportement des particules après application topique. En utilisant des drogues déjà étudiés dans notre groupe, nous avons également pu montrer qu'une seule application du traitement pouvait induire un effet positif chez nos animaux testés.

Mot clés : nanoparticules magnétique, application topique, administration de médicaments, maladies rétiniennes, modèle de souris.